FACULTY OF AGRICULTURAL SCIENCES

Institute of Plant Production and Agroecology in the Tropics and Subtropics

University of Hohenheim

Field: Geomorphology and plant production

Prof. Dr. Georg Cadisch

Sediment, carbon and nitrogen capture in mountainous irrigated rice systems

Dissertation
Submitted in fulfillment of the requirements for the degree
"Doktor der Agrarwissenschaften"
(Dr.sc.agr. / Ph.D. in Agricultural Sciences)

to the
Faculty of Agricultural Sciences

presented by:
Johanna Irma Franciska Slaets

born in:
Herk-de-Stad, Belgium

submitted in: November 2015

This thesis was accepted as doctoral dissertation in fulfilment of the requirements for the degree “Doktor der Agrarwissenschaften” (Dr.sc.agr. / Ph.D. in Agricultural Sciences) by the Faculty of Agricultural Sciences at the University of Hohenheim on January 25, 2016

Date of oral examination: February 15, 2016

Examination committee

Supervisor and Reviewer	Prof. Dr. Georg Cadisch
Co-Reviewer	Prof. Dr. Hans-Peter Piepho
Additional Examiner	Prof. Dr. Roel Merckx
Vice-Dean and Head of Committtee	Prof. Dr. Markus Rodehutscord

Acknowledgements

First off, I would like to thank my supervisor, Georg Cadisch, who gave me the chance to work in this project and in this topic. I was very lucky to have him visit me often in the field, during which he taught me many things – from operating a four-wheel drive vehicle, to looking at the big picture and avoiding scientific tunnel vision. Whenever I hear myself saying the words "Well, it depends – what's your hypothesis?" it will be due to his training. To my second supervisor, Hans-Peter Piepho, from whom I have learned everything I know about statistics, who was always willing to borrow his editorial hawk eye and who taught me how to bootstrap, thank you ever so much, and this thesis would have looked very different without you coming on board.

A big thank you also goes to Thomas Hilger, my direct supervisor, who helped me solve so many logistical crises and equipment failures in the field that I cannot even count them, and who always supported me in pursuing new ideas. To Petra Schmitter, my predecessor, whose many ideas formed the initial seed for this thesis, I am glad she always stayed involved, no matter where on the globe she found herself throughout the last years.

As this thesis was part of the Uplands Program, there were a great number of people instrumental in the logistics and local support. I would like to thank Gerhard Clemens, Pepijn Schreinemachers and Holger Fröhlich, the project coordinators in Vietnam, Thailand and Germany, who made life so much easier for all of us PhD students in the project. Mrs. Hong, Julia Rietze and Birgit Fiedler were very helpful in navigating the administrative mill that was involved. Peter Elstner assisted me with the GPS data. Thank you also to all project colleagues, German, Thai and Vietnamese, without whom the field experience would have been much more lonely and much less gratifying.

To my wonderful, splendid, spectacular field team, Do Thi Hoan and Nguyen Duy Nhiem, without whom the dataset would have never existed: thank you for braving torrential rains, tropical storms, and dirt roads on motorbikes to collect these samples. You were the best field team I could wish for and it was my privilege to

work with you. The people of Chieng Khoi commune, especially Mr. Ngoc, Lam, An and Keo who assisted in the data collection, and lake manager Nguyen Xuan Truong, thank you very much for making the experience about real people and putting a face on the “local stakeholders” from literature. Cam on nha, and I hope to visit you all in Vietnam again one day.

Special thanks also to the lab team at the Central Water and Soil Lab of Vietnam National University of Agriculture, Dang Thi Thanh Hue and Phan Linh under supervision of Nguyen Huu Thanh. The field work also wouldn’t have been possible without the logistic and scientific support of Tran Duc Vien at the Center for Agricultural Research and Ecological studies of Vietnam National University of Agriculture.

To Gaby Kircher who was my main German conversation partner and the secret driving force behind Institute 380a, thank you for everything. And to all my colleagues at 380a, thank you for years of positive atmosphere, international food, entertaining Christmas parties and barbecues in summer, and I hope we meet each other again, someday, somewhere. It’s a small world! To all friends, whether still in Hohenheim, or now departed, who were there to celebrate the good parts with me and commiserate through the less good: Scott, Anna and Michelle, Victor, Susanne and Toa, Martina, Angela Bernal (my fitness-inspiration), the Mensa-gang, old and new (Daniela, Christian, Judith, Rong, Lucia), thank you all for your support and friendship.

I want to thank my friends and family in Belgium, who managed to keep up with me throughout so many changes and chaos and sometimes non-responsiveness, your support has meant so much to me. To my sister, my mother and father, thank you for always being there for me, whether in person or Skype, through many time zones. Jullie relativeringsvermogen is onmisbaar en ik denk dat ik er zonder jullie steun niet aan begonnen was! To Juan Carlos, thank you for everything, but most of all thank you for simultaneously fuelling my love for science and yet reminding me that when push comes to shove, life is more important than research, always.

And finally I thank you, unknown reader, for showing interest in my work.

Table of Contents

List of Tables

List of Figures

Chapter 1 General introduction

1.1 Overview

Quantification of sediment and nutrient transfers within and between landscapes is essential to monitor and mitigate impacts of anthropogenic changes in mountainous watersheds in Southeast Asia. These watersheds have been subjected to intense land use change under the influence of population pressure and market mechanisms in the last decades (Fox *et al.*, 2009). The nutrient loss and productivity decline associated with changing from traditional swiddening systems to continuous maize cropping has been well documented (Häring *et al.*, 2014), but impacts beyond the plot scale, in the watershed or off-site, remain poorly understood. Within landscapes, nutrient re-allocation through irrigation systems acting as conveyor elements can be substantial (Schmitter *et al.*, 2012) and could potentially affect both upland and irrigated crop production, but these consequences are not yet evaluated. Additionally, Southeast Asia's mountainous areas are considered a hotspot for global sediment and nutrient yield to oceans (Beusen *et al.*, 2005; Ludwig *et al.*, 1996; Milliman *et al.*, 1992; Seitzinger *et al.*, 2005).

Therefore, reliable estimates of sediment and nutrient loads are imperative for and a first step in making suitable recommendations to stakeholders. These include farmers who need to preserve the long-term fertility of their production system, extension workers who can provide site-specific fertilizer recommendations, policy makers involved in food security planning in the area and scientists performing nation-wide environmental impact assessments. To address this knowledge gap, in this thesis sensor-based and statistical methodologies were developed to quantify sediment and sediment-associated nutrient transport in heterogeneous, cultivated mountainous watersheds, which have the potential to impact plant production. The developed methodology was applied to assess sediment fluxes for a typical maize-paddy rice cropping system in Chieng Khoi watershed, Yen Chau district, Son La province, Northwest Vietnam as a case study.

1.2 A history of plant production and land use change in montane Southeast Asia

1.2.1 From traditional swidden agriculture to intensive upland cropping

The highlands of Southeast Asia, encompassing the mountainous areas of Vietnam, Laos, Thailand, Northern Myanmar and Southern China, are the home of ethnic minorities who traditionally practice shifting cultivation agriculture – also known as swiddening. The estimated number of people still farming in a swidden system in mainland Southeast Asia varies widely, as these systems are complex, hard to quantify and there has been little political interest in doing so. Mertz *et al.* (2009) suggested a conservative estimate between 14 and 34 million. Pressure on the land in traditional swidden systems is low, and plots are normally used for cultivation one to three seasons and subsequently given ample time to regenerate, the fallow period usually lasting six to fifteen times the cropping duration (Mertz *et al*., 2009).

These true swidden systems, extensive both in space and time, have a very low environmental impact at the landscape level. They are characterized by low erosion and runoff, little to no soil fertility loss, and preservation of soil organic carbon stocks and biodiversity, even though the perception of shifting cultivations by governments in the region is often negative (Bruun *et al.*, 2009; Jamieson *et al.*, 1998; Valentin *et al.*, 2008; Ziegler *et al.*, 2009a). This unfavorable impression partly results from a confusion of true swidden systems with intensified swidden systems associated with forest conversion and land degradation (Ziegler *et al.*, 2009a), and partly results from cultural frameworks, in the sense that modern nation-states and development projects often treat ethnic minorities in ways that make them appear in need of "help" in order to pursue their own agenda (Dove, 1983; Fox *et al.*, 2009). In China, Vietnam and Laos, the historic Marxist/Stalinist world view associating production systems with ethnicity has also been stated to have influenced the governmental position on shifting cultivation, which is that these cropping patterns should be seen as a primitive "stage" in a social evolution (Jamieson, 1991; Rambo, 1995).

While these myths persist until the present day (Mai and To, 2015), Scott (2009) has argued that swiddening is neither archaic nor undeveloped. He considers this

cropping system to be rather a form of "Escape-Agriculture", a conscious and political choice of hill populations to remain outside of state space. Shifting cultivation fields, and by extension swiddeners themselves, are dispersed, hard to monitor, difficult to tax and onerous to collect for forced labor. These are precisely features that would make this cropping system attractive to ethnic minorities wanting to stay out of reach, fleeing both state-making projects in the valleys and lowland officials who see the technique as primitive and environmentally destructive. In this light, the widespread failure of development schemes involving swiddeners (Dove, 1983) is not surprising.

While shifting cultivation in its pure form has a low environmental impact, it is prone to suffer rapid degradation or even collapse in the face of population pressure, leading to excessive environmental degradation (Rambo, 1995). In many areas, a hybrid system referred to as composite swiddening has been adopted by more recent generations, in which paddy rice is cultivated in terraces in the valleys and shifting cultivation is practiced on the upland fields (Jamieson *et al.*, 1998). These composite systems are common in Northern Vietnam (Cuisinier, 1948), Burma and Northern Thailand (Durrenberger, 1981), Southwestern China and the Philippines (Rambo, 1995).

Composite swiddening is more robust than traditional shifting cultivation against population increase and it offers potential for intensification (Rambo, 1995), but population changes and associated land use dynamics in Vietnam during the last decades have been nothing short of extreme. Until the middle of the twentieth century, the mountainous North was largely covered by forests (Poffenberger and Nguyen, 1998). Since then, rapid decrease in forest cover and agricultural intensification in the uplands took place under the influence of high natural birth rates and migration from the lowlands due to resettlement policies, which led to a 300% population increase between 1960 and 1984 (Jamieson *et al.*, 1998).

Deforestation culminated in the late 1980s (Meyfroidt and Lambin, 2008). In recent years, governmental re-allocation of land to forestry (Fox *et al*., 2009; Nguyen, 2009), privatisation of land known as the Doi Moi reform (Fox *et al*., 2009; Meyfroidt and Lambin, 2008) and market opportunities brought about by the

development of market infrastructure, roads and the expansion of capitalism have again propelled land use change in montane Vietnam. Population growth has continued, with a population increase of 46% between 1981 and 2001 (Clemens *et al.*, 2010). In combination with the policy changes and economic development, this increased number of people has resulted in land shortages and the collapse of traditional swiddening in Northern Vietnam – a trend that persists across most of montane Southeast Asia. These same transformations characterize the study area of this thesis: in Yen Chau district, where the Black Thai ethnic minority traditionally were swiddeners, agricultural land has decreased from 0.5 ha per person in 1980, to 0.2 ha per person in 1998 (Statistical Department Yen Chau, unpublished data, 1999; cited in Wezel *et al.*, 2002).

The successors of shifting cultivation systems in Southeast Asia are various intensive cropping systems, ranging from large scale permanent cultivation of annual crops to monoculture plantations and greenhouse vegetable or flower production, all of which are more demanding on the land in space and time than shifting cultivation (Fox and Vogler, 2005; Rerkasem and Rerkasem, 1994; Schmidt-Vogt *et al*., 2009; Thongmanivong *et al*., 2005; Xu *et al.*, 2005*).* The environmental impacts of this demise of shifting cultivation are detrimental and well documented. Biodiversity loss is exacerbated by large areas of land being cultivated simultaneously (Rerkasem *et al.*, 2009). With limited or non-existing fallow periods, infiltration properties of the soil have no chance to recover (Ziegler *et al*., 2009a) resulting in increased water and tillage erosion, decreased soil quality and reduced carbon storage (Bruun *et al.*, 2009). The increased soil loss propagates, as upland fields in an intensive setting are often directly linked to connective elements in the landscape, such as roads or stream networks (Ziegler *et al*., 2009a). With reduced root strength on the permanently converted hillslopes, areas converted to permanent upland cultivation also become increasingly susceptible to landslides (Ziegler *et al.*, 2009a). Increased use of herbicides and pesticides diminishes water quality in fish ponds in cultivated watersheds (Anyusheva *et al*., 2012).

While environmental impacts are negative for almost all intensive systems that have replaced swiddening, permanent maize cultivation in particular has been reported to have one of the highest erosion rates (Tuan *et al.*, 2014; Valentin *et al.*, 2008). Plots

are cleared and lay bare at the start of the rainy season, which can lead to losses of up to 174 Mg ha^{-1} a^{-1} at the plot level (Tuan *et al.*, 2014). And maize is the prevalent crop on the upland fields in Chieng Khoi commune, as the demand for maize has grown strongly since the 1970s fueled by population increase, rising meat consumption and an ever growing demand for animal fodder (Keil *et al.*, 2008). In the 1990s, the advent of new improved varieties and chemical fertilizer substantially improved yields and, for a while, these developments masked soil degradation (Lippe *et al.*, 2011; Wezel *et al.*, 2002). But in recent years, cassava has often been the only crop that can be grown on fields where the soil has degraded too much (Wezel *et al.*, 2002). High maize prices on the world market, however, make it a difficult-to-resist choice for struggling people in rural areas with little access to other labor opportunities – even if the ecological consequences are well known.

1.2.2 Rice cultivation in changing mountainous landscapes

Rice feeds almost half of humanity, and in Vietnam, it is simultaneously the main staple food for small-scale rural farmers and the most important export product (FAO, 2014). In Northern Vietnam, 60% of paddy cultivation is located in hilly areas, in terraces forming cascades. While rice is a more important source of income for the lowland regions in the South of Vietnam, it still accounts for 46% of the net value of crop production in the mountainous North. And its role as a staple is larger than in the flat river deltas in the South, as the Northern uplands are more subsistence-oriented (Minot, 2006).

Rice cultivation has been present in these areas for centuries, and is considered to be one of the most sustainable agricultural systems (Cao *et al.*, 2007). Integrated pest management and resistant varieties can prevent major problems with insect pests, and salinization is not a threat in most areas (Heong *et al.*, 1995). Long-term sustainability of irrigated rice production then mainly depends on the effects of intensification on the soil resource base (Cassman and Pingali, 1995). In fact, before the Green Revolution, rice was the only major crop that could be grown for centuries in monoculture without collapse of soil fertility (Bray, 1986; Uexkuell and Beaton, 1992), supporting yields of one to two tons per hectare. Productivity was low, because rainfall only provided sufficient water for a single crop, bunding and levelling were not yet applied, and due to poor management by cooperatives in the

mountain paddies and lack of incentives inherent to that cooperative system (Meyfroidt and Lambin, 2008).

Since then, pressure on the soil has multiplied as a result of increased cropping intensity and yields. In Vietnam, allocation of paddies to households, liberalization of rice trade, improved seed varieties and fertilizers all influenced agricultural intensification (Meyfroidt and Lambin, 2008). More recently, the Vietnamese government has given priority to the development of small scale irrigation systems in the Northern provinces, as is the case for Chieng Khoi commune, where a surface reservoir built in 1963 allows people to produce two rice crops per year. Almost all of Vietnamese rice is irrigated, and surface reservoirs provide water for the vast majority of irrigated crops in Southeast Asia (FAO Aquastat, 2014). Up to date, increases in Vietnamese rice yields have been able to keep up with the rising demand from the growing population: yields in the country have risen from 4.14 Mg ha^{-1} in 2000 to 5.89 Mg ha^{-1} in 2015 (International Rice Research Institute, 2015). But paddy rice area is declining in Vietnam and is expected to keep doing so in the future, due to a reorientation of the economy towards services and manufacturing (Rutten *et al*., 2014), even though close to 70% of the population still resides in rural areas and works in the agricultural sector.

Intensification of rice production has also been associated with trends of declining productivity, originating from a gradual decline in soil quality caused by the intensification (Reichardt *et al.*, 1998). Depletion of soil nutrient reserves and reduced nitrogen supplying capacity of the soil in particular are reported as driving forces (Cassman and Pingali, 1995). Nitrogen deficiency is a general feature of modern irrigated paddy rice in Southeast Asia, while phosphorous and potassium are typically less limiting (Dobermann *et al*., 2003). Soil organic carbon content has also been found to decrease over time with application of chemical fertilizer (Lee *et al.*, 2009).

1.3 The role of sediment in the indigenous nutrient supply of rice

The function of the indigenous nutrient supply in sustaining rice yields in intensive, modern systems has rarely been quantified. Before the Green Revolution, soil fertility was maintained exclusively by flooding and puddling (Bray, 1986; Uexkuell

and Beaton, 1992). Reichardt *et al.* (1998) stated that maintaining the indigenous nutrient supply and positive nutrient balances are key factors in preserving sustained high yields in intensive production systems. Irrigation water transports and re-allocates sediments in watersheds, especially in intensely cultivated upland areas (Gao *et al*., 2007). Surface irrigation contributes sediments to paddy fields, for example in the Yellow River basin where Mingzhou *et al.* (2007) found paddy fields raised by four to five centimetres over fifty years due to sediment inputs.

Simultaneously, irrigation systems are conveyors for nutrients (King *et al.*, 2009; Poch *et al.*, 2006), and have been reported to contribute up to 800 kg a^{-1} of organic carbon and 700 kg a^{-1} of nitrogen per hectare of irrigated crop (Schmitter *et al.*, 2012). In comparison, biologically fixed nitrogen is estimated to contribute around 15 to 50 kg per crop (Koyama and App, 1979; cited in Roger, 1996*)*. Cassman *et al.* (1998), however, reported that in most irrigated rice systems, nitrogen inputs from rainfall and irrigation do not represent a significant input. In paddy rice production in a mountainous setting, in light of increased erosion and decreasing fertility of the upland fields where the sediment inputs originate, the contribution of sediment to the nutrient balance of rice could be negligible in intensive cropping. But beyond that, a change to an increased input in coarse and unfertile material may not only reduce the sediment-associated nutrient input to inconsequential levels, but could also have an adverse effect on paddy topsoil texture and puddling, reversing the previously beneficial role of irrigation water sediments. Surface reservoirs form the water source of the vast majority of irrigated crops in Southeast Asia, and therefore these changes potentially affect a large cropping area.

The actual effect of sediment inputs on rice production additionally depends on the net sediments remaining behind in the fields, but little is known about the trapping efficiency for sediment of paddy fields at the watershed scale. Plot-scale studies have indicated that sediment trapping capacity changes over time (Kundarto *et al.*, 2002; cited in Maglinao *et al.*, 2003; Mai *et al.*, 2013). But as spatial variability is present at the cascade level, showing the coarser particles deposit closer to the irrigation source and the finer material further away from it, plot-level studies cannot be considered representative at the landscape scale (Schmitter *et al.*, 2010).

1.4 Effects of sediment re-allocation beyond the catchment

The sediment trapping capacity of paddy fields not only has potential impacts on rice productivity, but also on sediment yield from catchments where wet rice is cultivated. As mountainous catchments in Southeast Asia are considered a hotspot for sediment and carbon export (Milliman and Syvitski, 1992), a filtering or accelerating function of paddy fields is important to realistically model contributions of these catchments to the global sediment and carbon yields. Surface reservoirs similarly trap constituents and change the particle size distribution of released sediments, and the speed with which constituents move within catchments (Kroon *et al.*, 2012).

Additionally, there are other effects of intensified land use in upland areas that are not limited to the field. Off-site effects at the landscape, regional or global scale are more difficult to quantify due to different processes at field versus landscape scale, and include flooding (Lopez-Tarazon *et al.*, 2010), siltation of irrigation systems and reservoirs (Lantican *et al.*, 2003), and eutrophication of oceans (Beusen *et al*., 2005; Ludwig *et al.*, 1996; Seitzinger *et al.*, 2005). Water quality studies often only focus on monitoring constituent concentrations, which are very informative in order to determine effects on in-stream pollution, eutrophication and ecology. But quantifying upland-lowland linkages within the watershed, between maize and rice, and beyond the watershed, such as the aforementioned off-site effects, necessitates the quantification of constituent loads (Horowitz, 2008).

1.5 Methodological knowledge gaps

1.5.1 Spatial and temporal measurement choices for sediment and nutrient loads

The vast majority of studies on sediment and nutrient loss have been done at the plot level, either on bounded or unbounded experimental plots, because measurements beyond the plot scale are more difficult to execute in practice, and therefore, data at the watershed level and beyond are scarce (de Vente and Poesen, 2005). Much has been learned from the plot-level studies regarding specific erosion rates for many land use types, but soil erosion rates measured at the plot scale are not accurate representations of sediment yield at the watershed, regional or national level: while

there is a lot of variation, sediment yield per unit area typically decreases with increasing area (de Vente and Poesen, 2005) due to internal deposition processes, variation in sediment supply and filtering elements such as river bank vegetation. For landscapes containing terraces, there is an additional effect of changed slope and different infiltration characteristics for the terraced units, which Van Dijk and Bruijnzeel (2005) found to result in an initial decrease in sediment yield with increasing slope length. Subsequently, a slight increase from the terrace scale to the catchment scale was observed, after which the sediment yield stabilized due to supply limitations. Therefore, in order to monitor constituent transport at watershed level, discharge and constituent concentrations need to be monitored at strategic locations in rivers and streams, typically by *in situ* sediment sampling in the main stream or at the outlet of the watershed of interest (Gao, 2008).

Not only is an appropriate choice of spatial monitoring scale required for meaningful constituent load estimates, in line with the objectives of the study, but also a satisfactory temporal resolution. Sediment transport processes are seasonal and strongly dependent on changes in rainfall, vegetative cover, sediment supply and soil moisture conditions. The sediment source or sink nature of paddy fields changes throughout the season, depending on the water status of the rice fields prior to rainfall (Mai *et al*., 2013), and the growing stage and activities in the field (Kundarto *et al.*, 2002; cited in Maglinao *et al.*, 2003); and without continuous data it remains unclear whether paddies are a net sediment source or sink over a whole growing season. Additionally, reliable load estimates and sediment budgets require frequent monitoring. If the time interval between measurements is too large, there is a high probability of missing peak events or reversely overestimating very short-lived, intense peaks, depending on the nature and responsiveness of the catchment, increasing uncertainty on the estimated loads. Therefore, there is a need for continuous constituent concentration data with a fine temporal resolution covering full cropping periods.

The need for continuous data to adequately capture seasonal trends additionally implies that the resulting discharge and constituent concentration data will be time series, with serial correlation present: two measurements taken at the same location, closely together in time, cannot be considered independent from each other. The

correlated nature of time series data requires the use of appropriate statistical methods that are able to account for autocorrelation, such as linear mixed models, which are not yet standard practice in hydrological studies.

1.5.2 Monitoring constituent concentrations in irrigated watersheds

Sediment and nutrient loads in natural streams are typically obtained by one of two methods (Gao, 2008). In direct measurement, water samples are taken and the loads at those sampling times are integrated over the whole period. The sampling can be at fixed time intervals, which is convenient but frequently fails to capture the highest constituent loads, or flow-proportional, with automatic water samplers. When using indirect measurement, typically constituent concentrations are predicted from a rating curve, which establishes a relationship between the constituent and discharge. Constituent loads are then calculated as the product of the concentration and discharge. In unmanaged watersheds, there is a natural link between an increase in discharge and an increase in sediment concentration, as both are usually caused by rainfall initiating overland flow.

In irrigated catchments, an increase in discharge is not necessarily related to an increase in overland flow, as irrigation management causes changes in water regime as well. Therefore, strategies that exploit this link, such as rating curves based on discharge, are not necessarily suitable. Flow-proportional automated sampling, on the other hand, requires a great number of samples to obtain high temporal resolution data, and can rapidly become expensive when several sites are monitored. Alternative predictor variables such as turbidity that function as proxies for constituent concentrations are thus required in order to obtain cost-effective, time-saving, continuous constituent concentration predictions where irrigation affects the hydrological conditions.

1.5.3 Uncertainty of constituent load estimates

Constituent loads based on continuous data are estimated as a product of concentration and discharge. As discharge is generally not measured directly, but rather estimated from water depth based on a stage-discharge rating curve, there are two components that introduce uncertainty into the sediment load: the prediction of discharge from water level, and the prediction of continuous constituent

concentrations. There is substantial literature discussing the uncertainty of both of these predictions, which differ vastly and depend on catchment size and geomorphological characteristics of the study area (Hamilton and Moore, 2012; Horowitz, 2008). But the resulting uncertainty on load estimates is almost never determined (Kulasova *et al.*, 2012).

As a consequence, there is an abundance of load estimates in literature, used to assess environmental impacts of a diverse array of processes such as erosion, sedimentation, eutrophication and degradation of aquatic ecosystems, but there is little information regarding the accuracy of these estimates. This lack of uncertainty measures puts constraints on the usefulness of the information – for everyone involved in the different levels of decision making concerning these environmental impacts.

1.6 Objectives and hypotheses

The main goal of this thesis was to develop sensor-based and statistical methods to quantify sediment and nutrient transfers beyond the plot-level in an intensely cultivated, irrigated tropical mountainous watershed, in order to assess the potential impact of these sediment and nutrient re-allocations on upland and lowland soil fertility and on watershed sediment and nutrient yield. The specific objectives were to:

(1) Develop a method to continuously predict sediment, organic carbon and nitrogen concentrations in waterways in a mountainous, fragmented, intensely cultivated watershed

(2) Quantify uncertainty on constituent load estimates in the form of confidence intervals

(3) Assess the contribution of irrigation water and direct overland flow to the sediment inputs of a paddy area in a mountainous watershed

(4) Determine whether the paddy area is a net source or sink for sediments

(5) Separate the different textural classes of the inputs and exports of the sediment budget

(6) Evaluate the contribution of sediment-associated organic carbon and nitrogen to the indigenous nutrient supply of the paddy fields at the watershed scale

Corresponding to these objectives, the hypotheses tested in this thesis are:

(1) Turbidity can be used as a predictor variable to obtain continuous estimates of sediment, organic carbon and nitrogen concentrations in irrigation channels and streams in a small mountainous watershed

(2) The uncertainty on discharge predictions is negligible in the calculation of confidence intervals for sediment loads

(3) Sediment, organic carbon and nitrogen inputs to the paddy area in Chieng Khoi watershed are driven by irrigation, rather than erosion from the surrounding upland fields

(4) The rice area in Chieng Khoi watershed is a net sink for coarse sediments

(5) Sediment-associated nutrients form a substantial contribution to the organic carbon and nitrogen balance of the rice fields in Chieng Khoi watershed

1.7 Outline of the thesis

This doctoral work is conceived as a cumulative thesis, where each chapter is a journal article. In Chapter 2, a method is developed to obtain continuous predictions of sediment, sediment-associated organic carbon and nitrogen concentrations in an irrigated watershed. Chapter 3 describes a bootstrap-based approach to assess sources of uncertainty on sediment load estimates. A case study follows, demonstrating the developed methods to obtain a sediment budget in a mountainous watershed in Northwest Vietnam: in Chapter 4, the sediment trap efficiency of a 13 hectare paddy area is determined, including a separation into particle size classes. The contribution of sediment-associated organic carbon and nitrogen in overland flow and irrigation

water to the indigenous nutrient supply of the same rice field area is quantified in Chapter 5, followed by a general discussion in Chapter 6.

Chapter 2 A turbidity-based method to continuously monitor sediment, carbon and nitrogen flows in mountainous watersheds[1]

J.I.F. Slaets[a], P. Schmitter[b], T. Hilger[a], M. Lamers[c], H.P. Piepho[d], T.D. Vien[e], G. Cadisch[a]

[a] Institute of Plant Production and Agroecology in the Tropics and Subtropics, University of Hohenheim, Stuttgart, Germany

[b] Singapore-Delft Water Alliance, Department of Civil and Environmental Engineering, National University of Singapore, Singapore

[c] Institute of Soil Science and Land Evaluation, Biogeophysics Section, University of Hohenheim, Stuttgart, Germany

[d] Institute of Crop Science, Bioinformatics Unit, University of Hohenheim, Stuttgart, Germany

[e] Center for Agricultural Research and Ecological Studies (CARES), Hanoi, Vietnam

2.1 Abstract

The aim of this study was to develop a method to continuously monitor sediment, carbon and nitrogen concentrations in streams using turbidity sensors. Field experiments were conducted in an irrigated and intensely cultivated watershed in Northwest Vietnam. Turbidity, discharge and rainfall were monitored during two successive rainy seasons from 2010 to 2011, and manual water samples were collected using a storm-based approach. Samples were analyzed for concentrations of suspended sediment (SSC), particulate organic carbon (POC) and particulate nitrogen (PN). A linear mixed model was developed to account for serial correlation,

[1] A version of this chapter is published as:
Slaets, J.I.F., Schmitter, P., Hilger, T., Lamers, M., Piepho, H.P., Vien, T.D. and Cadisch, G. (2014). A turbidity-based method to continuously monitor sediment, carbon and nitrogen flows in mountainous watersheds. Journal of Hydrology 513, 45-57.

with turbidity, discharge and rainfall as predictor variables. Turbidity was the most important predictor variable in all models. Five-fold cross-validation showed best model performance for POC with a Pearson's correlation coefficient of 0.91, while predictions for SSC and PN achieved a satisfying correlation of 0.86 and 0.87, respectively. Laboratory testing of the turbidity sensors showed that the turbidity signal is sensitive to differences in organic matter content, and has the smallest variance for fine textures, both of which are correlated to POC and thus supporting the higher predictive accuracy for this variable. The developed methodology is widely applicable and can be used to simultaneously obtain reliable, cost-effective and continuous estimates of SSC, POC and PN with a single sensor.

Keywords: turbidity, sediment, particulate organic carbon, particulate nitrogen, linear mixed model, serial correlation

2.2 Introduction

Techniques to monitor sediment transport in waterways provide essential data, not only on erosion processes at watershed scale (Gao, 2008), but also on eutrophication of freshwater bodies and coastal regions (Beusen *et al.*, 2005). Traditionally, automatic water samplers have been used to quantify suspended sediment concentrations (SSC), by sampling either at fixed time intervals or proportionally to stream flow. As the majority of the sediment is typically transported during uncommon storm events with extreme rainfall, regular but infrequent sampling can lead to an underestimation of sediment loads (Walling and Webb, 1981). And frequent sampling can be impractical – especially in remote areas – being time consuming and expensive. Therefore, efforts have been made to establish relationships between sediments and other variables, in order to obtain continuous data. Initially, the focus was on discharge (e.g. Duvert *et al.*, 2011; Porterfield, 1972; Williams, 1989). But many discharge-SSC relationships exhibit substantial scatter, due to the fact that SSC does not only vary with discharge, but also with upstream sediment availability (Gao, 2008). Typically, the variance for sediment rating curves also increases with the mean, violating the assumption of stable variance needed for simple linear regression. For this reason, Cox *et al.* (2008) suggested to use a generalized linear model with a gamma distribution for the errors. Moreover, in man-

made channels such as irrigation channels, changes in stream flow are not necessarily related to changes in sediment and associated nutrient concentrations, because irrigation management can cause changes in discharge that are not associated with an increase in Hortonian overland flow and corresponding sediment input (Schmitter *et al*., 2012).

As a solution to these limitations, turbidity has been explored extensively as an alternative to discharge as a proxy variable for SSC. Turbidity is a measure for the optical properties of a sample which cause light rays to be scattered and absorbed, rather than transmitted (Anderson, 2005) and has often been found to be proportional to the SSC in various environments: streams (e.g. Lewis and Eads, 2001; Minella *et al.*, 2008; Navratil *et al.*, 2011), regulated rivers (Gilvear and Petts, 1985), estuaries (Krause and Ohm, 1984), river deltas (Hung *et al.*, 2013) and irrigation and drainage systems (Gao *et al.*, 2008). It is generally considered the most reliable, easiest and cost-effective proxy (Lewis, 1996). Most authors have used simple linear regression (e.g. Brasington and Richards, 2000; Wass and Leeks, 1999), polynomial regression (Gao *et al.*, 2008; Lewis, 1996; Minella *et al.*, 2008; Riley, 1998) or multiple regression, combining turbidity and discharge (Ziegler *et al.*, 2011), to establish the relationship between turbidity and SSC.

The accuracy of the developed relationship between sediment concentrations and turbidity varied widely between reported studies. Regression resulted in an R^2 ranging from 0.55 (Riley, 1998) to 0.98 (Minella *et al.*, 2008). Similar values are reported for mountainous headwater catchments: Brasington and Richards (2000) reported results of a simple linear regression with an R^2 of 0.75 for SSC for a small watershed in the Himalaya, although the authors mentioned that due to the small sample size (n=31), the results should be interpreted with caution. Ziegler *et al.* (2011) found an R^2 of 0.96 for a simple linear SSC regression in a mountainous catchment in Thailand. Navratil *et al.* (2011) collected data in a mountainous headwater catchment of the Rhone (France), with badlands topography. They found it necessary to split the dataset in two. Using a quadratic regression on the one subset with 28 events achieved an R^2 of 0.97. The ten events in the remaining subset all showed different hysteresis effects in the SSC-turbidity relationship, requiring the development of individual relationships.

Regardless of their success in explaining the variability in SSC, these regression methods are based on linear models, and therefore they require constant variance and independent errors. The first condition is often problematic as the scatter in the data typically increases with increasing turbidity (Minella *et al.*, 2008; Riley, 1998). The second condition requires that there is no temporal correlation, which can be a problematic assumption for most hydrologic datasets, as they are normally time series (Helsel and Hirsch, 2002). Göransson *et al.* (2013) for example found a temporal autocorrelation for lags of approximately ten days for turbidity data of a large river in Sweden. But in practice, independence is often uncritically assumed. When these two conditions are not met, alternatives to simple linear or non-linear regression are required. This study aims to develop a method to reliably estimate SSC concentrations using turbidity in conditions, where simple regression does not provide satisfying predictions, where the errors are not constant but increasing with the mean, and where samples are taken so closely together in time that observations cannot be assumed to be independent.

Not only sediment concentrations require quantifying, but also nutrient concentrations are of interest: to study nutrient depletion through erosion from the uplands (Gao, 2008) but also to monitor stream quality and nutrient redistribution through irrigation (Gao *et al.*, 2008; Schmitter *et al.*, 2012) and nutrient export to and eutrophication of oceans (Beusen *et al.*, 2005; Seitzinger *et al.*, 2005). Southeast Asia in particular is considered a key region for C and N export (Beusen *et al.*, 2005; Ludwig *et al.*, 1996; Seitzinger *et al.*, 2005), having been especially subject to population increase and associated land cover changes (Valentin *et al.*, 2008; Ziegler *et al.*, 2009a).

Ideally, sediment and nutrient concentrations could be monitored with a single device. Turbidity sensors have already proven to be instrumental in monitoring total phosphorous (Grayson *et al.*, 1996; Istvanovics *et al.*, 2004; Jones *et al.*, 2011; Kronvang *et al.*, 1997; Rasmussen *et al.*, 2002; Ryberg., 2006; Stubblefield *et al.*, 2007), either directly via regression, or through establishing a relationship between SSC and turbidity, and total phosphorous and SSC. Particulate organic carbon (POC) and particulate nitrogen (PN) concentrations are traditionally either interpolated from discrete samples (Lu *et al.*, 2012), or calculated as a function of discharge and/or

other environmental predictors (Alvarez-Cobelas *et al.*, 2012), or as a function of the sediment flux (Ludwig *et al.*, 1996). The first method does not provide continuous data, and the results are strongly dependent on the sampling interval, with too few samples potentially leading to an underestimation of nutrient loads. The second strategy, establishing a relationship between Q and POC, suffers from the same difficulties as using Q as a proxy for SSC: an increase in discharge is not necessarily related to an increase in POC or PN concentrations, especially in irrigation channels where irrigation management also affects discharge. Additionally environmental predictors such as discharge and rainfall generally perform poorer for smaller catchments (Alvarez-Cobelas *et al.*, 2012). Finally establishing a relationship between SSC and POC is also not necessarily straightforward, as POC content of the sediment often decreases with increasing SSC (Lu *et al.*, 2012; Ludwig *et al.*, 1996). Turbidity sensors could provide an alternative. Némery *et al.* (2013) have successfully used turbidity indirectly to predict POC, by establishing a relationship between turbidity and SSC, and SSC and POC. Additionally, several authors discussed the effect of particle size on turbidity (Foster *et al.*, 1992; Lewis, 1996; Pfannkuche and Schmidt, 2003; Teixeira and Caliari, 2005, Thollet *et al.*, 2013; Wass and Leeks, 1999), showing that for the same SSC, a coarse fraction will result in a lower turbidity than a fine fraction. Foster *et al.* (1992) reported that at high concentrations of dissolved organic matter, turbidity is often a poor predictor for the mineral fraction. All this suggests that turbidity signals are sensitive to particle size and organic matter content, both related to nutrient content, and therefore turbidity sensors could potentially provide a continuous estimate of sediment-associated nutrient content – in particular of POC and PN. However, a direct relationship between turbidity and particulate nutrient content is to date missing.

The specific aims of this paper were (i) to investigate the factors influencing the turbidity signal in laboratory conditions, in particular the influence of organic matter, thereby testing the theoretical feasibility of using turbidity as a direct proxy for sediment POC and PN content, (ii) to develop a statistical model that accurately predicts the suspended sediment concentration when regression is not appropriate, and (iii) to assess the possibility of using turbidity as a direct predictor for POC and PN in field conditions.

2.3 Material and Methods

2.3.1 Exploratory laboratory test: effect of texture and organic matter on turbidity signal

Prior to deployment in the field, the turbidity sensors (ANALITE NEP395, McVan, Australia) were tank tested. The measuring range of the sensors is 0 to 3500 NTU. The aim was to enhance the understanding of the sensor's response to different qualities of sediment material in terms of particle size composition and organic matter content: if the turbidity sensor would be able to detect differences in organic matter content for the same SSC and particle size, that would indicate that turbidity is a potential predictor variable for POC.

Therefore three soils with contrasting dominant textures (a sandy podzol, a loamy luvisol and a clayey gleysol) were selected from a reference library at the Soil Science Institute of the University of Hohenheim. The particle size distribution was determined by laser diffraction and the organic matter content by loss on ignition. The soils were mixed with water at different concentrations, and the resulting turbidity signals were assessed. For each dominant texture, two different organic matter (OM) levels (Table 2.1) were evaluated. The effect of sediment texture on the turbidity response has been well established (Foster *et al.*, 1992; Thollet *et al.*, 2013). It was hypothesized that organic matter can alter reflectance properties, and therefore can cause a change in turbidity signal, due to particle aggregation or coating effects, both affecting reflectance behavior. Hence the following treatments were applied: (i) no treatment, (ii) free organic matter removal, (iii) free organic matter removal and aggregate disruption, and (iv) free organic matter removal, aggregate disruption and soil organic matter removal. First, the free organic matter was removed using a density fractionation with water, by swirling 10 g of soil in 200 ml of water. Second, the aggregates were disrupted by sonication at 22 kJ following Amelung and Zech (1999). Finally, hydrogen peroxide was used to remove soil OM (van Reeuwijk, 2002) by adding 7.5 ml of H_2O_2 (30%) to 10 g of soil.

Table 2.1: Textural properties and organic matter content of tested sediments in the laboratory experiment. Soils with three different dominant grain sizes were selected from a reference library, and for each of those, two different organic matter contents were chosen.

	Sand (%)	Silt (%)	Clay (%)	Organic matter (%)
Sandy - High OM	92	8	0	6.71
Sandy - Low OM	95	5	0	0.84
Loamy - High OM	7	64	30	4.65
Loamy - Low OM	5	62	34	1.90
Clayey - High OM	6	39	55	3.30
Clayey - Low OM	3	55	55	1.00

To minimize external influences, the sensor was positioned in a large black plastic tub filled with four liters of water. For each treatment, combinations of texture and organic matter were measured in completely randomized order. For each treatment and soil type (Table 2.1), first a zero concentration control was measured. Then soil was added to the water under continuous stirring and turbidity values were logged every second for two minutes and averaged for further analysis. This was done each time at four equal increments of the concentration that saturated the sensor, covering the measuring range of the turbidity sensor. As there was not enough soil material available to measure the concentrations in randomized order, the concentrations were measured consecutively for each combination of treatment, texture and organic matter content. Therefore all observations measured for one treatment, texture and organic matter content were considered as repeated measures and an autoregressive structure was specified for the residual variance covariance matrix with PROC MIXED in the statistical software package SAS (version 9.3). First the effect of texture was confirmed, by performing linear regression with turbidity as response variable, concentration (as the only quantitative predictor) and texture, organic matter content and their interactions with concentration as predictive variables. Secondly, to assess the effect of organic matter, for each treatment, linear regression was performed with the same autoregressive structure, with turbidity as response, concentration, the interaction of concentration and texture, and the three-way interaction between concentration, texture and organic matter as predictors. In all of the models, the intercept was not significant, confirming there was no overall time effect and therefore all regressions were forced through the origin.

2.3.2 Study site

This study was performed under the umbrella of the Collaborative Research Center "The Uplands Program", a DFG-funded international research project on sustainable land use and the improvement of livelihoods of rural populations in mountainous regions. Data collection was conducted for two consecutive years (2010 - 2011) in Chieng Khoi commune (350 m a.s.l), Yen Chau district, Northwest Vietnam. The area is located in the tropical monsoon belt, with a rainy season beginning in April and ending in October. Average annual precipitation is around 1200 mm and average annual temperature 21°C. The soils are dominantly alisols and luvisols, and topsoil organic matter content ranges from 0.7 to 2.4% (Clemens *et al.*, 2010). Dominant crops in the area are maize (*Zea mays L.*) and cassava (*Manihot esculenta* Crantz) on the hills, and irrigated paddy rice (*Oryza sativa L.*) in the valleys. This study focused on a subwatershed of 2 km^2 downstream of a man-made reservoir, created by damming up a river that collected overland flow from the steep mountainous area upstream of the reservoir. The reservoir feeds irrigation channels, providing water for two rice crops per year in the paddy rice area (Figure 2.1). The rice fields that are irrigated by the channels drain into a river which is additionally fed by a spillover that drains the excess water when the maximum storage volume is reached (i.e. around July-August).

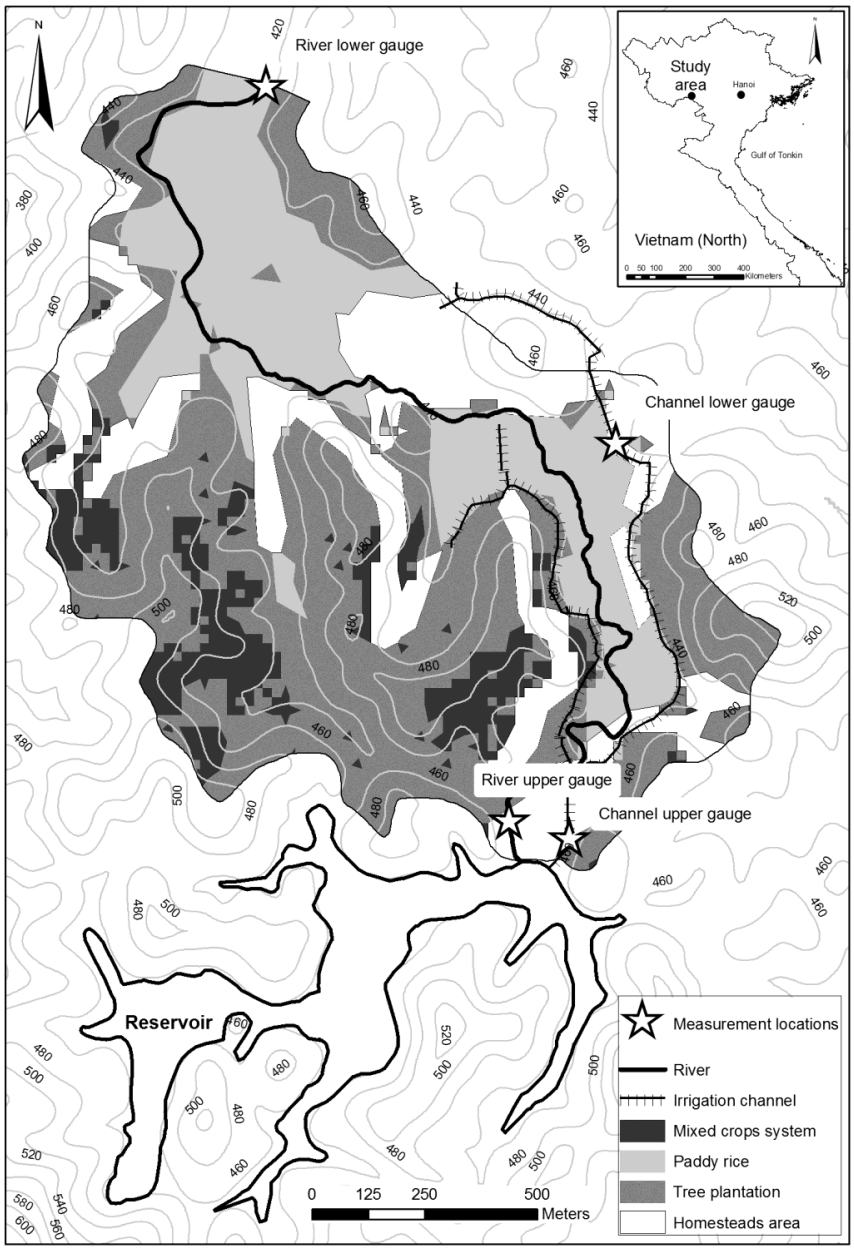

Figure 2.1: Overview of the study area, the main occurring land uses and the selected upstream and downstream measurement locations at the irrigation channel and river within Chieng Khoi watershed (Son La province). The outlet of the watershed is at the River Lower Gauge measurement station. Mixed crop systems consist of maize, cassava and maize-cassava intercropping. Mixed tree systems consist of orchards and teak plantations.

2.3.3 Field monitoring

In order to test if a reliable prediction of SSC, POC and PN could be established for a small mountainous catchment, four turbidity sensors were installed in Chieng Khoi watershed: the sensors were placed both upstream and downstream in one of the irrigation channels and the river (Figure 2.1). The irrigation water originates from the reservoir. During rainfall events, overland flow from the surrounding upland fields and homesteads are additional sediment sources contributing to the overall sediment concentration irrigated to paddy fields. The chosen locations enabled the quantification of carbon and nitrogen flows through irrigation and erosion and their ramifications for long term paddy sustainability: the upstream and downstream channel positions allowed separating the nutrient concentrations in the overland flow from irrigation water, while the upstream and downstream river positions enabled quantifying the sediment, carbon and nitrogen concentrations draining from the paddy rice. The lab tested turbidity sensors measure in the near-infrared spectrum and are equipped with a self-cleaning wiper. The sensors were checked for fouling every two weeks, but fouling was very rare, especially in the rainy season when discharge was high. Sensors were installed vertically (optical eye down) at the center of the channel/river, suspended in a perforated PVC pipe that floated in the center point of flow of the water column as rising water level caused the pipe to be pushed upwards. Turbidity was recorded every two minutes by a data logger (CR200, Campbell Scientific, USA), except for the downstream irrigation channel location where the turbidity during rainfall changed rapidly so that data needed to be recorded every minute. Pressure sensors (Ecotech, Germany) were used to measure the water level at the river and channel locations at a five and two minute interval, respectively. The pressure heads were converted to flow rates by means of stage-discharge relationships, established using the velocity-area method (river) and salt dilution method (irrigation channel) (Herschy, 1995). Rainfall was homogeneous over the watershed and was registered by an automatic rain gauge associated with a weather station (Campbell Scientific, USA) installed within the vicinity of the upper monitoring locations (Lamers *et al.*, 2011). Rainfall events were separated on the condition that no precipitation occurred for thirty minutes due to the short lag time observed in the catchment (Schmitter *et al*., 2012).

In order to establish a relationship between the turbidity data, sediment, carbon and nitrogen content, water samples were taken at the four sensor locations in 2010 and 2011. Flow proportional sampling with autosamplers is challenging in irrigation channels, as discharge not only increases during storm events but also is subject to irrigation management. For this purpose, manual sampling was performed. Sampling was conducted with a higher sampling frequency at the downstream channel and river locations as higher variability was expected due to the influx of sediment-loaded overland flow during rainfall events. Each sampling consisted of two 0.5 liter samples, taken simultaneously. The samples were taken opposite to the flow direction in order to minimize suspended particle disturbance. Base flow samples at each monitoring location were collected once a month. Storm-based water sampling was performed covering the rising limb, peak and falling limb of the event hydrograph. This was done to catch the full range of discharge, sediment, carbon and nitrogen concentrations. The sampling interval depended on the intensity of the rain and the responsiveness of the location. Typically ten to twenty samples were taken per rainfall event, and the minimal sampling interval when the sediment content of the water was seen to increase most rapidly, was two minutes. An example of a sampled event can be found in Figure 2.2. Samples were refrigerated on site and transported to the lab immediately after the event, where they were frozen until analysis. The total number of events sampled was 30 in 2010 and 50 in 2011, resulting in 867 storm flow grab samples. Additionally, 376 base flow samples were collected.

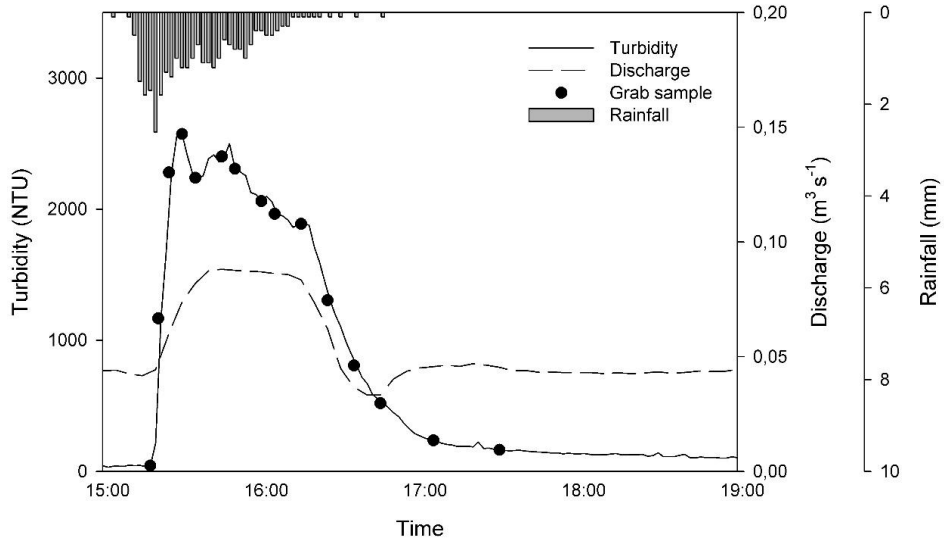

Figure 2.2: Storm based water sampling during the event of the 4th of August 2010 at the downstream channel position, showing rainfall, discharge, turbidity and grab sampling points.

2.3.4 Water sample analysis

As this dataset contained water samples with very high sediment concentrations, and filtering is not recommended for those samples (ASTM, 2013), sediment quantity was determined gravimetrically on one sample of 500 ml by letting it settle overnight in refrigerated conditions (<4 °C), prior to siphoning off the supernatants and drying the remaining sediment at 35°C. Total nitrogen (N) and total organic carbon (OC) were determined by combustion method using a LiquiTOC II (Elementar, Germany) on both the water sample containing sediment and the supernatants containing no sediment – the latter giving the dissolved concentrations (DN and DOC, respectively). Samples were homogenized before analysis as the LiquiTOC was equipped with an automatic sample feeder with stirring function. Three analytical replicates per sample were processed and averaged for further analysis.

Particulate concentrations for each element (PN and POC, respectively) were calculated as the difference between the measured concentration in the sample containing the sediments, and the dissolved concentrations and thus correspond to the mineral or sediment-associated OC and N. Directly determining the particulate concentrations in the sediment was deemed not feasible, due to the low POC and PN

concentrations (respectively <0.5% and <0.1% for half of the samples) and the small amounts of sediment available to do the analyses (<40mg for 10% of the samples). The LiquiTOC has a detection sensitivity of 0.05 mg l^{-1}. In samples where the dissolved and/or total OC and N concentrations were very close to this limit, the method to calculate the particulate fractions yielded negative results (124 out of 1144 for POC, 430 out of 1143 for PN). Whenever this was the case, the particulate concentration was considered as missing data. Significance of the selected parameters was not altered when values under detection limit were removed.

2.3.5 Model selection

2.3.5.1 Linear mixed model

Simple linear regression was performed with SSC, POC and PN as response variables and turbidity as the only predictor variable. The residual plots displayed heterogeneity of variance. Therefore, a Box-Cox transformation was applied on the response variables using the macro described by Piepho (2009). As the grab samples during storm events were taken closely together, in some cases as little as two minutes apart, this made it unlikely that the observations have independent errors. To account for this serial correlation, the use of a linear mixed model was explored. The model was developed using the MIXED procedure in SAS 9.3. All observations at the same location were considered as repeated measures, by using the repeated statement with the sampling location as the subject. The structure of the residual variance-covariance matrix was specified as a spatial power structure with time as the coordinate. This was done by converting the time the sample was taken into seconds, with the first sample of the entire dataset as point zero. This allowed for a correlation that decays exponentially in time, between samples taken at the same location.

To validate the models, five-fold cross validation was carried out, followed by a calculation of Pearson's correlation coefficient (r) between the observed and predicted values. In five-fold cross validation, the dataset is split into five folds, four folds forming the calibration dataset and the fifth fold the validation set. This process is repeated five times, so that each observation is in the validation set exactly once. As SAS does not have a procedure that performs cross validation with mixed models,

a macro was developed for this purpose (available online at https://www.uni-hohenheim.de/bioinformatik/beratung/index.htm).

2.3.5.2 Input variable selection

In order to further improve model fit, the use of multiple predictor variables was explored. Eight variables were considered as candidates for the fixed effects: 30 minute average rainfall (Pav), maximum rainfall (Pmax), cumulative rainfall since the start of the event (Pcum), time elapsed since the start of the event (Pdur), duration of the dry period before the event (tdry), total rainfall during the previous event (Pprev), discharge at time of sampling (Q) and turbidity at time of sampling (Turb). Forward selection was carried out using the Akaike Information Criterion (AIC, Akaike, 1974) as the selection criterion. Models were fitted using Maximum Likelihood estimation to allow comparison through AIC. A drop in AIC smaller than five points was considered not enough of an improvement to add an additional variable.

As there were not enough observations to fit a location specific model (i.e. four sensor locations), all observations were combined and one overall model was fitted, with a fixed effect for the measurement location. In this way, the selected predictor variables were the same for all locations, but the coefficients could be location-specific. Predictor variables of the selected models were standardized using the STANDARD procedure to allow direct comparison of the regression coefficients.

In order to get an idea of the minimal number of water samples that would be required to obtain models with the same predictive power as the full dataset, the effect of sample size on Pearson's r was assessed. This was done by repeatedly taking random subsamples of incrementing sample size from the full dataset with PROC SURVEYSELECT. Eight subsamples were taken for 100 to 800 samples, with increments of 100, and then the selected statistical models were fitted to the subsets and five-fold cross validation was carried out. For PN there were more missing observations due to the overall lower concentrations of nitrogen in the samples, under the detection limit of the TOC analyzer, hence the maximum subsample size for this variable was 600. For the smallest subsamples (n=100), there were not enough observations to fit the full model with the temporal correlation.

Therefore the variance components - obtained from the full model - were fixed for all subsamples.

2.4 Results

2.4.1 Effect of organic matter and texture on turbidity signal

In the laboratory experiment, differences in the texture of sediment led to different turbidity signals for equal concentrations (Figure 2.3), as is shown by the significant interaction term between concentration and texture in the linear model with turbidity as response ($P < 0.01$). The same concentrations resulted in a lower turbidity signal with a higher variance for sandy sediments (not shown) compared to loamy sediments. Furthermore, the SSC-turbidity relationship was affected by the organic matter content of the sediment: suspended sediments with the same texture, but different organic matter content had a significantly different turbidity response for the same suspended sediment concentration ($P < 0.01$ for both clayey and loamy sediment) (Figure 2.3). For sand however there was no significant difference due to organic matter ($P=0.19$). Therefore the subsequent treatments were tested only on the clayey and loamy sediment.

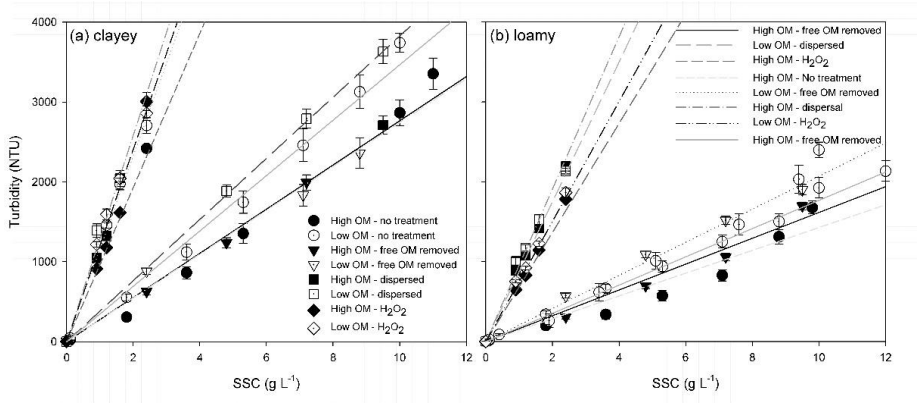

Figure 2.3: Changes in turbidity signal caused by organic matter, removal of free organic matter, dispersal of aggregates and destruction of organic matter by hydrogen peroxide at different concentrations, for a predominantly clayey sediment (a) and loamy sediment (b).

After removal of free organic matter by density-separation, the effect of organic matter remained significant ($P<0.01$) as without treatment. Dispersal of aggregates, however, caused the regression lines of the sediments with high and low organic

matter to fall together corresponding to a higher turbidity for the same concentration after dispersal, the effect of organic matter being no longer significant (P=0.09). Subsequent treatment with hydrogen peroxide to completely destroy organic matter resulted in a slight decrease in turbidity for the same concentration again. However the change was much smaller than the change caused by the dispersal alone.

2.4.2 Spatial and temporal variation of hydrological and water quality characteristics

In the field experiment, the suspended sediment concentration of the samples ranged from 0.003 to 34 g l^{-1}, with an average of 2.3 g l^{-1} (Table 2.2). Particulate organic carbon and nitrogen values were between 0.05 and 272 mg C l^{-1}, and 0.05 and 53 mg N l^{-1} respectively. Turbidity values covered the whole spectrum of the sensor, going from 8 to 3500 NTU, discharge varied between 0.05 and 7.61 m^3 s^{-1} for the river with an average of 0.65 m^3 s^{-1}, and between 0 and 0.26 m^3 s^{-1} for the channel with an average of 0.06 m^3 s^{-1}. Average rainfall intensity during the sampled events was 5 mm hr^{-1}. Cumulative average rainfall amounted to 10 mm for all sampled events. The largest event sampled consisted of 182 mm rainfall in 194 minutes. Duration of the rainfall ranged from 10 to 332 minutes with an average of 89 minutes. Duration of the dry period before the sampled event was between 32 minutes and 18 days. For SSC, POC and PN, the standard deviation was larger than the mean, indicating skewness of the data, confirmed by the histograms of these variables, as there were more observations for the low ranges.

Table 2.2: Descriptive statistics for storm flow and base flow samples for the following variables: sampled event rainfall (Pav), discharge (Q), turbidity (Turb), suspended sediment concentration (SSC), particulate organic carbon (POC) and particulate N (PN). The total number of events sampled was 30 in 2010 and 50 in 2011, resulting in 867 storm flow grab samples. Additionally 376 base flow samples were collected. (Pos=Position, U=Upper gauge, L=Lower gauge, NA=Not Applicable).

			Storm flow					Base flow				
Variable	**Stream**	**Pos**	**Med**	**Mean**	**Min**	**Max**	**n**	**Med**	**Mean**	**Min**	**Max**	**n**
Pav	River	U	0.1	0.4	0.0	6.0	102	NA	NA	NA	NA	NA
(mm 30min^{-1})		L	0.1	2.8	0.0	40.9	147	NA	NA	NA	NA	NA
	Channel	U	0.1	2.8	0.0	80.1	105	NA	NA	NA	NA	NA
		L	0.6	5.4	0.0	82.9	331	NA	NA	NA	NA	NA
Q	River	U	0.42	0.50	0.20	0.88	102	0.67	0.54	0.20	0.75	9
(m^3 s^{-1})		L	0.52	0.86	0.05	7.61	147	0.55	0.56	0.05	2.05	139
	Channel	U	0.10	0.11	0.00	0.26	105	0.09	0.10	0.06	0.18	35
		L	0.05	0.06	0.02	0.09	331	0.04	0.04	0.02	0.06	129
Turb	River	U	47	194	11	1859	102	190	187	11	444	9
(NTU)		L	77	143	8	912	147	46	150	10	1943	139
	Channel	U	51	364	17	3253	105	535	804	32	2152	35
		L	807	1260	15	3575	331	455	782	10	3561	129
SSC	River	U	0.331	1.046	0.003	22.075	102	1.603	1.561	0.004	3.041	9
(g l^{-1})		L	0.485	1.530	0.010	10.102	147	0.337	0.680	0.013	4.129	139
	Channel	U	0.232	0.360	0.003	3.865	105	0.288	0.406	0.006	1.719	35
		L	2.618	4.813	0.052	34.468	331	0.633	1.884	0.019	11.714	129
POC	River	U	3.17	5.33	0.13	60.00	102	1.27	2.69	0.61	7.26	9
(mg l^{-1})		L	2.93	11.33	0.09	131.15	147	1.44	3.04	0.05	17.11	139
	Channel	U	1.38	7.32	0.05	180.05	105	0.81	1.32	0.05	3.26	35
		L	9.54	39.75	0.05	272.44	331	3.73	12.26	0.05	207.98	129
PN	River	U	1.25	2.10	0.05	16.00	102	1.69	1.69	0.48	2.90	9
(mg l^{-1})		L	0.51	3.70	0.05	35.50	147	0.61	0.93	0.05	4.31	139
	Channel	U	0.88	1.70	0.05	20.60	105	2.67	2.67	2.67	2.67	35
		L	3.04	8.44	0.05	53.01	331	0.75	2.85	0.05	31.41	129

2.4.3 A linear mixed model to predict SSC, POC and PN

A simple linear regression model with turbidity as the only quantitative predictor variable, using the untransformed data, explained approximately half of the variability in the data for SSC, POC and PN (R^2 of 0.49, 0.61 and 0.51, respectively, first model in Table 2.3). The residuals of the simple linear regression model showed heterogeneity of variance for all response variables. Applying a Box-Cox transformation (with transformation parameter γ=0.3) to the linear regression model with turbidity as the only quantitative predictor variable, resulted in an R^2 of 0.55 but more importantly, stabilized the variance (second model in Table 2.3). In order to improve the predictions of these variables, a linear mixed model was developed. Accounting for serial correlation improved model fit, lowering the AIC and increasing Pearson's correlation coefficient[2] for all three response variables (third model in Table 2.3). When selecting multiple predictor variables, forward selection resulted in the same selection of turbidity, discharge and cumulative rainfall for all three variables SSC, POC and PN. Only for POC, adding rainfall duration as a fourth variable continued to lower AIC. When comparing mixed models containing multiple predictor variables (fourth, fifth and seventh model in Table 2.3) to the mixed model with turbidity alone (second model in Table 2.3), the model fit improved, but only in terms of AIC, and the effect was small compared to the effect of the data transformation and the serial correlation. Pearson's r resulting from the cross validation did not improve for any of the response variables after adding more predictor variables to the mixed model.

[2] As R^2 cannot be used as a measure of performance for mixed effects models, AIC and Pearson's correlation coefficient from the five-fold cross validation are given in Table 2.3 for the simple regression to allow for comparison between all models.

Table 2.3: Model fit shown by AIC and Pearson's correlation coefficient (r) for Suspended Sediment Concentration (SSC), Particulate Organic Carbon (POC) and Particulate Nitrogen (PN) for the tested models, starting from simple linear regression with turbidity (no transformation applied or autocorrelation fitted) and stepwise showing the effect of adding a data transformation, accounting for serial correlation, and adding predictor variables (n= 756 for SSC, 730 for POC and 478 for PN).

				AIC	r	AIC	r	AIC	r
Predictors	**Transform.**	**Serial corr.**	**Model**	**SSC**		**POC**		**PN**	
Turb	None	No	Simple Linear Regression	14235	0.69	6929	0.77	3119	0.69
Turb	Box Cox	No	Simple Linear Regression	3659	0.72	1374	0.79	569	0.78
Turb	Box Cox	Yes	Linear Mixed	3470	0.86	1129	0.91	386	0.89
Turb, Q	Box Cox	Yes	Linear Mixed	3418	0.87	1043	0.91	318	0.87
Turb, Q, Pcum	Box Cox	Yes	Linear Mixed	3406	0.86	1026	0.91	NA	NA
Turb, Q, Pcum	Box Cox	No	Multiple Linear Regression	3569	0.78	1209	0.87	NA	NA
Turb, Q, Pcum, Pdur	Box Cox	Yes	Linear Mixed	NA	NA	1019	0.91	NA	NA

Turb=Turbidity (NTU), Q=Discharge (m s^{-1}), Pcum= Cumulative rainfall (mm), Pdur=Time elapsed since start of the event (min), NA=Not Applicable.

When not fitting an effect for the temporal correlation, Pearson's r did improve by adding variables (sixth model in Table 2.3): for SSC, Pearson's r increased from 0.72 for simple regression (with turbidity alone) to 0.78 for multiple regression (with turbidity, discharge and cumulative rainfall). The fit never became as good as for the mixed model (Pearson's r=0.86). Thus, the effect for the temporal correlation is at least partially taken over by the other variables in the multiple regression, which is expected as those variables are all changing in time. Furthermore, the estimates of the variance components showed that the autocorrelation becomes nearly zero for samples taken more than 80 minutes apart (Figure 2.4) – which coincides with the average duration of the sampled events. Regardless of which candidate model was selected, POC predictions were most accurate, while PN and SSC predictions showed a similar, slightly lower accuracy.

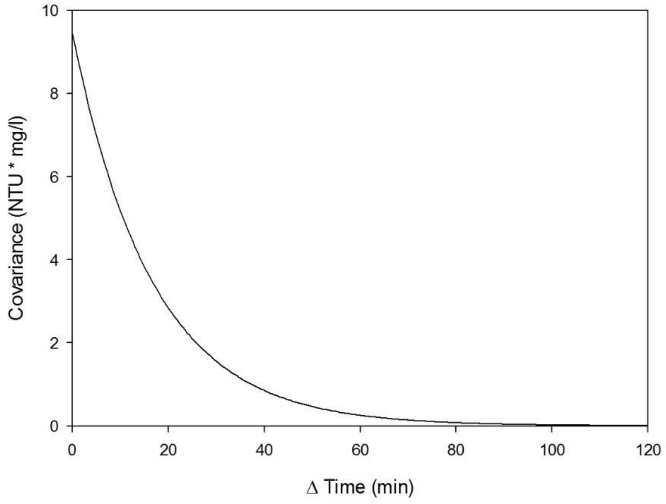

Figure 2.4: Change of the modeled covariance in time for the SSC – turbidity mixed model (model 3 in Table 2.3), showing that the autocorrelation approaches zero when samples are taken further than 80 minutes apart.

Plots of observed versus predicted data resulting from the cross-validation for the full mixed models with multiple predictor variables can be seen in Figure 2.5, showing that the fit was satisfying for each of the four sites. The models were used to estimate sediment and nutrient flows during the sampled rainfall event shown in Figure 2.2 at the channel downstream location. Resulting predictions for SSC, POC and PN can be

seen in Figure 2.6. Pearson's r for this event was 0.81 for SSC, 0.93 for POC and 0.93 for PN. Normalized Root-Mean-Square Error (obtained by dividing RMSE by the mean observed SSC, POC and PN value respectively) amounted to 0.21 for SSC, 0.23 for POC and 0.19 for PN.

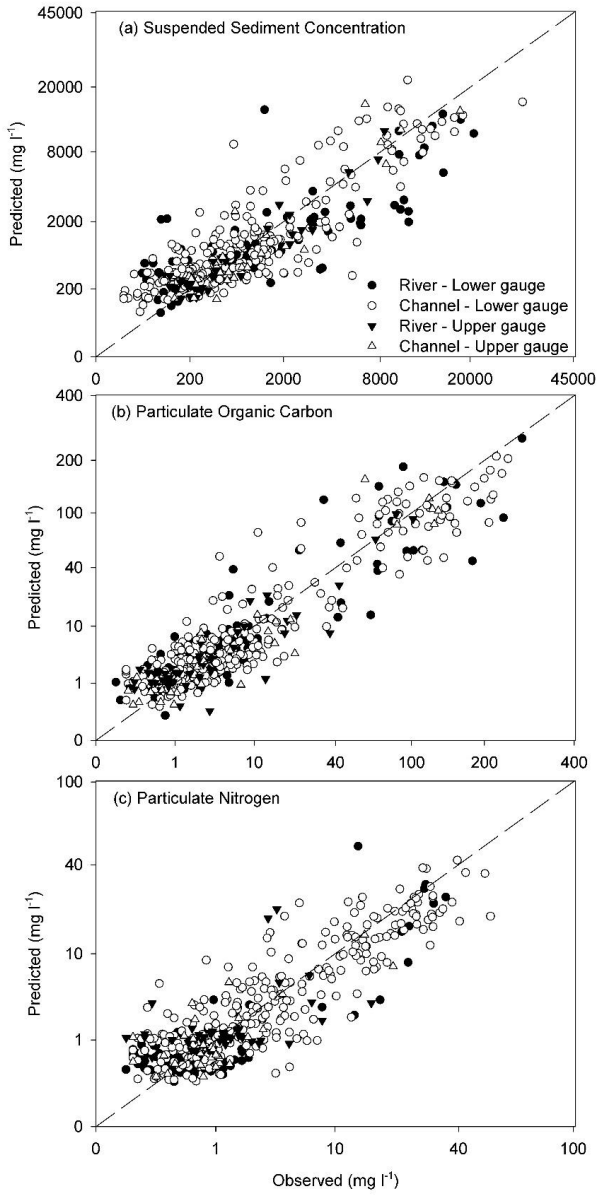

Figure 2.5: Predicted versus observed values resulting from five-fold cross validation of best performing linear mixed models for: (a)suspended sediment concentration, (b) particulate organic carbon and (c) particulate nitrogen according to Table 2.4, after Box Cox transformation (γ=0.3). Plots are shown on the Box Cox transformed scale.

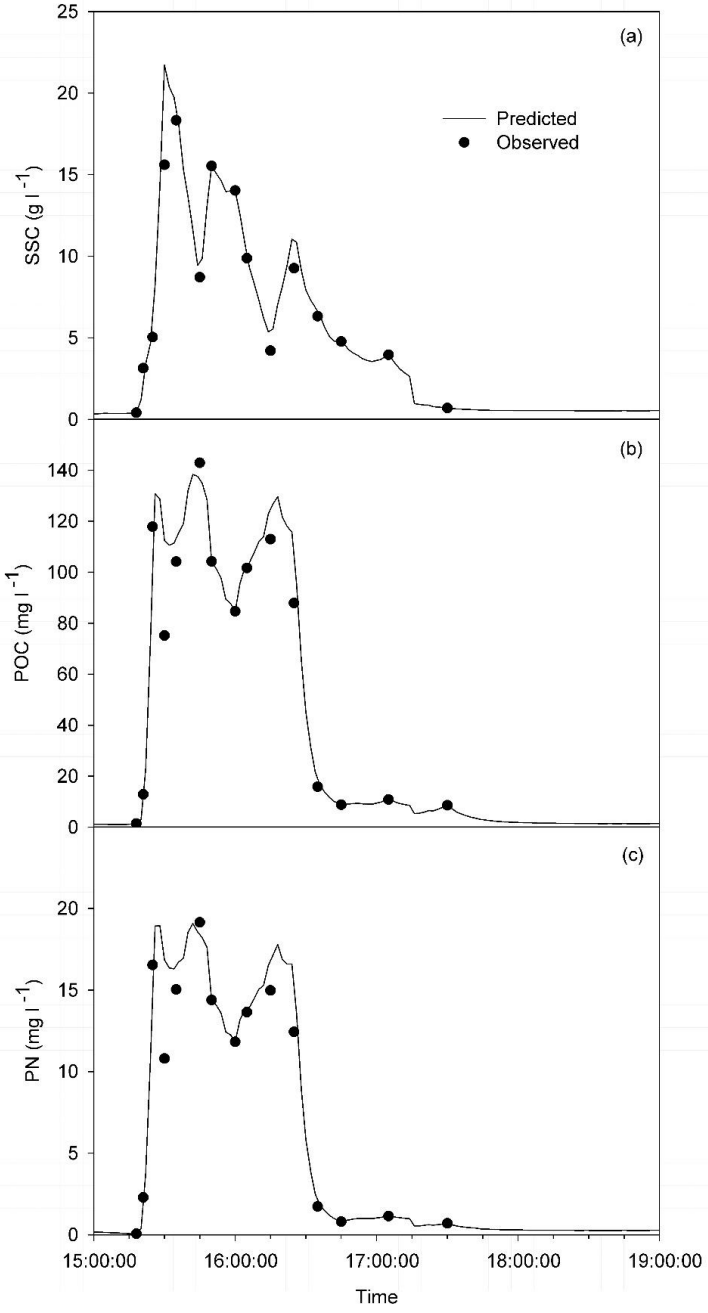

Figure 2.6: Observed and predicted suspended sediment concentration (SSC) (a), particulate organic carbon (POC) (b) and particulate nitrogen (PN) (c) at the downstream channel station corresponding to the event shown in Figure 2.2.

As was indicated by the forward selection, standardized parameter estimates of the multiple regression models show that turbidity is the most important predictor variable for all three responses and for all locations (Table 2.4). The only exception is the channel's lower gauge position, where discharge had the highest coefficient estimate, making turbidity the second most important predictor variable. Turbidity did not show site-specific effects for PN, as the parameter estimates were not significantly different between the locations. Discharge only had a significant effect for the downstream positions, both for the river and the channel, and was not significant for the upstream positions. Cumulative rainfall had a significant effect on the channel's lower gauge for SSC, and on both channel gauges for POC, although the effect was small compared to that of discharge and turbidity. Only for the downstream position in the channel did rainfall duration significantly contribute towards the prediction for POC.

Table 2.4: Standardized regression coefficients ± standard errors for fixed effects of selected linear mixed model for Suspended Sediment Concentration (SSC), Particulate Organic Carbon (POC) and Particulate Nitrogen (PN) for each of the four measurement locations: the upper and lower gauge of the river and the irrigation channel. * and ** indicate that the coefficient is significant at the level α=0.05 and α=0.01, respectively. (Turb=Turbidity (NTU), Q=Discharge (m s^{-1}), Pcum= Cumulative rainfall (mm), Pdur=Time elapsed since start of the event (min), NA=Not Applicable)

	Intercept	Turb	Q	Pcum	Pdur
			SSC		
River Upper	8.09 ± 0.70 **	3.14 ± 0.91 **	-1.12 ± 1.25	0.04 ± 0.14	NA
River Lower	7.94 ± 0.46 **	3.38 ± 0.74 **	0.71 ± 0.17 **	0.21 ± 0.38	NA
Channel Upper	5.46 ± 1.73 **	2.02 ± 0.59 **	-0.49 ± 4.71	0.78 ± 0.49	NA
Channel Lower	25.33 ± 3.78 **	1.51 ± 0.17 **	39.13 ± 8.89 **	1.48 ± 0.35 **	NA
			POC		
River Upper	1.82 ± 0.21 **	0.58 ± 0.25 *	-0.42 ± 0.39	0.03 ± 0.04	-0.06 ± 0.08
River Lower	1.75 ± 0.15 **	0.84 ± 0.22 **	0.18 ± 0.04 **	0.16 ± 0.11	0.08 ± 0.04
Channel Upper	1.23 ± 0.39 **	0.73 ± 0.15 **	-0.21 ± 1.30	0.38 ± 0.12 **	0.02 ± 0.10
Channel Lower	6.09 ± 0.68 **	0.68 ± 0.03 **	11.4 ± 1.79 **	0.39 ± 0.10 **	-0.19 ± 0.06 **
			PN		
River Upper	1.39 ± 0.17 **	0.50 ± 0.18 **	-0.25 ± 0.36	NA	NA
River Lower	1.02 ± 0.10 **	0.39 ± 0.16 *	0.13 ± 0.03 **	NA	NA
Channel Upper	0.63 ± 0.52	0.42 ± 0.17 **	-0.80 ± 1.54	NA	NA
Channel Lower	3.50 ± 0.52 **	0.44 ± 0.03 **	6.43 ± 1.38 **	NA	NA

Plots of sample size versus Pearson's correlation coefficient showed that a smaller sample size is needed to establish the prediction models for POC and PN compared to the SSC model (Figure 2.7). For SSC, the improvement in model fit leveled off at around 300 - 400 samples, while in the case of POC and PN, a sample size of about 200 sufficed to achieve a model fit approximating that of the full dataset.

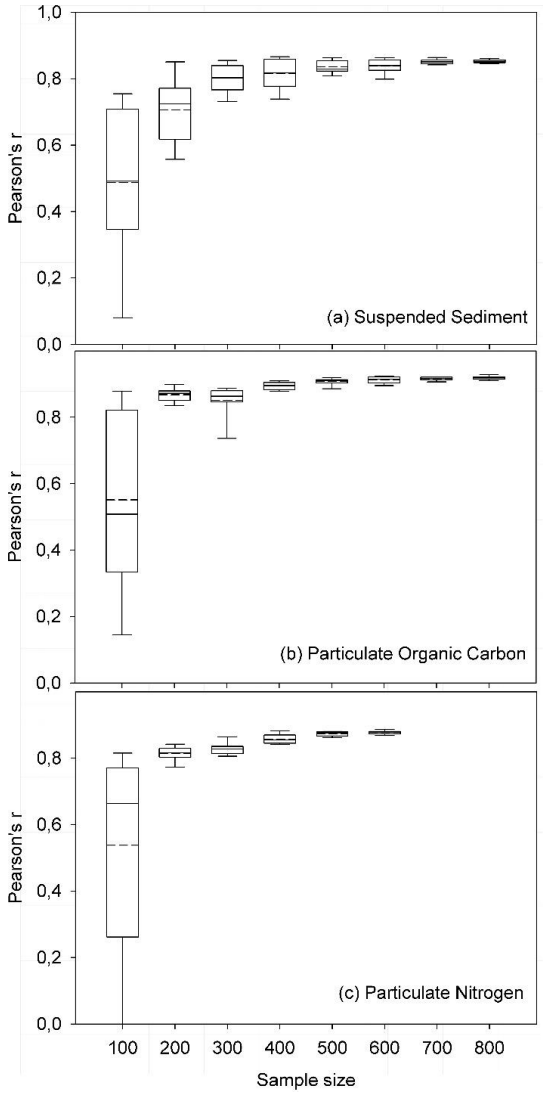

Figure 2.7: Effect of sample size on Pearson's correlation coefficient resulting from the five-fold cross validation for suspended sediment concentration, particulate organic carbon and particulate nitrogen. Ten subsamples were taken for each sample size. Full line indicates median, dashed line shows mean.

2.5 Discussion

2.5.1 Linear mixed model more adequate than regression

The use of a linear mixed model, taking into account temporal correlation, significantly improved the predictions for SSC compared to single and multiple linear regression functions without serial correlation. While classic simple linear regression with turbidity underperformed for the presented dataset explaining slightly less than half of the variability in the data (first model in Table 2.3), the linear mixed model with turbidity resulted in a model fit with a cross-validation Pearson's r of 0.86, or 74 % of explained variability (third model in Table 2.3). Care must be taken when comparing results of cross-validation with a coefficient of determination resulting from linear regression, as the former is a stronger measure of accuracy. But keeping this in mind, the linear mixed model performed equally well as or better than results from other mountainous catchments reported in the literature: For example, Brasington and Richards (2000) found an R^2 of 0.75 for a small Himalayan watershed. Ziegler *et al.* (2011) report an R^2 of 0.96 for a simple linear SSC regression in a mountainous catchment in Thailand, but SSC concentrations were significantly lower than the concentrations found in this study. In spite of the high SSC maxima in our study due to the high rainfall, erodible soils and poor soil cover during maize establishment in the area, the mixed model performed well in the high ranges, which is crucial to accurately predict loads and which is typically where a classic regression on SSC-turbidity exhibits the largest variance (Gippel, 1995).

The linear mixed model is also able to account for SSCs that are over the detection limit of the sensor. The maximum SSC measured in the sample set is well over the saturation limit (which is, as the lab tests show, around 12 g l^{-1} for clay and around 18 g l^{-1} for silt) and the limit was surpassed for about 5% of the dataset. While this would be a problem in a conventional linear regression, the fitted random effect for temporal correlation implies that the predictions are not solely based on the turbidity: concentrations surrounded in time by other observations with high turbidity will have a higher probability of a high SSC as well, so the saturation effect doesn't limit the model predictions in the same way as simple linear regression would.

A further advantage of the described method is that by adding a fixed effect for location, it allows to have just one model for all locations, with site-specific coefficients. This approach makes it possible to have a smaller number of samples compared to developing a separate model for each site. Further research could show if this approach remains possible in catchments that are larger, have more heterogeneous sediment sources or strongly mixed land uses. Repeatedly sub-sampling the dataset demonstrated how the sample size affects the accuracy of the predictions. For catchments with similarly high ranges of SSC, a sample size of 400 should suffice to obtain good predictions for all three variables, provided that the samples cover the full range of the variables. As the model fits all four measurement locations simultaneously, this number corresponds to a setup with four sites - and therefore translates into 100 samples per measurement station as an optimal amount, as larger sample size would no longer result in an increase in predictive power. This corresponds quite well with the sample size of most existing studies, with for example 98 samples for one location in Ziegler *et al.* (2011), 175 samples for two sites in Gao *et al.* (2008) and 354 samples by Navratil *et al.* (2011). The turbidity method has the additional advantage of estimating continuous particulate C and N concentrations reducing load uncertainties. As the established relationships are a function of hydrological and climatic variables, a yearly validation of the established relationship using a few monitored events would be sufficient to ensure continuous prediction of particulate associated C and N with similar accuracy. As it is usually easier to obtain samples with low SSC, special efforts should be aimed at collecting as many samples as possible during peak flow.

2.5.2 Turbidity as a direct proxy for catchment nutrient flows

This study demonstrates the potential of predicting sediment associated organic carbon and nitrogen concentrations directly using turbidity signals. As it has been well documented in the past that POC fluxes can be calculated as a function of sediment fluxes (Ludwig *et al.*, 1996), turbidity has been used to predicted POC indirectly based on the SSC – turbidity relationship (Némery *et al.*, 2013). The established linear mixed models in this study performed equally well for PN, and even better for POC than for SSC (r=0.87 and 0.91, respectively), showing that in the presented dataset, the indirect method would have resulted in predictions with lower accuracy than those from the direct approach, as there was a rather poor correlation

between SSC and POC (Pearson's correlation coefficient r of 0.66, P<0.01). This relatively weak correlation was most likely due to a high sand fraction, low in organic carbon, within some samples – pointing towards heterogeneity of suspended sediments within and between events. Uncles *et al.* (2000) also found a decrease in POC with increasing SSC, related to coarser particle size of sediment. Ludwig *et al*. (1996) report a similar trend and scatter in the SSC-POC relationship and relate it to an increase in mineral matter with higher turbidity. Additionally, the laboratory tests showed that the sand fraction is the most difficult fraction to estimate, as it was the least responsive for turbidity and had the highest variance. Furthermore, the turbidity signal was not only affected by SSC and particle size distribution but also by particulate organic matter content. More specifically, the results showed that the effect of organic matter arises largely through aggregation, as dispersion caused the strongest change in slope of the SSC-turbidity relationship. Fewer, larger, aggregated particles will give a smaller NTU value for the same concentration, therefore an increase in OM leads to a decrease in NTU for sediment with the same textural classes. This gives rise to equifinality, where samples with different combinations of SSC, texture and OM can have the same turbidity value, lowering the accuracy of SSC predictions based on turbidity with increasing heterogeneity of sediment sources. But as POC is associated with the finer particle size fractions for which the turbidity – SSC relationship has smaller variance, and associated with the organic matter content which the sensors were shown to detect, the model for POC showed a better fit than that for SSC. In the future, grain size could be determined on all the sediment samples and models could be fitted for each fraction to show if the silt- and clay-sized fraction could indeed be predicted with a similar accuracy as POC.

Adding variables to the mixed model may not have increased Pearson's r, but it did result in lower AIC values for all three response variables. This difference can be understood in light of the different theoretical concepts underlying these two measures of model fit: AIC assumes that there is an underlying true model, and therefore tends to select more complex models (Burnham and Anderson, 1998). The cross validation solely looks at the predictive power. When the main focus is on obtaining good predictions, the mixed model with only turbidity could be selected - although arguably all of the mixed models are good candidates.

When there is interest in the underlying processes affecting the sediment transport, however, the mixed model with multiple predictor variables can be exploited to gain information about the drivers behind SSC, POC and PN in the different water sources; with the upstream channel location representing the reservoir irrigation water, the downstream channel a mix of irrigation water and overland runoff, the upstream river location representing the river baseflow and the downstream river site containing both river water and paddy runoff. For all three established models (i.e. SSC, POC and PN), the standardized regression coefficients showed that turbidity was the most important predictor for all locations except for the channel's downstream position where discharge was more important. Both for SSC, POC and PN, discharge was only significant for the downstream and not for the upstream channel and river locations. The coefficients of the downstream stations were positive; the coefficients of the upstream positions were not significant. This difference reflects the different water sources and their contributing sediment quality. The upstream locations only receive water from the reservoir which has relatively constant, rainfall independent POC and PN concentrations, explaining the non-significant parameter estimates for discharge in explaining POC and PN. Downstream, an increase in stream flow would be due to an increase in overland flow – mainly from upland maize and cassava fields, roads and homesteads -, and this overland flow has a higher sediment and associated nutrient concentration compared to the water released from the reservoir (Schmitter *et al.*, 2012). Cumulative rainfall parameter estimates were significant for the lower channel gauge for SSC, and both channel gauges for POC, with the magnitude of the coefficient decreasing in that order. No effect was found for PN. Schmitter *et al.* (2012), who monitored the same channel locations, found that overland flow induced an influx of material with a higher organic C to total N ratio compared to the C/N ratio of the irrigation water from the reservoir (2 for irrigation water, and up to 6.8 for overland flow), supporting that cumulative rainfall would indeed be expected to be associated with rise in POC and not with PN. Finally, rainfall duration parameter estimates were only significant for POC at the channel's lower gauge, and the coefficient was negative, indicating that for the same turbidity, discharge and cumulative rainfall, the POC at this site is lower if sample was taken further after the start of the event. This could be indicative of a depletion effect, where all the easily erodible material with fine texture and high OM content is exhausted early in the event.

These findings point towards the possible impact of irrigation and overland flow on the redistribution of C/N to paddy fields and the future potential of the methodology. Since there was a significant effect of discharge on SSC, POC and PN for the downstream river position but not for the upstream one, this suggests that the sediment and nutrients brought in by overland flow are at least partially leaving the paddies again. However, average OC and N content of the sediment in the storm flow samples from the downstream river site was higher than in the downstream channel site (1.3% vs 1.0% OC and 0.32 vs 0.18% for N, respectively). This could indicate that, while irrigation water in this watershed is an important contributor to paddy soil fertility (Schmitter *et al*., 2012), a coarser fraction of sediment that contains less OC and N brought in by overland flow, remains behind in the paddies. Upland topsoil nutrient content, ranging between 3.8 and 14 g C kg^{-1}, and 0.2 to 1.2 g N kg^{-1} (Clemens *et al*., 2010), is much lower compared to the paddies with 17.5 g kg^{-1} C and 1.8 g kg^{-1} N (Schmitter *et al*., 2010). In order to assess the annual net OC and N input from overland flow to the paddy area, the established monitoring method can be combined with the flow component separation for the channel water into irrigated amount and overland flow, developed by Schmitter *et al*. (2012). In the future, this will allow for the continuous quantification of the sediment-associated OC and N balance for the paddy rice, determining the overall effect of upland erosion on paddy fertility.

2.6 Conclusions

The developed methodology and the optimization of the sample size provide a cost-effective way to obtain continuous, reliable and long-term estimates of sediment and particulate nutrient concentrations in challenging environments, using basic hydrological characteristics. The results showed that turbidity can be used directly to obtain reliable continuous estimates for SSC, POC and PN even where simple linear regression is underperforming, by applying data transformations and accounting for serial correlation. The method performed better for predicting POC and equally well for predicting PN as for SSC, which is supported by the laboratory tests where the results showed that turbidity sensors can pick up differences in organic matter, which is related to the POC and PN content of the sediment. Parameter estimates from the mixed model with multiple predictor variables elucidated the drivers behind

sediment and nutrient transport: turbidity was the most important predictor variable, followed by discharge. These results open up new ways to monitor movement of sediment and nutrients in headwater catchments, and allow for more accurate calculations of load estimates and sediment and/or nutrient budgets. Especially in Southeast Asia, where demographic pressure, economic and policy changes since the 1990's have led to rapid land use change and agricultural intensification in the uplands, the effects on environmental repercussions, sustainability of agriculture and food security have yet to be assessed. Likely, changes in the hydrological cycle due to climate change could further change sediment and nutrient export, and affect large populations in the downstream areas of these headwaters by altering downstream soil fertility. Additionally, policy measures such as carbon footprints, ecosystem services and adequate land use planning depend on reliable data regarding sediment quantity and quality. Further research is needed to test how the method is applicable at different scales, and if the developed equations are stable over time, as erosion of the topsoil could eventually lead to changes in source material.

Chapter 3 Quantifying uncertainty on sediment loads using bootstrap confidence intervals[3]

J.I.F. Slaets[a], H.P. Piepho[b], P. Schmitter[c], T. Hilger[a], G. Cadisch[a]

[a] Institute of Plant Production and Agroecology in the Tropics and Subtropics, University of Hohenheim, Garbenstrasse 13, 70599 Stuttgart, Germany

[b] Biostatistics Unit, Institute of Crop Science, University of Hohenheim, Fruwirthstrasse 23, 70599 Stuttgart, Germany

[c] The International Water Management Institute, Nile Basin and East Africa Office, Addis Ababa, Ethiopia

3.1 Abstract

Load estimates are more informative than constituent concentrations alone, as they allow quantifying on- and off-site impacts of environmental processes concerning pollutants, nutrients and sediment, such as soil fertility loss, reservoir sedimentation and irrigation channel siltation. While statistical models used to predict constituent concentrations have been developed considerably over the last years, measures of uncertainty on constituent loads are rarely reported. Loads are the product of two predictions, constituent concentration and discharge, integrated over a time period, which makes it not straightforward to produce a standard error or a confidence interval. In this paper, a linear mixed model is used to estimate sediment concentrations. A bootstrap method is then developed that accounts for the uncertainty in the concentration and discharge predictions, allowing temporal correlation in the constituent data, and can be used when data transformations are required. The method was tested for a small watershed in Northwest Vietnam for the period 2010-2011. The results showed that confidence intervals were asymmetric, with the highest uncertainty on the upper limit, and that a sediment load of 6262 Mg a^{-1} had a 95% confidence interval of [4331, 12267] in 2010 and a load of 5543 Mg a^{-1} had an interval of [3593, 8975] in 2011. Additionally, the approach demonstrated

[3] A version of this chapter is in revision for Water Resources Research as:
Slaets, J.I.F., Piepho, H.P., Schmitter, P., Hilger, T., Cadisch, G. Quantifying uncertainty on sediment loads using bootstrap confidence intervals.

that direct estimates from the data were biased downwards compared to bootstrap median estimates. These results imply constituent loads predicted from regression-type water quality models could frequently be underestimating sediment yields and their maximum environmental impact.

Keywords: constituent load, concentration prediction, discharge rating curve, sediment yield, resampling method, Monte Carlo-method

3.2 Introduction

The environmental impact of processes such as erosion, sedimentation, eutrophication or degradation of aquatic ecosystems can only be quantified through reliable estimates of sediment, nutrient or pollutant loads (Walling and Webb, 1996). Monitoring constituent concentrations alone does not suffice as these provide information on in-stream quality, but offer no means to evaluate outcomes such as reservoir siltation, soil fertility loss and pollution at the watershed scale – both on- and off-site. Despite abundant literature developing appropriate procedures for load estimates, most studies do not report a measure of uncertainty on the load (Kulasova *et al*., 2012).

In this paper, we will use the example of one of the most commonly measured constituents, sediment, but the methodology developed is applicable to any constituent load. For sediment, the most frequently used method to estimate loads is the so-called rating curve method (Gao, 2008; Horowitz, 2008). In this approach, the suspended sediment concentration (SSC) is predicted by some form of least squares regression with (often log-transformed) discharge as the explanatory variable. This approach introduces two sources of uncertainty in the load equation: the uncertainty on the sediment concentration equation (the so-called sediment rating curve), and the uncertainty in the discharge (Q), as discharge is usually not measured directly, but rather predicted from a regression with water level as predictor variable, the stage-discharge rating curve. Any measure of uncertainty on the constituent load must take into account the uncertainty on both the constituent concentration, and the discharge.

Uncertainty of the sediment concentration prediction has been extensively discussed and, depending on the catchment characteristics, generally good concentration

predictions are obtained with errors smaller than 15% (Horowitz, 2008). In some studies, however, the uncertainty is stated to be considerable. Smith and Croke (2005) for example reported that discharge only explained a quarter of the variability in the concentration data. Walling and Webb (1988) also found poor predictive power and suggested that seasonal differences of the relationship between discharge (Q) and constituent concentration, non-simultaneity of Q and concentration peaks during storms, hysteresis and exhaustion effects are the most important causes of inaccuracy in concentration predictions. In their dataset, the sediment rating curve explained only 14% of total variance in the data and concentrations at the same level of discharge ranged over more than three orders of magnitude.

Furthermore, there are situations where the use of the rating curve method based on discharge is inherently unviable. For example, in irrigated systems, the natural link between discharge and constituent load is disturbed (Slaets *et al.*, 2014). As an alternative to the sediment rating curve method, turbidity sensors have often been employed – either as a substitute or in addition to discharge as predictor variable. Navratil *et al.* (2011) gave an overview of sources of uncertainty in sediment concentrations introduced by using turbidity sensors. They found that the most important ones were short-term turbidity signal fluctuations, the mechanism of the automatic water samplers and uncertainty on the discharge introduced by the fact that discharge is not measured directly, but rather estimated from water level and a certain number of velocity measurements.

Assessments of sediment load uncertainty generally assume that this error on the discharge rating curve is negligible (Vigiak and Bende-Michl, 2013; Rustomji and Wilkinson, 2008). Uncertainties of discharge, however, depend on several factors: the method chosen to estimate the discharge, site conditions and the time interval over which water levels are measured (Hamilton and Moore, 2012; Harmel *et al*., 2009; Tomkins, 2014). Additional factors include errors in measuring the cross section, in determining the mean stream velocity, and field conditions during measurement such as change in stage, wind or ice obstruction (Sauer and Meyer, 1992). In general, discharge is estimated more accurately than constituent concentration. But discharge enters the load equation twice – once as predictor variable for the concentration, and once multiplied with the concentration to get the

instantaneous load. Therefore, it deserves further investigation whether or not the error on the discharge estimate can safely be ignored, and in which circumstances. Finally, as discharge is frequently used as a predictor for constituent concentration, the two variables are correlated and their errors cannot be assumed to be independent. As a result, there is no textbook formula to estimate the variance of a constituent load.

Therefore, authors that do report a measure of uncertainty often select a method that is specifically geared towards the application of load estimation at hand, and not necessarily applicable to other sites, making it hard to compare results throughout literature. Harmel *et al.* (2009), for example, developed a software tool to assess the errors introduced from estimating discharge, sample collection, preservation and storage, and lab analysis. In this tool, each of these sources is considered to be the result of random variability following a normal distribution and the sources of error are assumed to be independent from each other, but these assumptions will not apply in all situations.

Moatar and Meybeck (2005) assessed uncertainty on nutrient loads by comparing loads based on a random subsample of measurement times, with a high-resolution load that is considered the "true" load. This approach is suitable for testing different methods and different temporal measurement resolutions of load estimation, but it does not assess the uncertainty of the "true" load, as it is assumed that with sufficiently high sampling frequency (in their case, daily), the measured load is equivalent to the actual load. More recently, two new candidate approaches have emerged to calculate confidence intervals on loads, that have the potential to be generally applicable, regardless of the method used to calculate the load and the distributional assumptions made: bootstrap methods (Mailhot *et al.*, 2008; Rustomji and Wilkinson, 2008; Vigiak and Bende-Michl, 2013) and Bayesian methods that result in credibility intervals (Pagendam *et al.*, 2014; Vigiak and Bende-Michl, 2013).

The bootstrap is a Monte Carlo-type method, where a large number (B) of datasets are simulated – either by sampling with replacement from the original data in the case of the non-parametric bootstrap, or by sampling from a fitted distribution in the

case of the parametric bootstrap (Efron and Tibshirani, 1993). Bootstrap methods, however, were originally developed for independent, identically distributed random variables. In the context of sediment monitoring the assumption is that the observations used to build the regression model are independent in time. This can be realistic in fixed-interval sampling schemes where the sampling time interval is large, or in the case of discharge where measurements to build the stage-discharge relationship are typically taken far apart in time. For sediment concentration though, flow-proportional sampling is often performed to obtain samples at the highest concentrations. Those observations are usually taken closely together during storms and thus most likely are not independent in time (Slaets *et al.*, 2014). In this case, it is necessary to use an adjusted version of the bootstrap that retains the serial correlation in the data intact (Lahiri, 2003). Such methods have already been explored in hydrology in relation to the discharge rating curve: Ebtehaj *et al.* (2010) and Selle and Hannah (2010) uses block bootstrap methods to assess uncertainty on and improve robustness of model parameter estimates for discharge prediction.

To assess uncertainty on constituent loads estimated from continuous concentration and discharge predictions where serial correlation is present, we propose a bootstrap-based method to assess uncertainty on constituent loads that can be used with transformed data, that accounts for the uncertainty in both the sediment rating curve and the stage-discharge rating curve, and that allows for serial correlation in the times series data. We checked if any of these requirements can safely be neglected in certain circumstances, and how they affect the resulting confidence intervals. Corresponding code in SAS was created and is available online to accommodate for these different scenarios (https://www.uni-hohenheim.de/bioinformatik/ beratung/index.htm).

Our specific aims were: (i) to establish a generally applicable method to calculate confidence intervals on constituent loads, using bootstrap methods, (ii) to account for serial correlation in the data, (iii) to assess whether or not the effect of the uncertainty on discharge is negligible, (iv) to evaluate how data transformations affect the calculations, and (v) to determine the number of bootstrap replicates required to obtain reliable confidence intervals.

3.3 Material and methods

3.3.1 Discharge and sediment concentration

Discharge and suspended sediment concentrations were continuously monitored for a period of two years (1/1/2010 – 31/12/3011) in a small agricultural catchment in mountainous Northwest Vietnam. The catchment is located in the Chieng Khoi commune (21°7'60''N, 105°40'0''E, 350 m a.s.l), Yen Chau district, in the tropical monsoon belt where the rainy season begins in April and ends in October. Average annual precipitation is around 1200 mm, average annual temperature is 21 °C. The occurrence of typhoons is not uncommon especially at the end of the rainy season, and daily rainfall amounts can rise to 200 mm. The largest storm during the two years of this study was on the 12th of July 2011 and consisted of 73 mm of rainfall in three hours. The dominant soils are alisols and luvisols (Clemens *et al.*, 2010). The landscape has an altitudinal range between 320 and 1600 m above sea level with slopes ranging from 0.05 to 65%. The measurement location is in a river at the outlet of a small watershed with a contributing area of 2 km^2, of which 0.6 km^2 consist of paddy fields. A 26.3 ha surface reservoir with a buffering capacity of 10^6 m^3 provides irrigation water for rice production via concrete irrigation channels, and the paddies drain into the monitored river. As the reservoir fills up with the progression of the rainy season, excess water is removed via a spillover which drains into the river, typically from July till October. During this period, discharge in the river is an order of magnitude larger than during times when the spillover is not active: mean daily discharge in the dry season equaled $7*10^3$ m^3 s^{-1} (with a standard deviation of $11*10^3$ m^3 s^{-1}) in 2010 and 2011, while mean daily discharge with the spillover active amounted to $105*10^3$ m^3 s^{-1} (with a standard deviation of $57*10^3$ m^3 s^{-1}).

For the discharge monitoring, water levels were measured every two minutes using pressure sensors (EcoTech, Germany). The stage-discharge relationship was established with the velocity-area method (Herschy, 1995), where the velocity is measured with a propeller-type current meter (OTT, Germany) at one or more points in each vertical, depending on the water depth. The discharge is subsequently derived from the sum of the product of mean velocity, depth and width between verticals. Discharge measurements were never taken on the same day, and the closest time

interval between two measurements was one week. The estimated discharge $\hat{Q}$ in m^3 s^{-1} at time *i* was then predicted from

$$log\hat{Q}_i = log\hat{\alpha} + \hat{\gamma}\log(h_i - \hat{\beta}), \qquad \text{(Equation 3.1)}$$

where h_i is the water level (in m) at time *i*, $\hat{\alpha}$ and $\hat{\gamma}$ the estimated rating curve constants and $\hat{\beta}$ the estimated sensor offset, with all parameters estimated using the method of least squares on the log-transformed scale. This transformation was done to stabilize the variance.

As the irrigation management disturbed the natural relationship between Q and SSC, a turbidity-based method was used to monitor SSC. Turbidity was measured every two minutes with NEP395 sensors (McVan, Australia). Rainfall was quantified with a tipping-bucket rain gauge on a weather station (Campbell Scientific, USA). 228 water samples were collected using a storm-based approach, by taking around twenty grab samples per sampled rainfall event in order to accomplish the best possible coverage of all concentration ranges. 188 storm flow samples were collected during 24 rainfall events over the two year duration of the study. Additionally, every two weeks a base-flow sample was taken. The sediment concentration was determined gravimetrically on a sample of 500 ml by letting it settle overnight in refrigerated conditions, prior to siphoning off the supernatant and drying the remaining sediment at 35 °C, as is recommended for samples with very high sediment concentrations (ASTM, 2013).

Continuous sediment concentrations were then obtained from a mixed model described in Slaets *et al.* (2014). The response variable, sediment concentration, was Box-Cox transformed to stabilize the variance using the SAS macro described in Piepho (2009). The optimal value of the transformation parameter was estimated by the maximum likelihood method, and the selected value was the log-transformation. Predictor variables were chosen with forward selection based on Akaike Information Criterion (AIC). The model uses turbidity and discharge as quantitative predictor variables, and accounts for serial correlation. As surface reservoir irrigation management was present in the watershed, classic variables related to catchment characteristics such as hysteresis patterns and exhaustion effects were not suitable

predictors of sediment concentration. The predictor variables turbidity and discharge were also log-transformed. All statistical analyses were performed using the MIXED procedure of SAS 9.4, which can fit linear models with more than one random effect. The covariance structure used to model serial correlation in the present study was a first-order autoregressive (AR(1)) model.

Conceptually, this concentration prediction error can also be separated into an underlying latent autoregressive process generating the true concentrations, and an independently distributed measurement error corresponding to white noise in time series data. The white noise is equal to the error that would remain if two measurements were conducted at almost coinciding time points. This variability is typically attributable to measurement error and in spatial statistics, this is what is known as a nugget effect. In the MIXED procedure, this effect was fitted by using the local option in the repeated statement.

Validation was performed using five-fold cross validation, in which the dataset is split randomly into five parts, and each part is used four times to calibrate the model, and one time for validation, so that each observation in the dataset is used for validation once. Pearson's correlation coefficient (r) was calculated between the observed and predicted values resulting from the validation. The SAS macro that performs k-fold cross validation for linear mixed models using the MIXED procedure is described in Slaets *et al.* (2014). Additionally, event-based five-fold cross validation was performed, where all samples belonging to single events were resampled jointly, rather than individual observations. Events were defined based on rainfall data (no pause in precipitation for longer than 30 minutes) and lag times were added based on cross correlation analysis as described in Schmitter *et al*. (2012). A total of 420 rainfall events took place and were monitored during the two year study period.

3.3.2 Bootstrap resampling procedure

The basic principle of the bootstrap is to mimic, as closely as possible, the original process of sampling from the population. To this end, the bootstrap draws a large number (B) of random samples, of the same size as the original dataset, by sampling observations with replacement from that original dataset – so that each observation

can enter a bootstrap sample multiple times. The sample statistic of interest (in this case, the sediment load) is then calculated for each of the B bootstrap samples, resulting in B load estimates. The resulting empirical distribution of the sample statistic allows us to calculate measures of uncertainty on the statistic, as B becomes large, but only if the bootstrap sampling mechanism is able to accurately reproduce the original sampling process (Efron and Tibshirani, 1993).

As the key point of the bootstrap is to recreate the original sampling process, we need to understand the sampling processes resulting in the annual sediment load. Since neither discharge nor constituent concentration are measured continuously, annual loads are normally estimated by calculating the sum of instantaneous loads, measured at equally spaced discrete points in time. The load at a time *i* is then generated from

$$\hat{L}_i = \hat{Q}_i \times \hat{C}_i \qquad \text{(Equation 3.2)}$$

where $\hat{L}_i$ is the estimated instantaneous load at time *i* in g/s, $\hat{Q}_i$ is the estimated discharge at time *i* in m^3/s and $\hat{C}_i$ is the estimated concentration at time *i* in g/m^3. These instantaneous loads are multiplied by a time factor accounting for the monitoring interval. In the present study, for example, the factor was 120 s, as measurements were done every 2 minutes. Monthly or annual loads in Mg can then be calculated by simply summing up the instantaneous loads for the whole time interval and multiplying by a factor 10^{-6} to convert from mg to Mg:

$$\hat{L}_{1\ to\ t} = \sum_{i=1}^{t}(\hat{L}_i \times 120 \times 10^{-6}) \qquad \text{(Equation 3.3)}$$

Looking at Equation 3.2 for the load estimate at a time *i*, there are really two separate sampling processes from two distinct populations at work in the load estimation: firstly the sampling for the discharge rating curve (pairs of Q and h from the full time series of Q and h pairs), and secondly, the samples used to build the sediment rating curve (observations of C and hydrological predictor variables from the full time series of C, Q and turbidity). In order to assess the uncertainty of the discharge equation, the bootstrap replicates can be created by simply sampling (Q, h)-pairs at random with replacement from the original dataset. Simple random resampling assumes independence, which is dependent on the monitoring scheme: in the case of our dataset, discharge measurements were never taken on the same day, and the

smallest interval between two measurements was one week. In order to test this assumption, an AR(1) variance-covariance structure was fitted to the discharge data. As the AIC showed an increase of two points compared to an independent structure, no serial correlation was present in the (Q, h)-pairs. Using Equation 3.1, bootstrap discharges $\hat{Q}_i^*$ can be generated according to

$$log\hat{Q}_i^* = log\hat{\alpha}^* + \hat{\gamma}^* \log(h_i - \hat{\beta}^*) \qquad \text{(Equation 3.4)}$$

where h_i is the water level at time *i*, and $\hat{\alpha}^*$, $\hat{\beta}^*$ and $\hat{\gamma}^*$ are the bootstrap estimates of the discharge rating curve parameters.

These B predictions of Q, B being the number of bootstrap repetitions, must subsequently be fed into the bootstrapped sediment rating curve, as discharge typically is one of the predictor variables for SSC. But the previously described resampling mechanism cannot be applied to the observations used to build the sediment rating curve, as the simple random sampling assumes that the observations are independent. Water samples are often collected in a storm-based approach, as was done in this study, where they were collected sometimes only minutes apart during rainfall events. For this type of hydrological datasets where temporal autocorrelation is present, Ebtehaj *et al.* (2010) recommended the use of specialized sampling procedures that keep the serial correlation intact, such as the moving block bootstrap, the circular block bootstrap or the stationary block bootstrap, described in detail by Lahiri (2003).

Amongst these specialized methods, no clear winner has emerged up to now, and they require many choices - for example in terms of the block size - for which no general recommendation exists. But as the goal of the bootstrap is to mimic the original sampling process, there is an intuitive choice in the case of event-based sampling: the rainfall events form natural “blocks” or sampling unit, which is why water quality models used to predict continuous time series and thus new events should be validated on an event basis, rather than on a sample basis (Lessels and Bishop, 2013). So rather than sampling with replacement from the individual observations (water samples representing a single time point), all samples belonging

to one event can be resampled with replacement, thus keeping all observations within one event together and maintaining the serial correlation intact.

On the other hand, base-flow samples are typically taken at fixed time intervals far apart in time (here every two weeks). They can therefore be considered to be independent and can be resampled by simple random sampling with replacement, thus bootstrapping individual water samples from single time points. An increase in AIC of one point when fitting a first-order autoregressive covariance structure confirmed the lack of serial correlation in the base-flow samples. By bootstrapping all water samples belonging to the same event for the storm flow samples and single water samples for the base flow samples, each bootstrap replicate contains a similar ratio of base flow and storm flow observations as the original dataset, and in this manner, B time series of predicted sediment concentration $\hat{C}_i^*$ are generated from

$$\hat{C}_i^* = \hat{\delta}^* + (\hat{v}^*)^T X_i \,, \qquad \text{(Equation 3.5)}$$

with $\hat{\delta}^*$ and $\hat{v}^*$ the bootstrap estimates of the intercept and the regression coefficients, respectively, $(\hat{v}^*)^T$ the transpose of vector $\hat{v}^*$ and X_i the design vector of the fixed effects. This is a generalized equation applicable to any linear model, regardless of the number of predictor variables. If the sediment concentration was predicted using turbidity and discharge, for example, the bootstrap time series of predicted sediment concentration would be generated from

$$\hat{C}_i^* = \hat{\delta}^* + \hat{\eta}^* \hat{Q}_i^* + \hat{\kappa}^* T_i \,, \qquad \text{(Equation 3.6)}$$

where $\hat{\eta}^*$ is the bootstrap parameter estimate of the regression coefficient for $\hat{Q}_i^*$, the bootstrap discharge at time *i* generated from Equation 3.4, and $\hat{\kappa}^*$ the bootstrap parameter estimate of the regression coefficient for T_i, the turbidity at time *i*, respectively.

This resampling process accounts for the uncertainty that arises from estimating the parameters of the sediment rating curve from a dataset with a limited number of observations. If there were an unlimited number of water samples available, the uncertainty of these parameter estimates would reduce to zero. But it is more realistic to assume that, even if there were a very large number of samples available, there would still remain scatter in the real constituent concentrations around the equation,

as the equation simply does not fully explain all the variation in sediment concentration.

Sediment loads vary not only with discharge, but also with upstream sediment supply, which in turn depends additionally on geology, soil types, land cover and land use change or management, all influencing sediment quantity and quality (Walling, 1977). Therefore, there is a fundamental reason for the scatter in the data: sediment loads are inherently non-capacity loads. Even if there were an unlimited number of samples available, this would not result in a perfect equation to predict sediment concentration. Therefore this additional uncertainty needs to be taken into account. For the discharge rating curve, if the river bed is stable and the stream bank vegetation does not change, the stage-discharge equation has a high accuracy and it is reasonable to assume the only error on the equation is measurement error, therefore this additional uncertainty is not a concern.

To introduce this second source of error on the sediment rating curve, Rustomji and Wilkinson (2008) and Vigiak and Bende-Michl (2013) added an additional step to the bootstrap process: a randomly drawn residual from the original regression equation was added to the expected value of the constituent concentration, so that the predicted concentration included both the uncertainty of the parameters of the rating curve due to having a finite sample, and the uncertainty that arises from the fact that sediment concentrations simply cannot be perfectly predicted by any equation, regardless of how large the observed dataset would be. However, by randomly resampling from the residuals, it is assumed that these residuals are independent.

When this assumption does not hold because samples are taken very closely together in time, as was the case for our dataset, the method can be modified so that the added errors reflect the temporal autocorrelation. To this end, the covariance parameter estimates from the original sample can be used as plug-in estimates. In the present dataset, an AR(1) structure was fitted to the data (Verbeke and Molenberghs, 2009), resulting in two covariance parameter estimates: one for the autocorrelation parameter ($\hat{\rho}$) and one for the residual error variance ($\hat{\sigma}_e^2$). The Restricted Maximum Likelihood algorithm was used to simultaneously estimate the fixed effects and the covariance structure (Patterson and Thompson, 1971). The use of the covariance

parameter estimates obtained assuming a normal distribution of errors implies that the method is partly parametric. This is necessary in order to take the serial correlation in the data into account. The bootstrap error term e^* at time i was then generated according to the following equation:

$$\hat{e}_i^* = \hat{\rho}^* \hat{e}_{i-1}^* + \sqrt{(1 - (\hat{\rho}^*)^2)} \times f_i^*, \qquad \text{(Equation 3.7)}$$

where $\hat{\rho}^*$ is the bootstrap estimate of the autocorrelation parameter, and the error f_i^* was randomly drawn from a normal distribution with mean zero and a bootstrap variance $(\hat{\sigma}_e^*)^2$. The bootstrap prediction of a sediment concentration at time i, including the error expected due to residual scatter in the data, is then given by

$$\hat{C}_i^* + \hat{e}_i^* = \hat{\delta}^* + (\hat{v}^*)^T X_i + \hat{\rho}^* \hat{e}_{i-1}^* + \sqrt{(1 - (\hat{\rho}^*)^2)} \times f_i^*. \qquad \text{(Equation 3.8)}$$

In summary, the complete bootstrap process that accounts for uncertainty in the parameter estimates of both the discharge and sediment rating curves, and uncertainty due to residual scatter in the sediment concentrations consists of three steps (Figure 3.1):

(1) Resampling with replacement from the (Q, h)-pairs B times, in order to get B bootstrap stage-discharge equations; applying these equations to the continuous water level data to obtain B bootstrap time series (Q^*) for discharge;

(2) Block-bootstrapping the (C, turbidity, Q^*, rainfall) dataset by drawing whole events and base-flow samples with replacement, in each i^{th} replicate plugging in the corresponding bootstrap Q^* from Step 1, in order to get B bootstrap sediment rating curves; then applying these bootstrap sediment rating curves to the continuous turbidity, Q^*, and rainfall data to obtain B time series for the continuous suspended sediment concentration;

(3) Adding an error term to the concentration predictions to account for the residual scatter that is inherent to the sediment concentration.

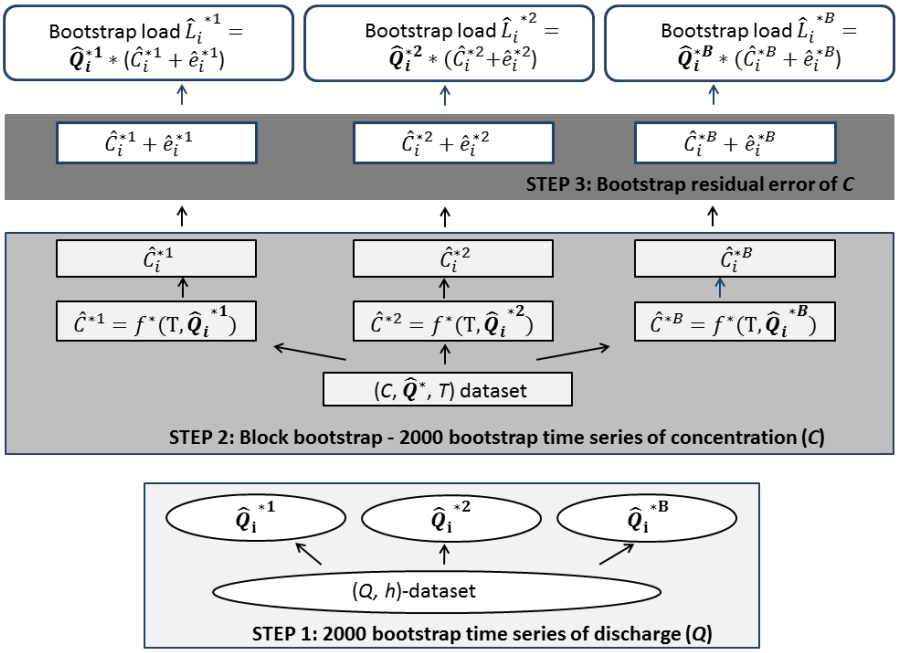

Figure 3.1: Flow chart showing the three-step bootstrap mechanism

In order to obtain a bootstrap estimate of the instantaneous load *L* at time *i*, the equation is:

$$\hat{L}_i^* = \hat{Q}_i^* \times (\hat{C}_i^* + \hat{e}_i^*) \qquad \text{(Equation 3.9)}$$

The residual scatter on the discharge is not added, as the stage-discharge rating curve has a much higher accuracy on the one hand, and on the other hand, velocity measurements are typically taken quite far apart in time, which would not allow modeling the serial correlation of the time series for discharge, but this would be needed because of the shortness of the time intervals considered here (2 minutes).

Finally, these bootstrap instantaneous load estimates can be summed up for the whole time interval, resulting in B estimates of monthly or annual loads:

$$\hat{L}_{1\ to\ t}^* = \sum_{i=1}^{t} (\hat{L}_i^* \times 120 \times 10^{-6}) \qquad \text{(Equation 3.10)}$$

3.3.3 Data transformations

If the data are not normally distributed, it can be necessary to transform variables, as was done for this dataset with a Box-Cox transformation. In this case, the variables in question can simply be transformed before starting the bootstrap, and all the bootstrap estimates are obtained on the transformed scale. The back-transformation is then performed in Equation 3.9 to obtain load estimates on the original scale. For example, in a typical case where both discharge and sediment concentration need to be log-transformed, the bootstrap predictions of discharge in Equation 3.4 and of concentration in Equation 3.8 will be on the log-scale. These predictors then need to be back-transformed to the original scale using the inverse of the logarithm.

This approach is applicable to any type of data transformation, and thus offers a flexible framework that can accommodate different methods of estimating the constituent concentration. However, if a modeled residual error term $\hat{e}_i^*$ is not included, care must be taken with the back-transformation. With many data transformations (the log-transformation and the Box-Cox transformation being prime examples), predicted means cannot be back-transformed and interpreted on the original scale. Adding the modeled residual error removes the need to apply a correction factor that compensates for the underestimation of SSC that arises from doing the predictions on the transformed scale, as pointed out by Rustomji and Wilkinson (2008) and is therefore the recommended approach.

While discharge is also typically predicted on the log-transformed scale, in our dataset the variance was much smaller than that of the concentration data. With a small variance, the log-normal distribution is nearly normal and therefore, the naïve back-transformation of $\log \hat{Q}_i^*$ should approximate the mean well.

3.3.4 Alternative option to simulate errors

If a data transformation is required and one does not want to explicitly simulate the residual scatter, then a correction factor must be applied to the back-transformed concentration. This correction is needed because the naïve back-transformation (for example, taking the exponent of the predictions if the predictions are on the log-scale) does not yield a predicted mean, but rather a predicted median. While medians

can be informative measures of central tendency for skewed datasets, they are not appropriate when the objective is to calculate a constituent load: loads are sums over equally-spaced time points, and in order to obtain an unbiased estimate of this sum over time intervals, we need to sum up estimates of the expected values, rather than the medians, for each interval.

The required correction factor is specific to the type of data transformation. For a logarithmic transformation, the expected value can be obtained by adding on half of the residual error variance to the predicted concentration on the log-scale before back-transforming. For other cases of the Box-Cox transformation, the correction depends on the selected transformation parameter. Solutions for specific examples of the transformation parameter can be found in Freeman and Modarres (2006). As the selected transformation in this dataset was the logarithm, the correction of adding half the residual error variance before back-transforming was compared to the approach where the error is simulated, in order to see how this affects sediment load estimates and resulting confidence intervals.

3.3.5 Bootstrap confidence intervals

A straightforward way to calculate a confidence interval (CI) on a parameter after bootstrapping is the bootstrap percentile method (Efron and Tibshirani, 1993). If one were to have 1000 bootstrap replicates and thus generate 1000 bootstrap parameter estimates (e.g. 1000 load estimates), and a 95% CI is required, the confidence interval would simply be calculated by ordering the 1000 load estimates from small to large, and taking the 25^{th} largest load estimate and the 975^{th} largest load estimate as the lower and the upper limit.

This method was used by Rustomji and Wilkinson (2008) on sediment loads and is transformation-respecting, also when the sample statistic is not normally distributed (Efron and Tibshirani, 1993). This property is important in the case of loads, because data are typically log-transformed. As a confidence interval depends on the tail of the empirical bootstrap distribution where fewer samples occur, a relatively large number of bootstrap replicates (upward of 500) are usually required to achieve acceptable accuracy (Efron and Tibshirani, 1993). How many exactly, depends on the statistic in question, and should be empirically tested for each case: when the

process is repeated, the resulting CI should not greatly differ, otherwise the number is too small. In the present dataset, a choice of 2000 bootstrap replicates yielded replicable results.

Improving upon the bootstrap percentile method, Efron and Tibshirani (1993) proposed bias-corrected and accelerated intervals, used by Vigiak and Bende-Michl (2013). Unfortunately, this approach requires an even larger number of bootstrap replicates than the percentile method to sufficiently reduce the Monte Carlo sampling error. This is a disadvantage when working with hydrological time series, as the datasets typically contain a large number of records already. This method then quickly becomes time consuming, and therefore in this paper, preference was given to the more intuitive and less computationally intensive bootstrap percentile method.

3.3.6 Identifying hydrological drivers of uncertainty

The proposed three-step bootstrap process offers an opportunity to assess the importance of different aspects of the load calculation on the accuracy of the estimate. By leaving out step 1 (bootstrapping the Q-h pairs) and just using Q as predicted by the discharge rating curve from all observed data points, confidence intervals can be obtained that only take into account the uncertainty on the sediment rating curve. If the resulting confidence intervals closely resemble the confidence intervals calculated with the full approach, this would mean that the uncertainty on the sediment concentration is what drives the uncertainty on the loads, thus supporting the common hypothesis (eg. Némery *et al.*, 2013, Vigiak and Bende-Michl, 2013) that the error on the discharge is negligible.

As the accuracy of the stage-discharge relationship depends on the type of streambed, the method chosen and the amount of measurements taken, this assumption might also hold true for some watersheds such as the one in this study, where the relationship had a high R^2, but not for others. To determine at which point the uncertainty on Q must be taken into account for the load confidence interval, data sets of (Q, h)-pairs were simulated with decreasing R^2 (0.95, 0.90, 0.85 and 0.80), and were each used as input dataset for bootstrapping the stage-discharge relationship (Step 1 in Figure 3.1) in order to test the sensitivity of the confidence intervals to the accuracy of the discharge rating curve. The datasets with a fixed

realized R^2 were simulated by a rescaling of errors which is described in Appendix A, as well as SAS code to perform the simulation.

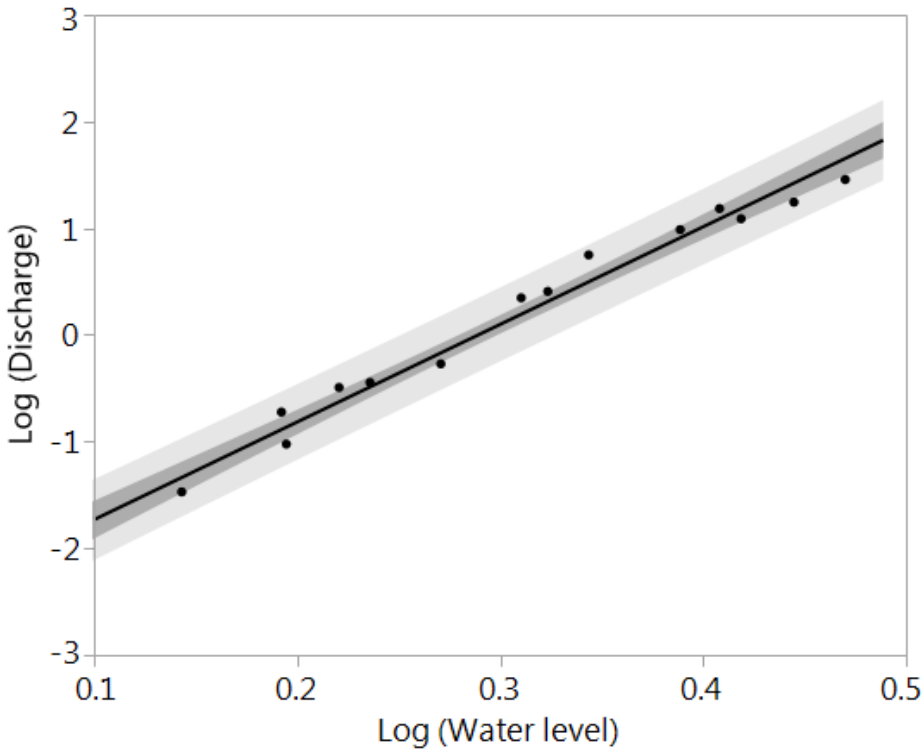

Figure 3.2: Discharge rating curve plotted on the log-transformed scale showing 95% confidence interval for the regression line (dark grey) and for new predictions (light grey). Stage-discharge rating curve: log(discharge) = (9.0819*log(water level)) - 2.6423 (n=15, R^2=0.98)

3.4 Results

3.4.1 Rating curves and load estimates

The coefficient of determination of the stage-discharge relationship was 0.98 (n=15, Figure 3.2). Homoscedasticity was observed on the log-transformed scale (Figure 3.3). For the sediment rating curve, Pearson's r between observed and predicted values on the log-transformed scale was 0.75 after five-fold cross validation (n=228, Figure 3.4). Event-based cross validation yielded very similar results, demonstrating the robustness of the model (Pearson's r=0.77). Thus in the case of our dataset, the discharge rating curve explained a higher proportion of the variance than the sediment rating curve, as is typical. Again, homoscedasticity was observed on the

log-transformed scale (Figure 3.5). The bootstrap parameter estimates for the rho of the AR(1) process varied from 0.56 to 0.93 with a mean of 0.77, showing the block bootstrap kept the serial correlation intact.

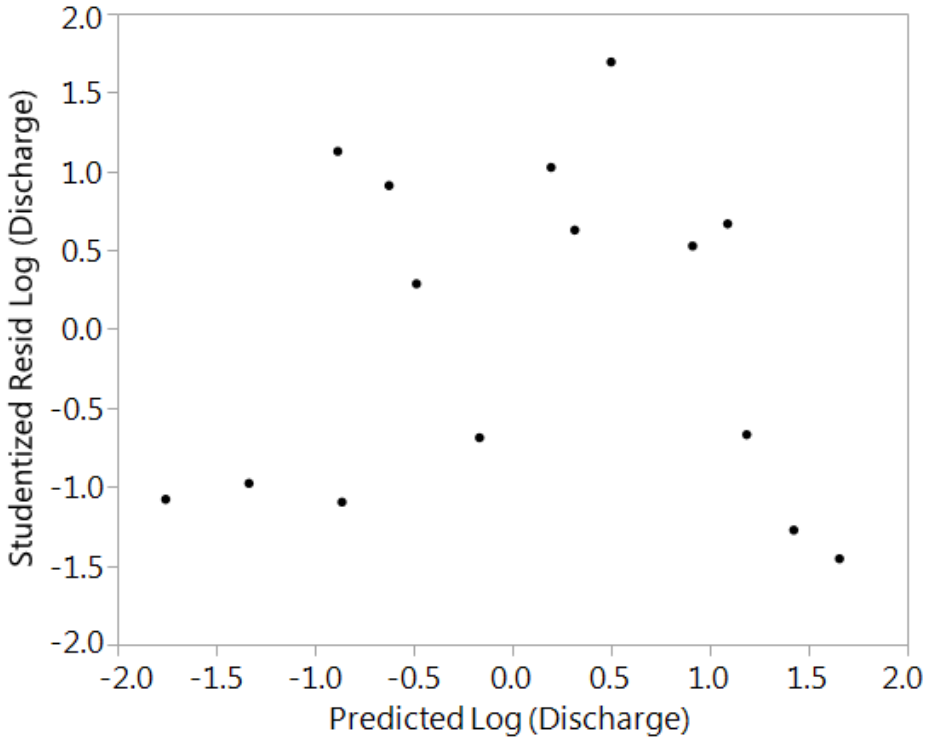

Figure 3.3: Residual plot for the discharge rating curve, showing studentized residuals versus the predicted discharge (on the log-transformed scale).

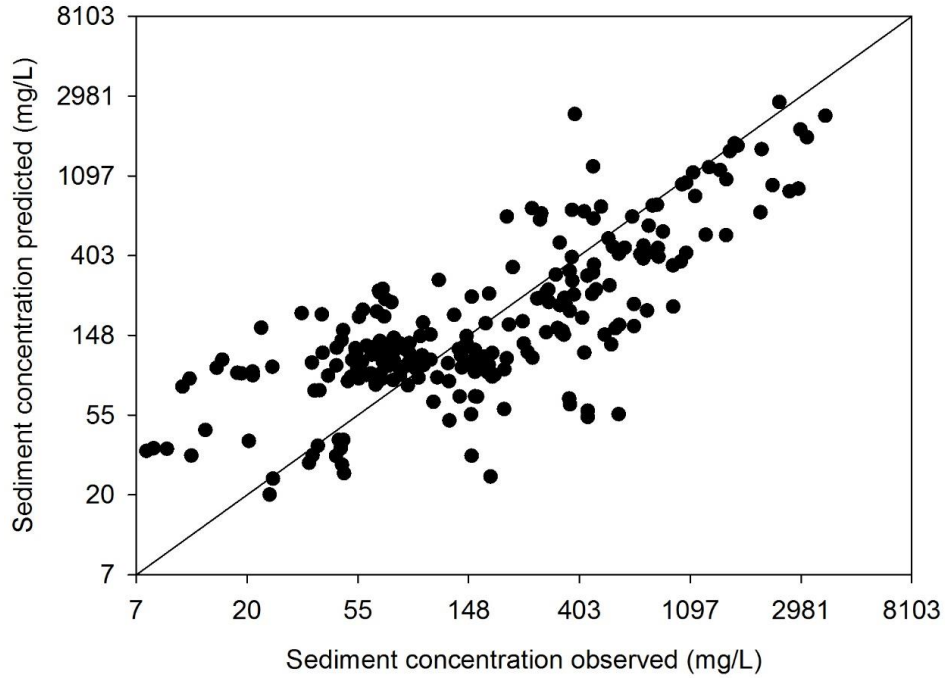

Figure 3.4: Observed versus predicted values of the sediment rating curve. Predictions are from the linear mixed model with turbidity and discharge as quantitative predictor variables, and after five-fold cross validation (n=228, r^2=0.56). Axes are on the log-transformed scale while tick labels show values on the original scale.

The size of the estimated load depended on the method chosen for estimation. First, the load was calculated directly from the model estimates based on the full datasets, without bootstrapping (Direct estimate in Tables 3.1 and 3.2). The sediment concentrations in this case were back-transformed by applying the correction appropriate for log-transformed data, which is to add half the residual error variance before back-transformation. Second, the median of the bootstrap estimates of the sediment load was taken, where, identically to the first case, the concentrations were corrected by adding half the residual error variance before back-transforming (Bootstrap without modeled error in Tables 3.1 and 3.2). Third, the median of the bootstrap estimates was taken for the bootstrap process that included a modeled, autoregressive error term (Full bootstrap method in Tables 3.1 and 3.2).

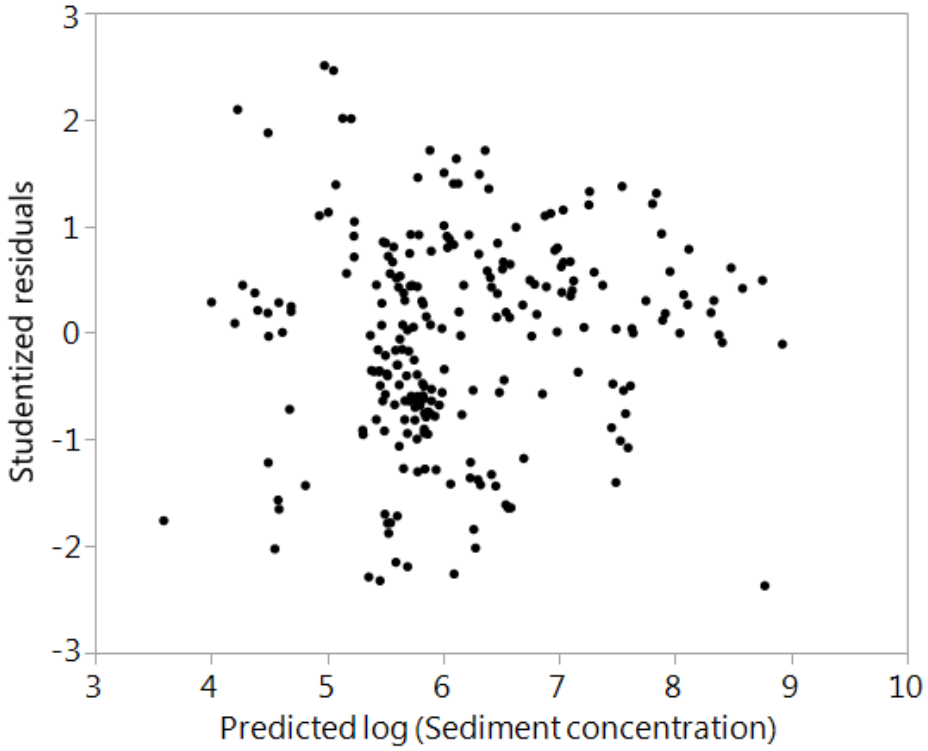

Figure 3.5: Residual plot of the sediment concentration prediction model, showing studentized residuals versus the predicted sediment concentration (on the log-transformed scale).

Table 3.1: Annual sediment load estimates (in Mg per year) for the two years of the study directly estimated without bootstrapping, and load estimates with 95% confidence interval limits and interval widths (difference between upper and lower limit) for the three different bootstrap methods: the full method shown in Figure 3.1, the method without modelled error (i.e. leaving out Step 3 in Figure 3.1) and the method without bootstrapping discharge (i.e. leaving out Step 1 in Figure 3.1). (Corr=Autocorrelation, Q= discharge, Est.=Estimate, Low.=Lower Limit, Up.=Upper Limit, n.a. = not applicable)

	Error source		2010				2011			
Method	**Corr.**	**Q**	**Est.**	**Low.**	**Up.**	**Width**	**Est.**	**Low.**	**Up.**	**Width**
			Mg a^{-1}				**Mg a^{-1}**			
Direct estimate			5607	n.a.	n.a.	n.a.	4997	n.a.	n.a.	n.a.
Full bootstrap method	✓	✓	**6262**	**4331**	**12267**	**7936**	**5543**	**3593**	**8975**	**5383**
Bootstrap without modelled error		✓	6575	4372	14586	10214	5839	3713	10410	6697
Bootstrap without discharge	✓		5944	4203	11649	7446	5413	3521	8394	4876

For this last estimation method, the annual sediment load was estimated to be 6262 Mg in 2010 and 5543 Mg in 2011 (Table 3.1). When the median from the bootstrap sediment load estimates was taken without modeled error, but rather applying the back-transformation correction, the load was approximately 5% higher for both annual and monthly load estimates (Tables 3.1 and 3.2). The annual loads thus amounted 6575 Mg in 2010 and 5839 Mg in 2011. Finally, if sediment loads were estimated not by bootstrapping, but directly from the data, then the results were around 10% lower compared to the first estimates, at 5607 Mg and 4997 Mg, respectively, in 2010 and 2011.

Table 3.2: Monthly sediment load estimates (in Mg per year) for the two years of the study directly estimated without bootstrapping, and load estimates with 95% confidence interval limits for the three different bootstrap methods: the full method shown in Figure 3.1, the method without modelled error (i.e. leaving out Step 3 in Figure 3.1) and the method without bootstrapping discharge (i.e. leaving out Step 1 in Figure 3.1). In January 2011, discharge was zero; therefore no sediment load was transported during this month.

Method	Direct	Full bootstrap method			Bootstrap without modeled error			Bootstrap without discharge		
		Estimate	Lower	Upper	Estimate	Lower	Upper	Estimate	Lower	Upper
Jan-10	31	52	21	163	55	21	199	45	20	128
Feb-10	39	62	22	167	66	23	205	54	22	137
Mar-10	39	63	25	194	68	26	233	55	24	158
Apr-10	45	76	27	301	81	28	361	63	27	237
May-10	185	175	123	305	187	137	321	168	121	274
Jun-10	397	332	189	654	353	224	656	310	183	567
Jul-10	1392	1550	1136	2590	1646	1151	3172	1552	1160	2620
Aug-10	971	1368	892	2557	1461	897	3103	1172	768	2528
Sep-10	914	1124	555	3039	1194	555	3635	1136	572	2932
Oct-10	967	1327	544	3435	1406	596	4028	1174	546	2937
Nov-10	62	93	35	254	99	36	304	81	35	215
Dec-10	6	10	4	32	10	4	38	8	4	23
Jan-11	.	.	.	.	.	.	.	.	.	.
Feb-11	5	9	4	22	9	4	26	8	3	19
Mar-11	17	24	13	51	26	13	61	22	12	45
Apr-11	9	15	7	44	16	7	52	13	6	36
May-11	220	214	149	341	226	150	396	210	150	317
Jun-11	488	382	233	613	411	279	592	388	240	618
Jul-11	1617	1325	770	1930	1396	877	2073	1404	796	2081
Aug-11	1437	1345	700	2658	1423	717	3072	1563	1078	2438
Sep-11	966	943	368	2083	1005	387	2443	1137	568	2279
Oct-11	506	699	166	1760	743	175	2052	602	236	1243
Nov-11	19	29	14	68	31	14	82	26	11	58
Dec-11	13	24	10	79	25	10	98	20	8	61

In all three approaches the difference between the two years remained consistent and all estimates were within the bounds of the confidence intervals, both for those calculated by modeling error and those calculated by adding half the variance before back-transformation.

3.4.2 Width of confidence intervals for sediment loads

Before looking at the bootstrap confidence intervals, the histograms of the bootstrap load estimates were evaluated (Figure 3.6). The histogram of the 2000 bootstrap estimates looked reasonably smooth, so we concluded that sample size was adequate for the percentile bootstrap. For both years and both for the full method and the method without modeled error, the histograms were found to be skewed to the right, even when the loads were log-transformed. This skewness means that, in the case of our dataset, the assumption of log-normality would not hold for estimated annual loads.

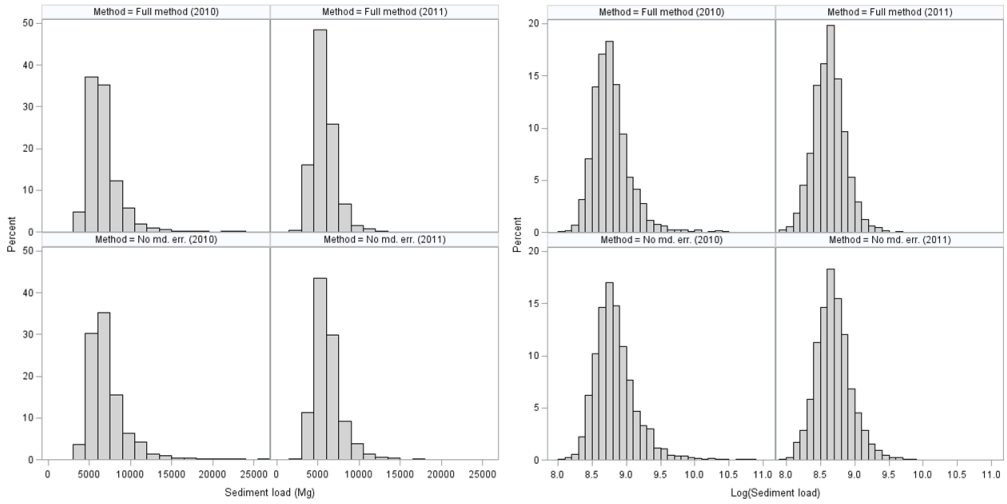

Figure 3.6: Histograms of bootstrap load estimates on the original scale (left) and the log-scale (right) for two study years and for two bootstrap methods: the full method with modeling the autocorrelated error ("Full method", (top), and without modeling the error ("No md. err.", (bottom)))

As a result of the distribution of the loads, the confidence intervals were always asymmetric, with the difference between the upper limit and the estimate around 80% larger than the difference between the estimate and the lower limit. As for the width of the intervals - the difference between the upper and lower limit of the interval, while remaining in the same order of magnitude, the width varied between years and between methods (Table 3.1). In 2010, the interval was always wider, regardless of which method was chosen, for the annual as well as for the monthly

loads (Tables 3.1 and 3.2). The year 2010 did contain a smaller proportion of the samples (73 out of 228) and this could be a cause for the difference.

The bootstrap method affected the width of the confidence interval as well. The monthly and annual intervals resulting from applying a back-transformation correction were consistently wider than those resulting from the bootstrap process that modeled the autocorrelated error: not modeling the error changed the interval (limits in Mg) from [4331, 12267] to [4372, 14586] in 2010 and from [3593, 8975] to [3713, 10410] in 2011 – in both cases an increase in width of about 20%. The change was due to an increase in the upper bound of the interval, while the lower limits remained very similar. These results show that performing the back-transformation correction is only a very rough method of adjusting the predicted concentrations on the original scale, as this approach does not take the serial correlation in the data into account.

3.4.3 Hydrological drivers of uncertainty

When, rather than applying the full bootstrap method, we did not bootstrap the discharge rating curve (meaning, we left out Step 1 of the process in Figure 3.1), the width of the confidence interval decreased, as one less source of error is taken into account. In 2010, this changed the CI from [4203, 11649] without accounting for uncertainty in the discharge rating curve to [4331, 12267] when accounting for this uncertainty on discharge; and from [3521, 8397] to [3593, 8975] in 2011 – including discharge therefore resulted in a respective increase in width of 6 and 9%.

The accuracy on the (Q, h)-relationship in this particular dataset was very high with an R^2 of 0.98. As not all monitoring programs can establish accurate discharge rating curves, the (Q, h)-dataset was replaced by a simulated dataset with increasingly lower coefficient of determination to test how this further affects the uncertainty on the load estimate (Figure 3.7). While the width of the confidence interval keeps increasing with decreasing R^2, including the discharge also affects the confidence interval for a high R^2. In fact, changing from not bootstrapping the discharge (”a” in Figure 3.7) to bootstrapping the real discharge dataset, which has an R^2 of 0.98, resulted in a 7% increase in width. On the other hand, the confidence intervals show little differences at an R^2 of 0.95, where the width was 9003 Mg, and at 0.90, when it

reached up to 8795 Mg, equivalent to an 11% increase in width. At a coefficient of determination of 0.85, the CI was 17% wider than the original CI and at 0.80 finally, the width increase reached 20%. As can be seen from Figure 3.7, the change in width was mainly due to an increase in the upper limit of the confidence interval. The lower limit decreased only slightly.

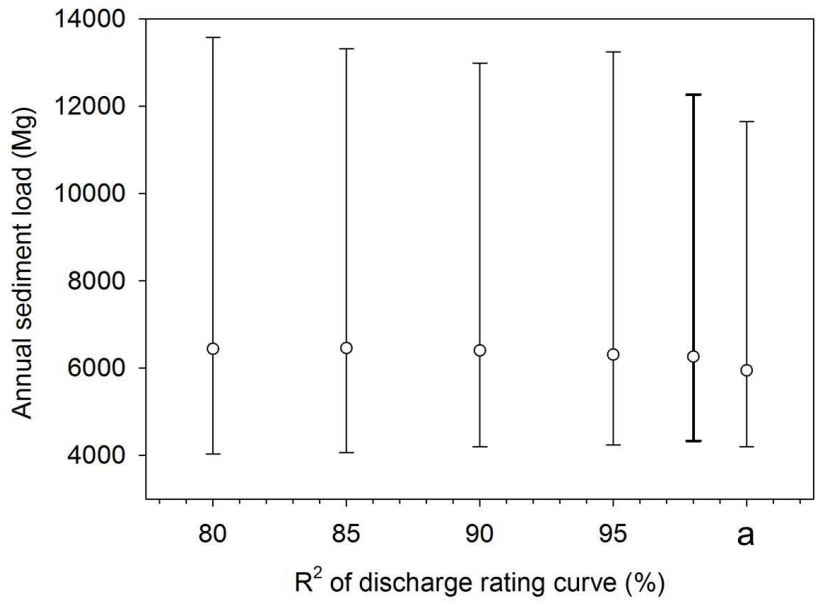

Figure 3.7: Change in median and 95% confidence intervals for the sediment load estimate of 2010 (in Mg) when decreasing the coefficient of determination of the discharge rating curve. The bold line indicates the CI width of the real (Q,h) dataset. The letter "a" corresponds to not bootstrapping the (Q,h) pairs.

The bootstrap approach where the concentration prediction error was separated into an underlying latent autoregressive process generating the true concentrations, and an independently distributed measurement error corresponding to white noise in time series data, did not converge for 906 out of 2000 runs. Convergence problems are very common when trying to fit nugget models as these models tend to be difficult to fit. Particularly AR(1) type error structures are prone to these issues, as there is an inherent confounding between parameters of the independent white noise component and the autocorrelated component (Piepho *et al*., 2015). In a bootstrap setting where convergence was already an issue, adding such an effect was not feasible in the case

of our dataset. For exploratory purposes, the nugget can be fitted to the original dataset without bootstrapping, in order to examine the contributions of the respective error components. Results of this exercise showed that indeed, the measurement error (0.67) was large compared to the latent process variance (0.09), the former being due to sensor error, both from the turbidity sensors and the pressure sensors for discharge, the manual grab sample process which may not always capture the center point of flow, and laboratory error in determining the sediment concentrations. The error separation thus indicates that focusing on these factors could yield substantial improvement in the sediment rating curve.

3.5 Discussion

3.5.1 Load estimates, data transformations and bias

As was shown in Table 3.1, the annual sediment load estimates differ depending on the method selected. While it is encouraging that all estimates are within the 95% confidence interval limits, choosing a different method can lead to anything from an underestimation of 10% to an overestimation of 20% compared to the median of the full bootstrap process. Two issues play a role in these differences: the back-transformation of the sediment concentrations, and bias in the estimate of the annual load.

The effect of back-transforming the concentration predictions is visible when comparing the medians of the bootstrap estimates with and without modeled autocorrelated error. When the error was not modeled, the estimate itself increased by around 5% in both years, corresponding to an absolute increase of around 300 Mg of sediment, and the CI became wider. Essentially, adding half the variance before back-transformation is a very rough way of estimating expected values of concentrations at original time points – as shown by the larger CI - because it does not take the serial correlation in the data into account. If the naïve back-transformation would be applied, without any variance correction, the resulting estimates would be even lower than those where we add half the variance before back-transformation: around 4200 Mg in 2010 and 3700 Mg in 2011, or an underestimation of approximately 2000 Mg.

While the latter is a relatively common approach to implement the back-transformation of constituent concentration predictions which are typically predicted on the log-scale, it may not be the most appropriate solution when the concentrations are used to calculate loads. The crucial issue with load calculations is that a load is a sum over time points, which is essentially the same as computing an arithmetic average, and for that we need to estimate the expected values for the individual time intervals. If the predicted value on the log-scale is simply back-transformed, we are estimating medians of the concentrations, and while this may be appropriate if one is only interested in the concentrations, these medians cannot be multiplied with discharge and summed up to get the load.

When the bootstrap process includes a simulated, autocorrelated error, the result of that process is not a mean or a median concentration, but rather a simulated realization of an observed process. When it is not desired to simulate the error in the bootstrap process, then applying a back-transformation correction is an alternative, but the confidence intervals should be expected to be wider compared to the confidence intervals where the serial correlation is modeled, as adding on half the residual error variance before back-transformation ignores the serial correlation. Another back-transformation correction often used in literature, Duan's smearing correction, similarly assumes iid errors and is therefore not suitable for datasets where serial correlation is present (Duan, 1983). Duan's is a non-parametric correction where the sample average of the exponentiated residuals from the model is used as the correction factor, in contrast with the two parametric approaches we used.

The back-transformation method of the concentration predictions, however, is not the only force at work: the direct estimate from the data and the bootstrap median without modeled error are quite far apart, even though they both use the same back-transformation correction. Statistics, unless they are very simple (for example a sample mean), will typically have some bias. Bootstrapping can in fact be used to identify and correct bias; therefore in most cases the bootstrap estimate will typically be different as it removes this bias (Efron and Tibshirani, 1993). There are alternative methods in literature intended to remove the bias on load estimates (Ferguson, 1986), but as the correction will depend on the variance of the data, numerical corrections are not generally applicable. However, as one would need to bootstrap in any case in

order to produce a CI of the load, taking the median of the bootstrap estimates is a straightforward way to obtain constituent load estimates.

Regarding the data transformation, while the sediment concentration was log-normally distributed, this does not imply that the annual load is also log-normally distributed. One could expect this assumption to hold based on the central limit theorem, but as can be seen from the bootstrap replicate histograms, it did not hold true for our dataset, because both the underlying discharge and concentration time series are strongly skewed. This non-log-normality of our loads does not affect the viability of the bootstrap approach, but it does limit the applicability of methods that use the log-normality assumption of the load to estimate a variance for the load, as was done for example by Wang *et al.* (2011) in an approach that used the delta-method as an alternative way to assess uncertainty on annual sediment load estimates.

3.5.2 Confidence interval width and model selection

The results showed that the CI's are relatively wide and asymmetrical with a much larger uncertainty on the upper limit. And comparing the two years, when the estimated load was higher, the uncertainty on it was larger as well (i.e. in 2010). This is a trend consistent with other studies (Kuhnert *et al.*, 2012; Rustomji and Wilkinson, 2008). Although it is difficult to compare uncertainty calculated with other methods in different catchments, our confidence intervals are of the same order of magnitude as the CI's in those two studies. For example, Kuhnert *et al.* (2012) calculated 80% confidence intervals on an annual load of 5232 Mg (n=122), and the resulting limits were [3512, 7775]. In comparison, 80% confidence intervals for our dataset were [4186, 7403] for a load of 5543 Mg in 2011.

The factors governing the width of a confidence interval are essentially the sample size and the accuracy of the two rating curve estimates. If the sample size is large and the variation explained by the rating curves large, but the confidence intervals are very wide, one possible cause is that the concentration prediction model was over-fitted, resulting in a very high apparent percentage of variance explained by the model but a poor predictive power when the model is interpolated to the whole time series. This can be shown by just adding additional predictor variables to our selected

model. If we add the variables ‘water height in the reservoir’, ‘discharge irrigated to the paddy fields’ and ‘Julian day-of-year’ (the last one both linear and quadratic) to the model, the percentage of variance explained increases from 58% to 71%. When this extended model was used to estimate the annual sediment load, however, the confidence interval was inflated by two orders of magnitude, resulting in a width of 5 564 076 Mg.

These effects on the CI indicate that indeed, overfitting is a concern even when interpolating within the time series. The risk of overfitting is particularly high with more complex models (Burnham and Anderson, 2002), as was demonstrated as well with the example above, and it is not uncommon in load estimations to fit models that are very flexible (eg. spline functions, sigmoid functions) and / or have used a large number of predictor variables to a relatively small dataset. In such cases, bootstrap uncertainty assessment can be an additional tool both for model selection, and for evaluating model fit. In the example of the over-fitted model above, the change in percentage variance explained is less pronounced after cross validation, and ranges from 56 to 64%, implying that the cross validation penalizes at least partially for any overfitting. Water quality models, however, are often not validated and only the R^2 resulting from calibration is reported, leaving readers no means of assessing over-parameterization of the model. Studies with smaller datasets where more variables are included in the model should be particularly encouraged to report measures of uncertainty on load estimates. In the case of large datasets where a simple model, such as linear regression with one or two predictor variables is used, the variability in the data explained by the model resulting from calibration only is less likely to deviate strongly from the result of a validation. Reporting bootstrap confidence intervals would offer readers an additional way of assessing over-parameterization.

An issue related to overfitting and model selection could also be seen in the selection of the variance-covariance structure. In a previous study on water quality prediction models (Slaets *et al.*, 2014), a power decay structure was selected based on AIC. But the power model gave convergence problems in some of the bootstrap replicates due to having fewer different observations to estimate the variance-covariance parameters. Based on these bootstrap results, the covariance structure that models

serial correlation in this paper was changed from the previous power model to a simpler first-order autoregressive structure which did not have any convergence issues.

3.5.3 Bootstrapping discharge and error propagation

The uncertainty on the load estimate resulting from the discharge rating curve was normally assumed to be negligible in previous uncertainty assessments (Mailhot *et al.*, 2008; Rustomji and Wilkinson, 2008; Vigiak and Bende-Michl, 2013). One would expect that, as the sediment rating curve has much more uncertainty than the discharge rating curve, excluding the latter would not affect the confidence intervals much, but for our dataset, this assumption did not hold: even having a discharge rating curve with high accuracy (R^2 of 0.98), its uncertainty had a considerable effect on the load estimate, which increased from 6389 Mg when not bootstrapping the discharge, to 6781 Mg when bootstrapping the discharge, as well as on the width of the confidence interval.

This result underscores the importance of error propagation in uncertainty assessments. Even though the discharge rating curve has a high accuracy, an estimate of Q is used as a predictor variable for concentration, and the concentration then gets multiplied with the estimate of Q, and so the effect is not as small as one would expect based on the R^2 of both rating curves. If we assume that most discharge rating curves have around 95% of explained variance, this could imply that most measures of uncertainty in literature are too conservative by about 10% in terms of width of the CI and that this increase would be mostly on the upper limit of the interval – implying that minimum impact estimates would not be affected much, but that literature to date would underestimate worst case scenarios of sediment yield, nutrient loss or erosion with about 10%.

3.6 Conclusions

The approach developed in this paper provides a means to assess uncertainty on any type of constituent load, which was calculated from continuous constituent concentration and discharge predictions estimated with regression-type methods. Compared to Ordinary Least Squares regression methods to obtain load estimates,

bootstrap estimates resulted in bias-corrected estimates that can take serial correlation into account when present, as well as providing a measure of uncertainty on the load estimate. Uncertainty assessments can be obtained, whether daily, weekly, monthly or annual loads are required.

The results show that, even when the uncertainty of the discharge rating curve is small, it is important to take into account that the errors propagate by using discharge both as a predictor variable for constituent concentration and in the instantaneous load equation. Application of the method in different watersheds, at different spatial and temporal scales could elucidate whether discharge is an important driver of uncertainty in those settings as well. The approach in its current form cannot, however, be extended to situations where loads are not estimated from regression-type models for concentration and discharge, such as in ungauged catchments.

The confidence intervals resulting from our proposed method showed that the uncertainty on the loads is quite large and is mostly on the upper limit of the estimate, as the intervals were strongly right-skewed. This asymmetry implies that, wherever load estimates are used to assess environmental impact, without reporting an uncertainty assessment, the maximum impact could be severely underestimated.

Additionally, the bootstrap process demonstrated that load estimates are biased downwards if calculated directly from the data. While some alternative bias corrections are available, these are not consistently used, and this is another factor contributing to the underestimation of constituent loads thus far reported in literature. Taking the median of the bootstrap estimates is an easy and generally applicable way to obtain unbiased estimates.

Reporting uncertainty is especially important when water quality models are complex. There has been a great increase in the use of more complex predictive methods for water quality, for example the use of Artificial Neural Networks, Random Forests or Generalized Additive Models (Berk, 2008). The advent of these methods makes the consistent reporting of measures of uncertainty even more essential: the more complex a model is, the more prone it is to overfitting (Burnham and Anderson, 2002), as was demonstrated by the inflated confidence intervals when

adding predictor variables to the sediment concentration model. Some measure of uncertainty should systematically be shown for any load estimate, and the method developed in this paper provides a flexible framework to do so.

Chapter 4 Sediment trap efficiency of paddy fields at the watershed scale in a mountainous catchment in Northwest Vietnam[4]

J.I.F. Slaets[a], P. Schmitter[b], T. Hilger[a], T.D. Vien[c], G. Cadisch[a]

[a] Institute of Plant Production and Agroecology in the Tropics and Subtropics, University of Hohenheim, Garbenstrasse 13, 70599 Stuttgart, Germany

[b] The International Water Management Institute, Nile Basin and East Africa Office, Addis Ababa, Ethiopia

[c] Centre for Agricultural Research and Ecological Studies (CARES), Vietnam National University of Agriculture, Hanoi, Vietnam

4.1 Abstract

Composite agricultural systems with permanent maize cultivation in the uplands and irrigated rice in the valleys are very common in mountainous Southeast Asia. The soil loss and fertility decline of the upland fields is well documented, but little is known about re-allocation of these sediments within the landscape. In this study, a turbidity-based linear mixed model was used to quantify sediment inputs, from surface reservoir irrigation water and from direct overland flow, into a paddy area of 13 hectares. Simultaneously, the sediment load exported from the rice fields was determined. Mid-infrared spectroscopy was applied to analyze sediment particle size. Our results showed that per year, 64 Mg ha^{-1} of sediments were imported into paddy fields, of which around 75% were delivered by irrigation water and the remainder by direct overland flow during rainfall events. Overland flow contributed one third of the received sandy fraction, while irrigated sediments were predominantly silty. Overall, rice fields were a net sink for sediments, trapping 28 Mg ha^{-1} a^{-1} or almost half of total sediment inputs. As paddy outflow consisted almost exclusively of silt- and clay-sized material, 24 Mg ha^{-1} a^{-1} of the trapped amount of sediment was estimated to be sandy. Under continued intensive upland maize cultivation, such a

[4] A version of this chapter has been submitted to Biogeosciences as:
Slaets, J.I.F., Schmitter, P., Hilger, T., Vien, T.D., Cadisch, G. Sediment trap efficiency of paddy fields at the watershed scale in a mountainous catchment in Northwest Vietnam.

sustained input of coarse material could jeopardize paddy soil fertility, puddling capacity and ultimately also food security of the inhabitants of these mountainous areas. Preventing direct overland flow from entering the paddy fields, however, could reduce sand inputs by up to 34%.

Keywords: Sediment budget, sediment particle size distribution, sediment yield, maize, irrigated rice, composite swiddening.

4.2 Introduction

Paddy cultivation is one of the most long-term sustainable cropping systems, as irrigated rice is the only major crop cultivated in monoculture for centuries without severe soil degradation (Bray, 1986; Uexkuell and Beaton, 1992). Two mechanisms facilitate this continuing productivity: first, flooding applies suspended particles and soluble nutrients to the fields that contribute to the indigenous nutrient supply (Dobermann, 1998; Schmitter *et al*., 2011). Second, puddling creates an environment of high input and low breakdown of organic matter (Cao *et al.*, 2006; Gong *et al.*, 2007; Huang *et al.*, 2015). As nutrient content of sediments is closely related to sediment particle size, and puddling is favored by high clay content (De Datta, 1981), the potential for long-term sustainable rice production is related to the soil texture in paddy fields.

Irrigated paddy fields, however, are not isolated elements in a landscape, as they are connected to surrounding upland areas. They receive sediments from those upland areas, both directly through overland flow, and indirectly from irrigation water released through surface reservoirs (Schmitter *et al*., 2012). These processes bring sediments into the rice fields, which can alter paddy soil texture (Schmitter *et al*., 2011). The vast majority of paddy fields in Vietnam are subject to these processes: 97% of Vietnamese rice is irrigated, and the main water source for irrigated rice in Southeast Asia is water from surface reservoirs (FAO Aquastat, 2014). Therefore, most paddy areas receive sediment-conveying irrigation water.

The amount and nature of sediments in irrigation water depends on their source, i.e. the upland fields surrounding both the paddy fields and the surface reservoirs. Traditionally, in the mountainous regions of Northern Vietnam, Thailand and Laos as

well as Southern China, paddy systems have been located in the valleys, surrounded by shifting cultivation on the hills. In Northern Vietnam, 60% of paddy cultivation is located in valleys of such hilly areas, on terraces that form cascades (Rutten *et al*., 2014).

In shifting cultivation systems, forest plots are cleared and burned followed by cultivation of subsistence crops. Cultivation lasts for one to three seasons, after which the plots are left fallowed for a prolonged time to recover soil fertility (often a minimum of six times the cropping duration (Ziegler *et al.*, 2009a)). Traditional shifting cultivation systems are very extensive in space and time, generating very limited runoff and erosion at the watershed scale (Ziegler *et al.*, 2009a). Gafur *et al.* (2003) reported soil losses amounting to 30 Mg ha^{-1} a^{-1} for an upland area with shifting cultivations, while the regional average sediment yield was 1.2 Mg ha^{-1} a^{-1}, as 43% of soil loss from upland areas was captured by filtering elements in the lower area of the watershed. Chaplot and Poesen (2012) similarly found large sediment accumulations downslope in a slash and burn system in Southeast Asia, pointing towards the lower impact of the land use at the watershed scale. In recent years, under the influence of market mechanisms and population pressure, the traditional shifting cultivation systems on the slopes have been replaced by permanent upland cultivation (Ziegler *et al.*, 2009a). Implications of these land use changes have been studied in detail on the upland fields, and the increased erosion due to these changes are well documented. Chaplot *et al.* (2007) found water erosion rates of 6 to 24 Mg ha^{-1} a^{-1} in an intensifying slash and burn system in Northern Laos. Lacombe *et al*. (2015) determined that conversion of fallow into teak plantation versus forest communities has opposite effects on catchment hydrology. Infiltration increased and runoff decreased for the forest communities, while the opposite was true for the teak conversion, illustrating how the effects of disappearing fallow strongly depend upon the replacing vegetation. In our study area, maize and maize-cassava intercropping on steep slopes with clay topsoil texture resulted in plot-level erosion rates in bounded plots of up to 174 Mg ha^{-1} a^{-1} (Tuan *et al*., 2014), coupled with a loss of soil organic matter reaching 1 Mg ha^{-1} a^{-1} (Häring *et al.*, 2014). Additionally, changes in texture occurred as fertile silt and clay fractions were exported from the upper and middle slope positions whereas sandy material was deposited at foot slope positions (Clemens *et al*., 2010). Differences in amount and texture of eroded material from

upland fields could therefore entail a shift in matter exchange between upland cultivation and valley paddy rice.

Increased erosion may thus not only jeopardize the continued production of the cash crop maize on upland fields, but also adversely affect the long-term sustainability of the food crop production in the paddies. Schmitter *et al.* (2010) showed that soil fertility in paddy cascades varies with distance to the irrigation channel, establishing a link between sedimentation processes and soil properties. Rüth and Lennartz (2008) and Schmitter *et al.* (2011) found that variability of paddy soil texture and yield were a function of position along the catena, related to differential settling of sediments in irrigation water. If soil properties and yield are closely linked to sedimentation processes, then changes in amount and texture of the sediment inputs have a potential effect on long-term soil fertility and crop production, and hence on food security in the area, as rice is the main staple food crop.

In order to assess these risks, there is a need for reliable data not only on the amount and texture of sediments entering the paddy fields, but also on the quantity and quality of the material exported from the paddies. Because of their terraced structure, paddies can function as a sediment filter in the landscape (Maglinao *et al*., 2003). But few studies have assessed both inputs and exports. Dung *et al*. (2009) monitored a watershed in Northern Vietnam with shifting cultivation in the upper area of the catchment and paddy rice in the valley. Annually, for an experimental plot of 0.3 ha, between 11 and 29 Mg of sediments entered the paddies, and from this amount, 27 to 63% was trapped within the field and the remainder was exported with the runoff. The proportion that remained behind was mostly sandy, and hence altered the soil texture in the experimental paddy plots.

While these results indicate that paddy fields act mainly as a net sediment trap, their function might differ when up-scaled to a larger area as sediment deposition changes over cascade length (Schmitter *et al.*, 2010). Thus, at the watershed level, it is not clear whether paddy fields act as sediment sources or sinks. For example, Mai *et al.* (2013) found that paddies acted as a green filter, reducing runoff peaks, when their water storage capacity was not yet fully used by irrigation at the onset of the runoff event. But if the maximum storage capacity was already reached, runoff increased, as

full paddies are not able to retain any water and so all overland flow was propelled through them, causing high runoff peaks at the catchment outlet.

Therefore, there is a need for a more detailed understanding of sediment fluxes and budgets in paddies at watershed-scale. Our specific aims were to (i) quantify the contribution of overland flow and irrigation water to the sediment inputs of a paddy rice area, (ii) determine if paddy fields are a net sediment source or a sink, (iii) assess the particle size distribution for the sediment input and export from paddy fields, and (iv) evaluate the potential effects of within-watershed sediment re-allocation on long-term soil fertility in Chieng Khoi watershed, Northwest Vietnam.

4.3 Material and Methods

4.3.1 Study site

The study was conducted in a small agricultural watershed, located in Chieng Khoi commune, Yen Chau district, Son La province, North-West Vietnam (21°7'60''N, 105°40'0''E, 350 m a.s.l., Appendix B). The catchment is 200 ha in size, and sediment re-allocation in a sub-catchment of 50 ha which consists of 13 ha of paddy rice and 37 ha of upland fields was monitored in greater detail. In the area, the dominant soil types are alisols and luvisols (Clemens *et al*., 2010) and the climate is monsoonal, with a rainy season from April till October and average annual rainfall of around 1200 mm. Land use in the watershed is characterized by maize and maize-cassava intercropping on the slopes, and irrigated rice in the valleys. The source of irrigation water is a surface reservoir that feeds a concrete irrigation channel, ensuring two rice crops per year: a spring crop from February till June, followed by a summer crop planted in July and harvested in October. The reservoir was formed by the damming of a river that originates in the karst mountains of the area. It has a capacity of 10^6 m^3 and a contributing area consisting of 490 ha of intensively cultivated upland fields and forest. The channel splits in two, just below the reservoir, and feeds two paddy rice areas (6.5 ha each), on the banks of a river that intersects the paddy fields. The irrigation water flows from the channel into the paddy fields, which drain into the river (Figure 4.1).

4.3.2 Hydrological monitoring

Discharge and sediment concentration were monitored at five different locations in the catchment (Figure 4.1, Appendix B and Table 4.1). As the irrigation management in the catchment disturbed the relationship between discharge and sediment concentration, a turbidity-based method was used to monitor the sediment concentration. Self-cleaning turbidity sensors (NEP395, McVan, Australia) were installed, with the optical eye down, in a vertically suspended pipe that could float with water level fluctuations, ensuring that the sensor remained approximately at the center point of flow.

Discharge was monitored using pressure sensors (Ecotech, Germany) and the stage-discharge relationship was established using the salt dilution method for the channel and the area-velocity method for the river (Herschy, 1995). Rainfall was measured with a tipping-bucket rain gauge (0.1 mm accuracy, Campbell Scientific, USA) in the upper part of the catchment. The water level of the lake was recorded on a daily basis.

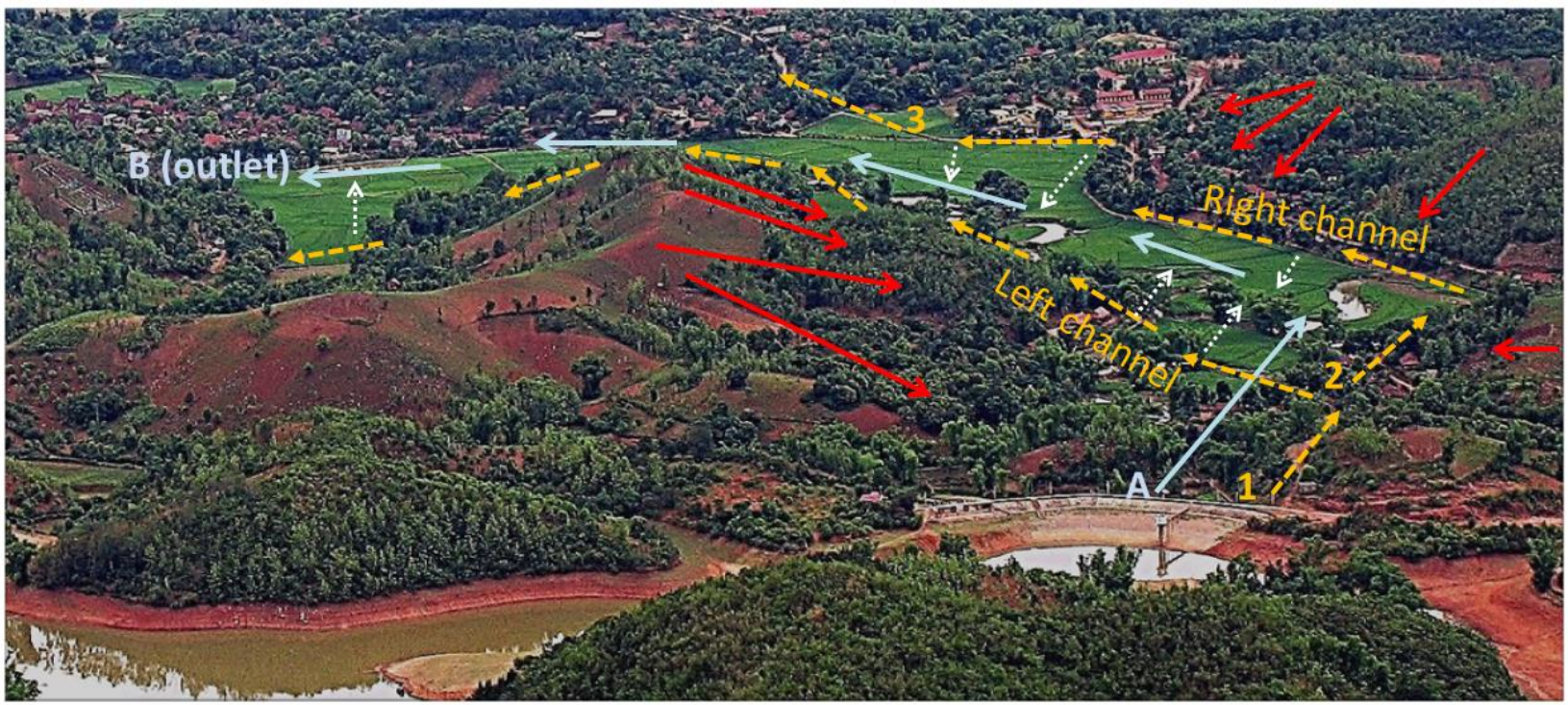

Figure 4.1: Sediment sources and water flows into and out of paddy rice fields in Chieng Khoi watershed. The dotted yellow arrows show the irrigation channel leaving the reservoir and splitting in two, feeding the two banks of paddy rice. The rice fields subsequently drain into the river, which is indicated by the blue arrows. During rainfall, runoff generated on the uplands flows into the irrigation channel and the paddy fields (red arrows). Measurement locations are indicated with numbers in the channel (1: reservoir outflow, 2: channel split, 3: channel leaving watershed) and with letters in the river (A: river before paddy fields drainage, B: river after paddy fields drainage).

4.3.3 Sediment concentration predictions

Water samples were collected manually with a storm-chasing approach, where more samples were taken when water level and turbidity were rapidly changing. The sampling interval depended on the hydrograph. During rapid changes in turbidity, samples were taken more frequently (up to two minutes apart) than at the end of the falling limb (up to 15 minutes apart). A typical sampled rainfall event thus consisted of ten to twenty water samples, depending on the duration of the event. Additionally, base-flow samples were collected every two weeks. Total sample sizes for each location are shown in Table 4.1 and ranged from 71 to 327 samples. Each sample consisted of a 500 ml bottle. Sediment concentration in the samples was determined gravimetrically (ASTM, 2013) as recommended for samples with very high Suspended Sediment Concentration (SSC), by letting the sediment settle overnight in cold storage (<4°C) and then siphoning off the supernatant followed by oven-drying of the sediment at 35°C until the sample weight remained constant.

Field calibration of the sensors resulted in continuous statistical predictions of sediment concentration for the two year study period (temporal resolution of two minutes) which were obtained from a linear mixed model (Slaets *et al.*, 2014). The linear mixed model is a regression-type model with SSC as response variable and turbidity, discharge and cumulative rainfall as predictor variables. As the storm-based approach resulted in samples taken at very short consecutive time intervals (i.e. 2 min), the assumption required for a traditional sediment rating curve of independence of errors was not fulfilled in this dataset. Similarly, we found the variance to increase with increasing sediment concentration, violating the assumption of homoscedasticity. To account for temporal correlation in the observations, an error with a first-order autoregressive covariance structure was fitted to the data. The response variable was log-transformed to stabilize the variance, as were the predictor variables discharge and turbidity. The models were validated with five-fold cross validation using a SAS macro described in Slaets *et al.* (2014).

4.3.4 Separating sediment sources

There are only two sources of sediment inputs to the paddy area: sediments in irrigation water from the surface reservoir, and overland flow which enters the paddies via the channel. The paddies are isolated from surrounding uplands by the channel, and no overland flow enters the paddies without passing through the

irrigation channel (Figure 4.1). The monitoring locations in the concrete irrigation channel were chosen in order to separate these contributions of irrigation water from the surface reservoir, and Hortonian overland flow, to the paddy fields. The station situated furthest upstream in the channel (Location 1 in Figure 4.1) was placed directly below the reservoir outlet, and thus monitored the discharge and water quality of the surface reservoir, which equals the sediment concentration of paddy inflow when it is not raining. An additional station (Location 2 in Figure 4.1) was installed directly below the split of the concrete channel, and monitored only discharge, as the water quality here was the same as at Location 1. This second location quantified how much of the irrigation was flowing to the left arm of the irrigation channel after the split, and how much was going to the right arm. As the water in the left channel was fully irrigated to the paddy fields in this watershed, no further measurements were conducted in this branch of the channel. But the right channel leaves the watershed, exporting part of the irrigation water from the catchment. Therefore, a measurement station was installed downstream in the channel, at the point where the irrigation channel crosses into a neighboring watershed (Location 3 in Figure 4.1). Thus, sediment inputs from reservoir outflow to both banks of the paddy area could be quantified.

In the absence of rainfall, Location 3 received water with the same sediment concentration as the reservoir outflow (Location 1). As there were no other water sources entering the concrete-lined waterway, the hydrological balance when it is not raining can be described by

$$Q_{in} = Q_{irr} + Q_{out}, \qquad \text{(Equation 4.1)}$$

where Q_{in} is the discharge measured at Location 2, consisting of the irrigation water originating from the reservoir, Q_{irr} the irrigated discharge to the paddies, and Q_{out} the discharge measured at Location 3, as not all irrigation water in the channel was used up fully in this catchment, but a part was transported further to irrigate rice in a watershed downstream. Since Q_{in} is the discharge measured at Location 2 and Q_{out} is the discharge measured at Location 3, Q_{irr} can be calculated as the difference in discharge between those two sites.

During rainfall events, Hortonian overland flow entered the channel directly from the upland fields (Figure 4.1), changing the water balance to

$$Q_{in} + Q_{pp} + Q_{of} = Q_{irr} + Q_{out}, \quad \text{(Equation 4.2)}$$

where Q_{pp} is the direct rainfall into the channel and Q_{of} the overland flow that enters the channel from the upland area between the upstream and downstream locations. During rainfall, Q_{pp} could be calculated directly from the rainfall intensity and the surface area of the channel. Assuming that the irrigated discharge to the paddy fields prior to the onset of a particular rainfall event remained constant during the duration of that specific rainfall event, Q_{of} can be calculated using Equation 4.2. Flow component separation was performed with the statistical software R. Details of the procedure can be found in Schmitter *et al.* (2012).

4.3.5 Sediment load estimates

Instantaneous sediment loads at a time *i* (*i*=1 to *t*) are generally estimated from the continuous discharge data and the continuous sediment concentration predictions according to

$$\hat{L}_i = \hat{Q}_i \times \hat{c}_i\,, \quad \text{(Equation 4.3)}$$

where $\hat{L}_i$ is the estimated instantaneous load at time *i* in g s^{-1}, $\hat{Q}_i$ is the estimated discharge at time *i* in m^3 s^{-1} and $\hat{C}_i$ is the estimated concentration at time *i* in g m^{-3}. These concentrations for each specific location were derived from the continuous sediment predictions using the location specific SCC regression function, where the time series consisted of two minute intervals. As such, the estimated monthly or annual sediment load $\hat{L}_{1\,to\,t}$ in grams can be computed by summing up the instantaneous loads, across *t* measurement intervals of turbidity and discharge:

$$\hat{L}_{1\,to\,t} = \sum_{i=1}^{t}(\hat{L}_i \times 120). \quad \text{(Equation 4.4)}$$

Rainfall does not contain sediment, so Q_{pp} makes no contribution to the sediment load. The full sediment load balance for the irrigation channel then equals

$$L_{in} + L_{of} = L_{irr} + L_{out}, \quad \text{(Equation 4.5)}$$

where L_{in} is the sediment load at Location 2, L_{of} is the sediment load brought into the channel by direct runoff during rainfall events, L_{irr} is the load irrigated to the paddies, and L_{out} is the sediment load exported from the channel at Location 3, with L_{in}, L_{irr} and L_{out} in Equation 4.5 computed using Equation 4.4. The sediment load from direct runoff during rainfall is then the only remaining unknown in Equation

4.5: The sediment concentration c_{in} of Q_{in} was monitored at Location 1, and c_{out} of Q_{out} at Location 3. The irrigated discharge to the paddy fields, Q_{irr}, had the same sediment concentration as the discharge exported from the watershed at Location 3, assuming full mixing. The sediment load from overland flow can then be calculated from

$$L_{of} = [(Q_{irr} \times c_{out}) + (Q_{out} \times c_{out}) - (Q_{in} \times c_{in})]. \quad \text{(Equation 4.6)}$$

In the river, the water sources are paddy outflow and reservoir overflow. The measurement stations were installed in a similar manner as they were in the irrigation channel, with one station upstream and one downstream of the paddy fields (Locations A and B in Figure 4.1). The only sediment input between these two locations was drainage from paddy fields and fish ponds in the paddy area. The river receives outflow from both banks of paddy fields, and we only monitored the overland flow entering the right bank. Therefore, in order to quantify the net sediment balance for the paddy fields, the assumption is made that the upland fields on the left bank of the river generated the same amount of erosion as those on the right bank, as the areas are very similar in land use, slope and size (17 and 20 hectares of contributing area).

There was one additional measurement location in the river further downstream (overall outlet, Appendix B), at the outlet of a larger watershed of 2 km^2 in which the monitored paddy area was nested, in order to assess scaling effects on paddy watershed sediment losses.

In order to calculate 95% confidence intervals on the sediment load, a bootstrap method was used that accounts for uncertainty in the discharge and sediment concentration predictions (Slaets *et al.*, in revision). The number of bootstrap replicates was 2000. As the direct sediment load estimation described in Equation 4.3 is typically biased downwards when concentration and discharge are predicted on the log-transformed scale (Ferguson, 1986), taking the medians of the bootstrap replicates is a simple approach to bias-correct the estimates (Efron and Tibshiriani, 1993). Therefore, the estimated sediment loads reported in this study are the medians of the bootstrap empirical distribution, rather than the direct estimates from Equation 4.3 (Slaets *et al.*, in revision).

4.3.6 Sediment texture with mid-infrared spectroscopy

Texture analysis with conventional methods typically requires a minimum of one gram of sample. Collecting this amount can be unpractical when the sediment is obtained from water samples which have a very low sediment concentration. The base-flow sediment concentrations in this study fluctuated around 250 mg L^{-1}, which would mean that samples of approximately 4 L would have to be collected, transported, refrigerated for storage and analyzed. Diffuse reflectance Fourier transform mid-infrared spectroscopy (MIRS) is a practical alternative to conventional methods for determining particle size distribution on sediment samples, as only 25 mg is needed for analysis and the measurement is not destructive (Schmitter *et al*., 2010). From the samples collected for sediment concentration analysis, the sediments of a total of 152 samples were selected to cover the full range of locations, seasons and flow regimes, and analyzed for texture. A Bruker Tensor-27 mid-infrared spectroscope (Bruker Optik, Germany) was used and three analytical replicates were measured per sample. Baseline correction and atmospheric compensation were performed on each spectrum before averaging the analytical replicates. As the MIRS method requires a subset of the samples to be analyzed with conventional wet analytical methods for calibration and validation, laser diffraction with a Coulter LS 200 (Beckman Coulter, Germany) was performed on 50 samples. Organic matter and carbonates were destroyed prior to laser diffraction analysis and samples were shaken overnight with a dispersing agent (5 ml 2% sodium metahexaphosphate for 5 g soil). Three analytical replicates were done per sample.

Sand, silt and clay were predicted from the spectral data using Partial Least Squares Regression (PLSR; Wold, 1966). All spectral manipulation and model selection was performed using Quant2 package within the software Opus 7.0 (Bruker Optik, Germany). Models were evaluated with leave-one-out cross validation. Opus offers several spectral processing techniques to enhance spectral information and reduce noise. The selection of the most suitable method can be automatized using the Optimization function, which selects the method resulting in the highest r^2 of observed versus predicted values after cross-validation. For sand, the pre-processing method was the calculation of the second derivative of the spectra, which can help to emphasize pronounced but small features over a broad background. After validation, an r^2 of 0.81 was obtained. For silt, multiplicative scattering correction was applied, which performs a linear transformation of each spectrum for it to best match the

mean spectrum of the whole set, and the model resulted in an r^2 of 0.83. For clay, no satisfactory model could be obtained, and so the clay percentage was calculated as the remaining amount of sediment after subtracting the sand and silt fractions.

4.4 Results

4.4.1 Hydrological processes driving sediment flows

Model fit for the discharge rating curves varied between locations, with the coefficient of determination ranging from 0.96 to 0.99 (Table 4.1). As expected, accuracy of the sediment rating curves was lower than that of the discharge rating curves, and explained between 52 and 72% of variability in the data after cross-validation.

Table 4.1: Number of observations (n), coefficient of determination (R^2) and method used for stage-discharge relationship (Q); and number of observations and Pearson's correlation coefficient (r^2) after five-fold cross-validation for suspended sediment concentration predictions (SSC). Details on the linear mixed model development can be found in Slaets *et al*. (2014).

	Stage-discharge relationship (Q)			Suspended sediment concentration (SSC)	
	n	**R^2**	**Method**	**n**	**r^2**
Channel (1)	6	0.99	Salt dilution	Identical to location 3	
Channel (2)	6	0.99	Salt dilution	Identical to location 3	
Channel (3)	6	0.96	Salt dilution	327	0.72
River (A)	9	0.99	Area-velocity	145	0.52
River (B)	8	0.98	Area-velocity	71	0.66
River (main outlet)	15	0.98	Area-velocity	228	0.56

In 2010, a total of 920 mm of rainfall was measured between April and October with the onset of the rainy season in April, whereas in 2011, 961 mm fell but rains were delayed, resulting in less rainfall in April- May and a precipitation peak in July, and 780 mm of the annual rain falling between June and October. The lower amount of precipitation in the spring of 2011 resulted in a lower amount irrigated during that period (Figure 4.2). Although the total amount of water irrigated to the 13 ha of paddy fields was similar, i.e. $3\,978 \cdot 10^3$ m^3 in 2010 and $4\,021 \cdot 10^3$ m^3 in 2011, the seasonal distribution of the irrigated amounts varied between the study years. As the rainy season started late in 2011, there was more water irrigated during the first rice season (February-June) in 2011 ($913 \cdot 10^3$ m^3) than in 2010 ($700 \cdot 10^3$ m^3). The opposite was true for the summer crop (July-October), during which $1\,308 \cdot 10^3$ m^3

was irrigated in 2011 compared with 1 448·10^3 m^3 in 2010. As the rains came late in 2011, the reservoir was not filled up yet in July at the start of the summer crop, and so there was less irrigation water available.

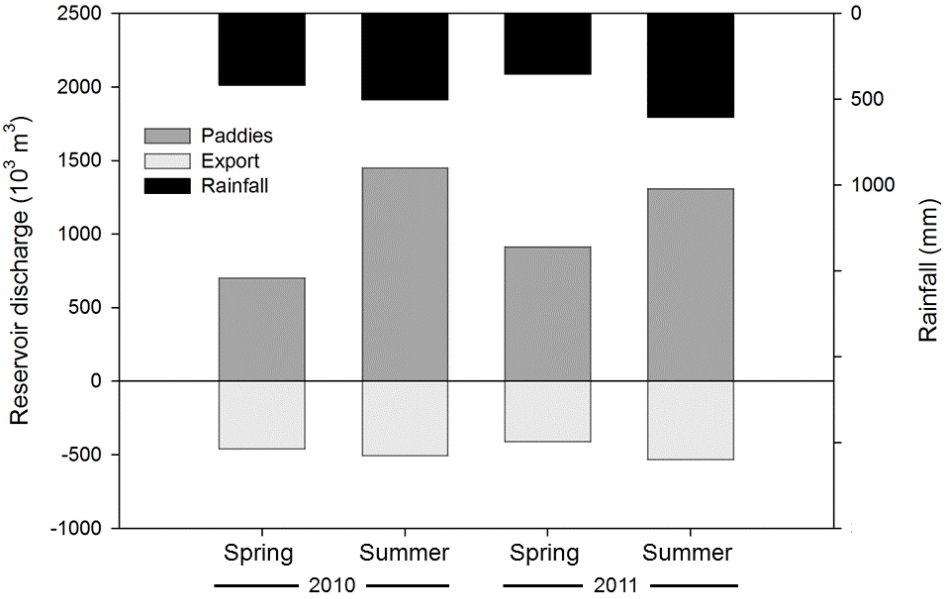

Figure 4.2: Total discharge from the reservoir irrigated to the 13 ha paddy area draining between Locations A and B in the river, and total discharge exported (negative on the Y-axis) from the sub-watershed via the irrigation channel at Location 3, per rice crop (spring, summer) per year, and amount of rainfall per rice crop per year.

Variation in rainfall throughout the year was also reflected in the sediment concentration of the irrigation water. In the irrigation channel, the median sediment concentration during base-flow regime was 240 mg L^{-1}. The predicted base-flow sediment concentration fluctuated seasonally, peaking in April and May 2010 and in April, May and June 2011 (Figure 4.3b), and resulting in a higher median in those months, between 350 and 430 mg L^{-1}. As for sediment texture, the sand content of the sediments in the irrigation channel during base-flow regime (n=18) varied between 0 and 50% with an average of 34% over the whole study period (Table 4.2). The silt content ranged from 14 to 58% with an average of 34%. For clay, the minimum measured content was 0%, the maximum was 86% and the average clay content of the sediments was 32%.

Table 4.2: Minimum, average and maximum sediment particle size distribution measured in the water samples collected at the different measurement locations for the different components of the paddy area sediment balance

Sediment source	% sand			% silt			% clay		
	min	av	max	min	av	max	min	av	max
Reservoir water – Location 1	0	34	50	14	34	58	0	32	86
Overland flow	0	50	100	0	30	61	0	20	61
River – Location A	29	61	89	9	22	40	0	17	80
River – Location B	1	47	74	17	33	47	9	20	53

The median sediment concentration in the irrigation channel during rainfall events was 1 200 mg L^{-1}, and the concentration reached a maximum of 70 000 mg L^{-1} (Figure 4.3a) during the rainfall event on 12th of July 2011, during which 70 mm of precipitation fell in just over one hour. The water samples taken during rainfall events in the channel (n=109) showed a different particle size distribution than those taken during base-flow, with higher proportions of coarser particles: on average, 50% of sand, 30% of silt and 20% of clay were measured during the full duration of rainfall event sampling (Table 4.2). When only looking at the peak sediment concentration of each event (thus excluding rising and falling limb samples), sand concentrations were higher and varied from 29 to 94% with an average of 72% for the 14 measured events.

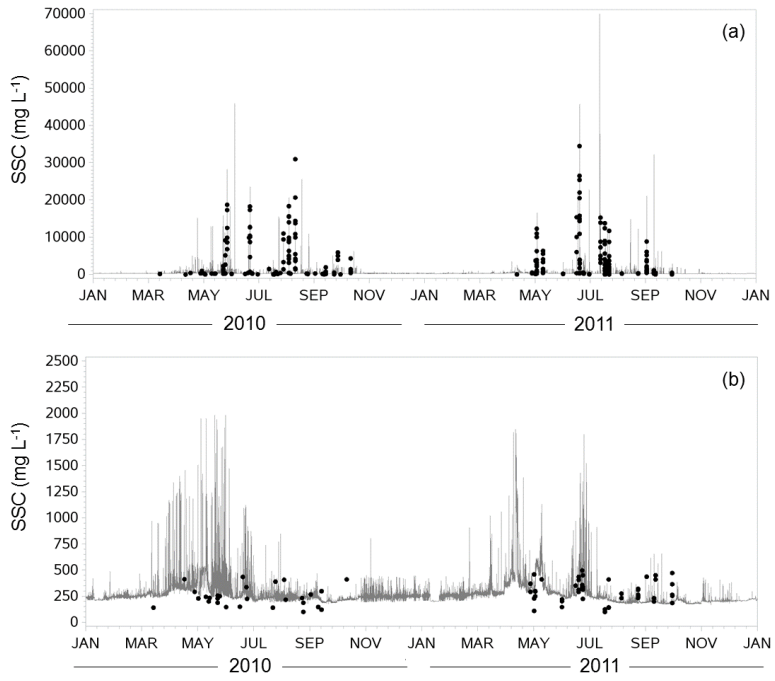

Figure 4.3: Observed and predicted sediment concentrations (in mg L^{-1}) for Location 3 in the irrigation channel (a), and zooming in on base-flow, showing only non-event samples and concentration predictions (b).

In the river, the median of the suspended sediment concentration predictions was 300 mg L^{-1} during periods of no rainfall (data not shown). There were no differences in base-flow concentrations between Locations A and B. The river sediment concentrations were very little affected by overland flow as the paddy fields buffered inputs from Hortonian overland flow, and so the maximum concentrations in the river only reached up to 5 000 mg L^{-1}. Water samples of Location A in the river, upstream of the paddy fields, had on average 61 % sand, 22% silt and 17% clay (n=12, Table 4.2). After paddy discharge, the river sediment texture on average had 47% sand, 33% silt and 20% clay (n=13, Table 4.2).

In the river at the overall outlet of the larger catchment, the median base-flow concentration was 190 mg L^{-1} (data not shown). Between Location B and the overall outlet, an additional 47 ha of paddy rice drain into the river, adding filtered irrigation water with lower sediment content to the river, resulting in a lower sediment concentration during base-flow at the overall outlet compared with Location B. During rainfall events, concentration increased at the overall outlet, with a maximum peak of 22 000 mg L^{-1} on June 5th 2010 when 46 mm of rain fell in 160 minutes.

These peak concentrations during rainfall events were higher than those measured at the same time at Location B. As there are point sources of overland flow that reach the stream directly at the overall outlet, the river is not completely isolated from overland flow as it is in Location B where the paddy fields buffered the input of runoff from upland fields, explaining the difference in peak concentrations between these two stations.

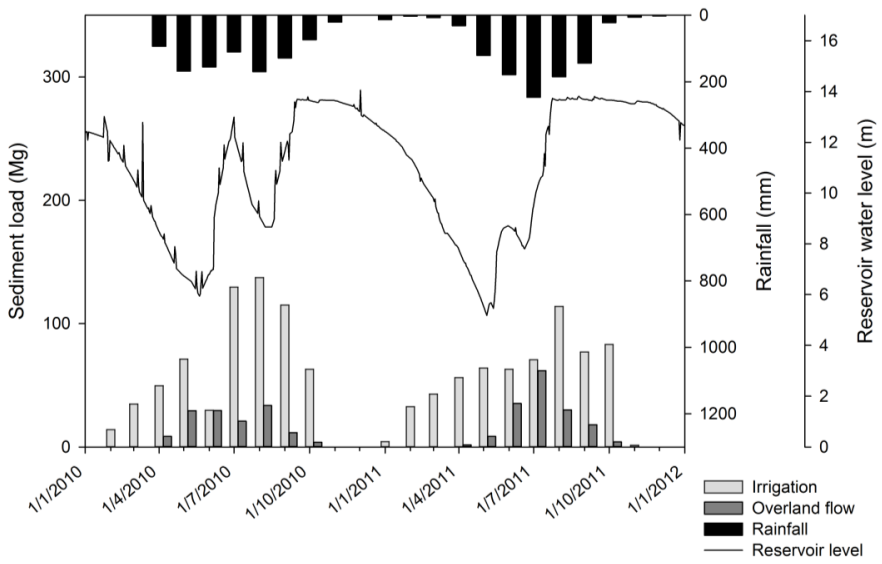

Figure 4.4: Monthly variations in rainfall, reservoir water level, and sediment load inputs to the paddy fields, both from the surface reservoir and from overland flow

4.4.2 Seasonal sediment load trends in the irrigation system

Monthly sediment loads from irrigation water (Figure 4.4) reflected changes in the suspended sediment concentration (Figure 4.3b), related to fluctuations in the level of the surface reservoir (Figure 4.4) as well as changes in amount of water irrigated to the paddy fields. The first rice crop (from February till June) received about half the water volume of the second crop (Figure 4.2), as a smaller area of the paddy fields was cultivated during the spring season, resulting in a lower sediment input from irrigation during the spring season (200 Mg in 2010, 263 Mg in 2011) compared with the summer season (445 Mg in 2010, 346 Mg in 2011). The difference in load between the spring crop and the summer crop was smaller in 2011, as the rains came late that year. Consequently, the reservoir was depleted during the first rice crop and the first rains fell on a much smaller volume of water, increasing the sediment concentration in the reservoir, thus causing the higher sediment load compared with

2010. In the summer season of 2011, the irrigated amount of water was 10% less than in 2010 (Figure 4.2), as the rains came late and the irrigation manager wanted to preserve water. Overall, the largest sediment inputs from irrigation occurred in August in both years of the study (Figure 4.4), with 137 Mg of sediments in 2010 and 114 Mg in 2011.

Table 4.3: Sediment inputs from irrigation water and overland flow from the 37 ha upland area in the sub-watershed, and sediment export and trapping by the 13 ha paddy area (Figure 4.1 and Appendix B). Loads are estimated as the median of the bootstrap estimates (Med) and therefore do not always sum up exactly within columns, and 95% confidence intervals are shown (LL=lower limit, UL=upper limit) in Mg per year (Mg a^{-1}).

	Sediment load (Mg a^{-1})					
	2010			2011		
Sediment source	**LL**	**Med**	**UL**	**LL**	**Med**	**UL**
Reservoir water:						
Total to channels …	617	806	1123	587	762	1331
… irrigated paddy area	492	646 (77%)	903	496	612 (74%)	1085
… exported via channel	124	160	222	117	150	248
Spill-over to river	nd	nd	nd	917	1556	18128
Overland flow:						
Total to channels …	121	249	303	129	278	516
… irrigated to paddy area	119	193 (23%)	302	110	219 (26%)	517
… exported via channel	36	56	88	35	59	135
Total paddy input		839 (100%)			832 (100%)	
Paddy outflow	nd	nd	nd	-361	469 (56%)	2555
Net paddy balance	nd	nd	nd	-1625	363 (44%)	1586
Paddy balance per ha					28 Mg ha^{-1} a^{-1}	

Even though the sediment concentration in the overland flow was orders of magnitude higher than the concentration in the irrigation water (Figure 4.3), over a full year, the contribution of irrigation water was about three times larger than the contribution of overland flow (Table 4.3). As the rainy season starts in April, paddy

water inputs from overland flow play a more important role during the second rice crop. The contribution of overland flow was almost negligible during the first rice crop, particularly in 2011 when the onset of the rains was late and the volume of overland flow was much smaller during the first crop (Figure 4.5). During that spring cropping season of 2011, the contribution of overland flow to the sediment input of the paddy fields was negligible, reaching only 46 Mg compared to 263 Mg from irrigation water. But during July 2011, the month in the study which had the highest rainfall (247 mm), direct overland flow provided almost as much sediments to the paddy fields as irrigation water from the reservoir (62 Mg versus 71 Mg).

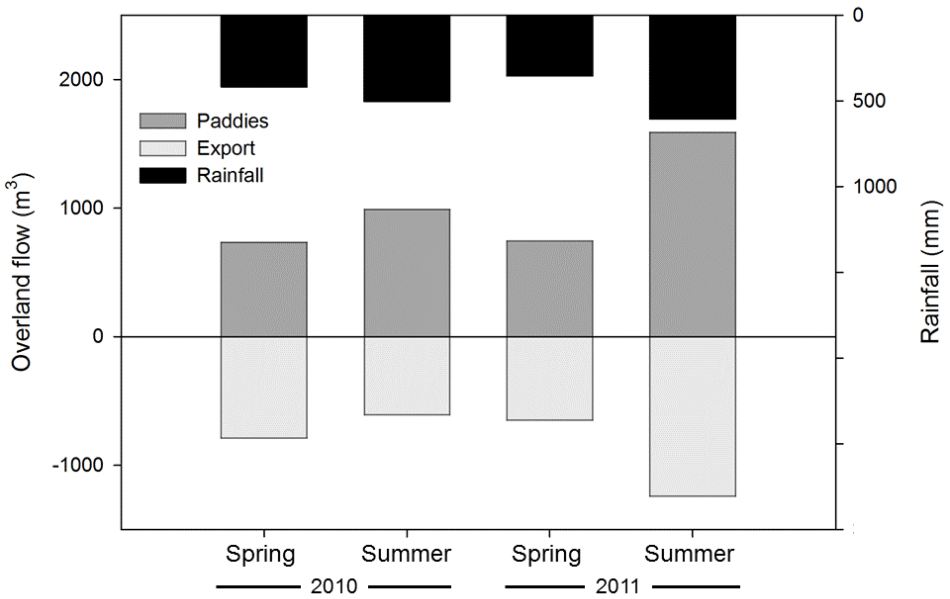

Figure 4.5: Total amount of water from overland flow during rainfall events, irrigated to the paddy fields and exported (negative on the Y-axis) out of the sub-watershed via the irrigation channel per rice crop per year, and amount of rainfall per rice crop (note the different units on the Y-axis compared to Figure 4.2).

4.4.3 Sediment budget for paddy fields

Irrigation water from the surface reservoir removed 806 Mg of sediment from the reservoir in 2010 (Table 4.3). Of this amount, 646 Mg entered paddy fields through irrigation and 160 Mg were exported from the sub-watershed, as the irrigation channel crosses the watershed border into a neighboring catchment. In 2011, the sediment load from the irrigation water was similar with 762 Mg, of which 612 Mg entered the rice fields, and 150 Mg were exported to the next catchment. Using the

average textural class percentages of the surface reservoir outflow, irrigation water can be estimated to have contributed 208 Mg of sand, 208 Mg of silt and 196 Mg of clay to the paddy rice fields in the watershed in 2011 (Table 4.4). As there were not enough samples analyzed to obtain continuous predictions of the different particle size classes using a regression model, simple averages were used for the texture loads. In this sense, all reported sand, silt and clay loads are more a semi-quantitative estimate that provides an order of magnitude, rather than an exact figure.

Table 4.4: Texture-specific sediment inputs from irrigation water and overland flow from the 37 ha upland area in the sub-watershed, and texture-specific sediment export and trapping by the 13 ha paddy area (Figure 4.1 and Appendix B). Percentages express proportions compared to total inputs (100%) of that textural class. (nd = not determined)

	Load (Mg a^{-1})					
	2010			2011		
Sediment source	**Sand**	**Silt**	**Clay**	**Sand**	**Silt**	**Clay**
Reservoir water:						
Total to channels …	274	274	258	259	259	244
… irrigated to paddies	220 (70%)	220 (79%)	207 (84%)	208 (66%)	208 (76%)	196 (82%)
… exported via channel	54	54	51	51	51	48
Spill-over to river	nd	nd	nd	950	343	265
Overland flow:						
Total to channels …	124	75	50	139	83	56
… irrigated to paddies	96 (30%)	58 (21%)	39 (16%)	109 (34%)	66 (24%)	44 (18%)
… exported via channel	28	17	11	30	17	12
Paddy input (100%)	316	278	246	317	274	240
Paddy outflow	nd	nd	nd	2	326	141
Net paddy balance	nd	nd	nd	+315 (99%)	-52	+99 (40%)

For the upland area bordering both irrigation channels (37 ha), overland flow generated a sediment load of 249 Mg in 2010 and 278 Mg in 2011. Of this total amount, 193 Mg of overland flow sediments actually entered the paddy fields in 2010 and 219 Mg in 2011. The remainder of the sediments was exported from the watershed through the irrigation channel (Table 4.3). Again assuming average

texture values, the input of overland flow to the paddy fields in 2011 hence consisted of 109 Mg of sand, 66 Mg of silt and 44 Mg of clay (Table 4.4). Thus the combined addition to the paddy fields from reservoir outflow and overland runoff amounted to 318 Mg of sand, 274 Mg of silt and 240 Mg of clay (Table 4.4).

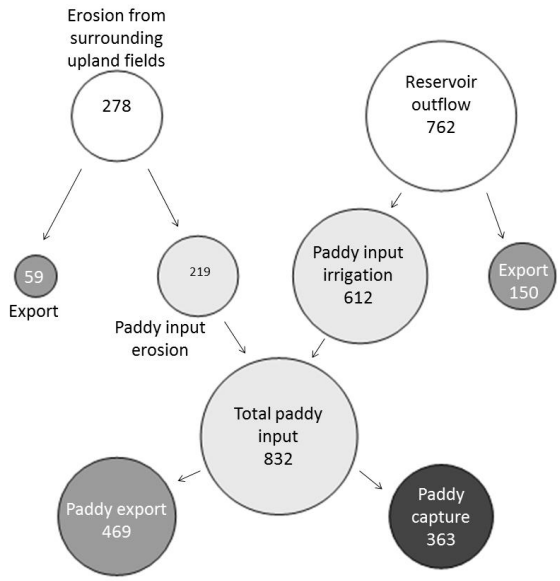

Figure 4.6: Sediment flow chart for 2011. Bubble size corresponds to size of the sediment load (in Mg a^{-1})

The sediment load exported from the paddy fields on both banks of the river, calculated as the difference between Location A and Location B, was 469 Mg in 2011 (Table 4.3), of which 60% was exported during the spring cropping season, and 40% during the summer crop. As the monitoring station in Location B was only installed in 2011, data for 2010 are not available. Combining all of these loads, the difference between inputs and export from the paddy area resulted in a sediment yield of 363 Mg in total, or 28 Mg ha^{-1} that remained in the rice fields in 2011. Since the load exported and the net paddy load are differences between positive numbers (loads measured at Location A minus B for the export, and inputs minus export for the net load), the lower limit of the confidence interval for these two estimates can become negative (Table 4.3). Negative load estimates can be interpreted as net sediment trapping of the paddy area. Looking at the texture-specific loads (Table

4.4), the sediments exported from the paddy fields consisted mostly of finer material. Thus, in 2011 approximately 326 Mg of silt and 141 Mg of clay were exported from the rice paddies. Combining inputs and losses, 315 Mg of sand and 99 Mg of clay remained behind in the paddy fields over the whole year, while a net amount of 52 Mg of silt was lost from the 13 ha paddy area (Table 4.4).

4.4.4 Watershed sediment yield

The total sediment yield of the sub-watershed, ending at Location B, was 2 234 Mg in 2011. This amount was exported via two pathways. First, the irrigation canal distributed 150 Mg from the reservoir and 59 Mg from the upland area through overland flow into the neighboring catchment (Table 4.3, Figure 4.6). Second, the river exported 2 026 Mg from the sub-watershed at Location B. Of these 2 026 Mg, a total of 469 Mg consisted of runoff from the paddy fields. The remaining 1 556 Mg that was lost through the river, originated from the surface reservoir as water released via the reservoirs spill-over, which allows excess water to flow into the river whenever the reservoirs maximum capacity is reached. For the larger watershed of 200 ha, which contains the aforementioned sub-catchment, the annual sediment yield was 6 262 Mg in 2010 and 5 543 Mg in 2011.

4.5 Discussion

4.5.1 Upland sediment contribution to the irrigation system

The largest peak of suspended sediment concentration found in this study was two to five times higher compared to the highest values found in other SE Asian studies (Ziegler *et al.*, 2014; Valentin *et al.*, 2008) and the corresponding event contributed 23% of the total annual sediment load transported by overland flow to the irrigation channel in 2011. The difference in sediment concentration with other studies is most likely due to the more gentle slopes (8 to 15 %) present in the watershed study of Valentin *et al.* (2008), whereas steep slopes up to 65% are found in our watershed. Both other studies, however, which contain the highest values found for Southeast Asia in literature, also used a storm-based sampling strategy, underscoring the importance of capturing the highest events in order to reliably assess the erosivity of mountainous catchments. Horowitz *et al.* (2014) reported that calendar-based sampling typically underestimates constituent transport, while event-based sampling does not. Capturing the highest peaks is crucial, as the importance of single, high-

intensity storms for sediment yield in tropical areas is increasing due to climate change. In the monsoon climates of Southeast Asia, a rise in extreme, high intensity rainfall events is expected (IPCC, 2013) and as single large storms already have such a substantial effect on the annual sediment load, in the future they can be expected to dominate annual sediment loads.

Our estimated upland sediment load of 278 Mg a^{-1} in 2011 translates into an annual soil loss of 7.5 Mg ha^{-1}, but this result should be interpreted as an average yield at the watershed level, not as a representative erosion rate at the plot level. This estimate is well within the order of magnitude reported by watershed-scale measurements. For instance, Valentin *et al.* (2008) monitored sediment yield from 27 catchments in mountainous Southeast Asia and found an average total annual sediment yield of 3.4 Mg ha^{-1}. Plot scale studies, however, frequently report larger erosion rates than the 7.5 Mg ha^{-1} found in our study. Also in the Chieng Khoi commune, Tuan *et al.* (2014) recorded an erosion rate averaging 44 Mg ha^{-1} a^{-1} for sediment fences in unbounded plots for maize-cassava intercropping systems. This discrepancy is typical when upscaling erosion rates (de Vente and Poesen, 2005), as processes are not linear. Erosion can be concentrated at certain hotspots and rill erosion, and internal deposition and filtering processes (e.g. hedges) leave part of the eroded sediments behind within the watershed (Verstraeten and Poesen, 2001). Indeed, in our watershed, the mix of homesteads, maize and maize-cassava cropping and trees on the hills affect both sediment delivery pathways and re-deposition opportunities. The plot-level soil loss on upland fields can thus be expected to exceed the value of 7.5 Mg ha^{-1} that enters the irrigation channel, as a proportion of eroded sediments will be deposited before ever reaching the channel. Nevertheless, even using the conservative estimate of 7.5 Mg and assuming a bulk density of around 1.2 g cm^{-3}, this result entails a loss of around 0.6 mm of soil per year, a value that is well above the soil loss of 2.5 Mg ha^{-1} a^{-1} that is generally considered tolerable (Schertz, 1983).

4.5.2 Sediment trap efficiency of paddy fields

Surface reservoir water was the largest contributing source to suspended sediment inputs for the paddy fields, with only one quarter of sediment inputs to the paddy fields coming from overland flow in both years. When looking at the sediment quality rather than sediment loads, however, the importance of overland flow increased for sand, with 34% of the total paddy inputs originating from erosion in

2011. Therefore, while irrigation was the main driver behind water and sediment fluxes in this irrigated catchment, overland flow plays an important role in transfers that could affect plant production and long-term soil fertility.

Paddy runoff amounted to a total of 469 Mg for the 13 ha area in 2011, or 36 Mg ha^{-1} a^{-1} of sediments leaving the rice fields. The majority of paddy sediment export (60%) took place during the spring season, and can thus be related to overland runoff flowing through the paddies early in the year, when upland fields were bare as the maize crop was not yet established. Hence, intensive land preparation for maize planting and lack of soil cover in spring resulted in a large supply of readily erodible material on the hills. Short-duration, high-intensity spring storms combined with this sediment supply, led to rapid and large inputs of sediment which passed through the paddies. As a result, sediments had little time to settle, thus reducing filter effectiveness of the rice fields and culminating in less trapping and more sediment export from the paddies during the first crop.

Comparing inputs to paddy field exports suggests that the rice area trapped 44% of the combined re-allocated sediments from reservoir irrigation water and direct runoff from the upland areas. Similarly, Mingzhou *et al.* (2007) found that the sediment load in the irrigation water resulted in a net deposition, rather than erosion from paddy fields, which led to an additional 4 cm of top soil through irrigation deposits after fifty years of irrigation. While the paddies in our study were a net overall sediment sink, results also showed that the sand fraction was preferentially deposited and was in fact almost entirely captured in the paddies, forming a net deposition of 23 Mg ha^{-1} a^{-1}. About half of the imported clay remained behind in the fields, or a total of 8 Mg ha^{-1} a^{-1}. For silt, the overall balance was negative, with 5 Mg ha^{-1} of silt exported on an annual basis. This preferential deposition is likely to have consequences, as long-term fertility of paddy fields is contingent upon the particle size distribution of the soils for physical soil properties, e.g. clay content exceeding 20% is favorable for puddling (De Datta, 1981). In our study area, top soil in the paddy fields is predominantly silty, with an average of 19% sand, 68% silt and 13% clay (Schmitter *et al.*, 2010). With an estimated deposition of 23 Mg ha^{-1} a^{-1} of sand and 8 Mg ha^{-1} a^{-1} of clay in the paddies, and a removal of 4 Mg ha^{-1} a^{-1} of silt, textural changes can be expected to take place over time. While the clay fraction is expected to add sediment-associated nutrients to the paddies, and thus increase the

indigenous nutrient supply for rice, the sand deposits are much larger (76% of all inputs) and will thus drive the long-term fertility changes in paddy topsoil. Assuming a puddling depth of roughly 25 cm and a bulk density of 1.2 g cm^{-3}, the sand fraction would dominate after approximately fifty years of these continued inputs. But not all fields would have the same longevity, as sediment inputs do not affect the fields equally. Previous research has shown that sedimentation in rice cascades shows spatial variability, and that fields closest to the water source receive most of the coarse material, the yield declining with decreasing distance to the water source (Schmitter *et al.*, 2010). Thus for certain fields closer to the water source, sand content would increase more rapidly, which is indeed already visible in the study area: paddies higher up on the cascades were often seen to display poor water holding capacity.

Similar composite agricultural systems with permanent upland cultivation on the hills and irrigated rice in the valleys contain 60% of the total paddy area in Northern Vietnam (Rutten *et al.*, 2014). Consequently, a large agricultural area is potentially affected by such upland-lowland linkages. Eliminating the direct entry of Hortonian overland flow into the irrigation channel, for example by runoff ditches, is one way to prevent up to one third of the total sand inputs from entering the rice fields and thus to protect the food security of the people in the mountainous areas of Northern Vietnam, who depend on rice as their staple food. This solution is not sustainable in the long run from a systems-approach perspective, as the fertility loss of the uplands would affect income when the cash crop income is declining. But with the current high maize prices, it is challenging to identify sustainable hillside land uses that are attractive to local stakeholders (Keil *et al.*, 2008), and deviating direct runoff from entering the paddies would at least be an interim solution. It would, however, also lead to substantial losses of nutrients (Dung *et al*., 2008) which could not be recycled.

4.5.3 Buffer capacity of the reservoir

For the sediment yield measured at Location B, the outlet of the sub-watershed, the vast majority of sediments (1 557 Mg out of 2 064 Mg) stem from the reservoir which spills over into the river when it reaches maximum capacity. In that sense, the bulk of sediments are merely passing through the sub-watershed, having been captured in the reservoir after runoff from the surrounding 490 hectares of upland

fields. Reservoir outflow is thus not only the largest contributor to sediment transport in our paddy area within the watershed, but also has a propagating effect beyond the watershed scale: the river water leaving the watershed is either re-used for irrigating paddies in downstream catchments, or will finally end up in the Da river. In either case, the surface reservoir buffers direct sediment inputs that could negatively affect paddy production and river water quality, as average sediment concentrations released from the reservoir were much lower than those measured during rainfall events in the channel (240 mg L^{-1} versus 1 200 mg L^{-1}).

The water in the reservoir also had a lower sand and higher silt and clay content, and sediment profiles in the lake indeed confirmed this preferential settling of coarse material. Weiss (2008) showed that soil profiles taken at the lake bottom had a sediment texture of between 40 and 75% sand, 20 to 50% silt and 5 to 14% clay. The reservoirs filtering effect can be expected to be stronger beyond the watershed, as coarser particles will be trapped preferentially in closer vicinity to the source. While large enough to substantially affect rice production, the amount of sediments trapped by the paddy fields is moderate (12%) compared to the total amount exported from the watershed by reservoir spillover export. In light of these proportions, effects of climate change and declining soil fertility in upland areas will not remain on-site but can be expected to propagate beyond the watershed, and also affect areas further downstream.

4.6 Conclusions

The sediment budget for a 13 ha paddy area in a composite agricultural system with permanent maize cultivation on the uplands showed that rice fields at the watershed level are a net sink for sediments, i.e. trapping 46% of the total sediment inputs. Irrigation water, providing 74% of the total inputs of 832 Mg, was a larger contributor than direct overland flow from the surrounding upland fields. The irrigation water, however, provided predominantly silty material, while direct runoff sediments had a sandy texture. In the past, extensive swiddening systems with their diverse landscape patterns would have delivered little and mostly fine, fertile sediments to paddy fields via direct overland flow. Recent intensification of upland cropping has transformed these previously beneficial inputs into an increased risk for the long-term sustainability of rice production, threatening both productivity of upland cropping and paddy yields. The reservoir, however, acts as a buffer by

protecting both the rice fields within the watershed, and paddies and water quality further downstream, from unfertile sediment inputs – thus expanding the life time of the paddies.

Our results show the importance of quantifying upland-lowland linkages within and between watersheds, and can be used by scientists, policy makers and extension services to give suitable recommendations to the large group of people in mountainous Southeast Asia who, under influence of population pressure, have gone from practicing composite swidden agriculture to an intensified cropping system with permanent maize cultivation on the hills. Preventing overland flow from reaching the paddy fields, for example, could prevent up to 8 Mg ha^{-1} a^{-1} of sand per year, or one third of the total sand deposits, from entering the rice fields. More diversified, sustainable and acceptable approaches, however, benefitting both upland fields as well as downstream paddies, need to be developed at the same time.

Chapter 5 Sediment-associated organic carbon and nitrogen inputs from erosion and irrigation to rice fields in a mountainous watershed in Northwest Vietnam

J.I.F. Slaets[a], P. Schmitter[b], T. Hilger[a], D.T.T. Hue[c], H.P. Piepho[d], T.D. Vien[e], G. Cadisch[a]

[a] Institute of Plant Production and Agroecology in the Tropics and Subtropics, University of Hohenheim, Garbenstrasse 13, 70599 Stuttgart, Germany

[b] The International Water Management Institute, Nile Basin and East Africa Office, Addis Ababa, Ethiopia

[c] Central Water & Soil Lab at Vietnam National University of Agriculture, Hanoi, Vietnam

[d] Biostatistics Unit, Institute of Crop Science, University of Hohenheim, Fruwirthstrasse 23, 70599 Stuttgart, Germany

[e] Centre for Agricultural Research and Ecological Studies (CARES), Vietnam National University of Agriculture, Hanoi, Vietnam

5.1 Abstract

Maintaining indigenous nutrient supply and positive nutrient balances are key factors in sustaining rice yields. Irrigation systems act as conveyers for water, sediments and nutrients throughout landscapes, especially in mountainous, cultivated tropical areas where erosivity is usually high. Contributions of erosion and irrigation to the nutrient balance of paddy fields, however, are rarely assessed. In this study, a turbidity-based method was used to quantify sediment-associated organic carbon and nitrogen as well as dissolved nitrogen inputs from erosion and irrigation to a 13 ha rice area in Northwest Vietnam. The irrigation source is a surface reservoir, and both reservoir and irrigation channel are surrounded by permanent upland maize cultivation on the steep slopes. Additionally, organic carbon and nitrogen loads in paddy outflow were determined to obtain nutrient budgets. Irrigation contributed 90% of sediment-associated organic carbon inputs and virtually all nitrogen inputs. Analysis of ammonium and nitrate in total nitrogen loads showed that 24% of the total N inputs

from irrigation to the rice area, or 0.28 Mg ha^{-1} a^{-1}, were plant-available. Loads measured at the outlet of rice fields showed that paddies were a trap for sediment-associated nutrients: balancing inputs and outflow, a net load of 1.09 Mg ha^{-1} a^{-1} of sediment-associated organic carbon and 0.68 Mg ha^{-1} a^{-1} of sediment-associated nitrogen remained in the rice fields. Sediment-associated organic carbon and nitrogen inputs thus form an important contribution to the indigenous nutrient supply of rice in these maize-paddy systems, while the rice fields simultaneously capture nutrients, protecting downstream areas from the effects of land use intensification on surrounding slopes. These results underscore the importance of upland-lowland linkages in tropical, mountainous, erosion-prone areas.

Keywords: nutrient balance, runoff, shifting cultivation, surface reservoir, nutrient yield, water quality

5.2 Introduction

Irrigation systems convey sediment and nutrients in landscapes (Schmitter *et al.*, 2012). At the field scale, King *et al.* (2009) found that irrigation increased the field nutrient status: furrow irrigation created a net input of organic carbon (OC) and nitrogen (N) by leaving behind nutrient-rich sediments. They estimated that irrigation water contributed 31.2 kg ha^{-1} sediment-associated OC to the irrigated fields. Beyond the field scale, man-made irrigation channels cross catchment boundaries, exporting surface water from the watershed into a neighboring one. Thus irrigation structures also cause nutrient transfers between catchments, the nature of which depends on the source of the irrigation water and its quality. Schmitter *et al.* (2012), for example, measured total OC and N in irrigation water, combining sediment-associated and dissolved nutrients, and reported that an irrigation channel exported 5.7 Mg of OC and 4.7 Mg of N from a small mountainous watershed in one rainy season (May to September).

The main irrigated crop in Southeast Asia is rice, and in Vietnam, where this study was conducted, 97% of paddy rice is irrigated – mainly with water from surface reservoirs (FAO Aquastat, 2014). But the contribution of sediment-associated nutrients from irrigation to the nutrient balance of paddy systems is not well known. And the impact of these nutrient transfers depends on other inputs and losses, which in turn depend on the nature of the rice cropping system. In traditional irrigated rice systems before the Green Revolution, nutrient uptake and removal rates were low.

Additions from sediment and rainfall were an important component of the nutrient balance in this setting, enabling even poor soils to sustain yields of 1 to 2 Mg ha^{-1} and allowing rice to be cultivated in paddy fields in monoculture for decades or even centuries (Reichardt *et al*., 1998).

In current, intensive rice production, inputs through irrigation water are rarely quantified. Cassman *et al.* (1998) reported that in most irrigated rice systems, N inputs from rainfall and irrigation are negligible. Schmitter *et al*. (2010), however, found that rice yields in paddy fields increase with distance to the irrigation channel, showing a distinct spatial trend in soil fertility induced by sediments from irrigation water. In the same watershed, Schmitter *et al.* (2012) measured nutrient contents of irrigation water combining sediment-associated and dissolved fractions, and reported an amount of 0.8 Mg ha^{-1} of OC and 0.7 Mg ha^{-1} N entering the paddies through irrigation water in one rice cropping season, an amount that could influence the indigenous nutrient supply of the fields. Dung *et al*. (2009) monitored a small catchment in Northern Vietnam with a composite swiddening system in the uplands, where between 50 and 227 kg of total N entered the paddies from upland slopes and even larger outflows were recorded, resulting in a slightly negative N balance. In the latter study, the negative balances indicated that the nutrients brought in by overland flow were lost again, going downstream.

Irrigation water not only provides nutrient inputs, irrigation management additionally affects nutrient losses from paddies and watersheds. Yan *et al*. (2010) found paddies to trap N and purify the N in rainwater, with riverine N output amounting to less than 1.5% of all combined N inputs. Kim *et al*. (2006) quantified N concentrations in paddy outflows during different rainfall events and reported that N export from paddy fields during storms depended on irrigation status of the fields (ponded or not) and fertilizer application. Marumaya *et al*. (2008) calculated a paddy mass balance for N and reported that 8.5% of N inputs were lost via percolation and runoff combined, indicating a filtering effect important in protecting a downstream lake.

These differing results indicate the importance of understanding upland-lowland linkages as well as the cropping systems surrounding the paddies and the irrigation system in place. The nutrient status of paddies cannot be seen separately from the erosivity of the uplands surrounding the rice fields and surface reservoirs. In

Northern Vietnam, 60% of the paddies are enclosed in hilly areas (Rutten *et al*., 2014). But the subsistence-based shifting cultivation systems with long fallow periods, which used to dominate these hills, have dwindled in the last decades. Under the influence of political decision making, market mechanisms, and population pressure, they have given way to intensified production systems such as permanent maize cultivation (Fox *et al*., 2009).

These changing farming systems have brought about an extensively documented deterioration of soil fertility on the slopes. Based on a review of studies in Southeast Asia, Bruun *et al.* (2009) report losses of soil organic carbon from 13 to 40% after converting a shifting cultivations system to continuous annual cropping. Specifically in Northern Vietnam, yearly N balances for a cropping cycle of two years of upland rice, followed by one year of cassava were found to be negative in the upland fields by Dung *et al.* (2008), with 247 kg of N per hectare lost cumulatively over five years.

Continuous maize cultivation in particular is often a culprit for declining soil quality on steep slopes (Valentin *et al*., 2008). Maize is known to cause especially high amounts of erosion during the onset of the rainy season, before establishment of the crop, when soil cover is very poor (Tuan *et al*., 2014). According to Pansak *et al*. (2008), under maize mono-cropping on moderate slopes in Northeast Thailand, between 12 and 15 kg of N ha^{-1} a^{-1} were lost via runoff, soil loss and leaching – amounting to almost one quarter of the amount of N applied through fertilizer. In Yen Chau district, the same district were this study was conducted, Häring *et al.* (2014) found SOC losses on steep slopes between 0.6 and 1.3 Mg ha^{-1} a^{-1} for fields converted from forest into maize 5 to 20 years ago resulting in an approximate average loss of 40 Mg ha^{-1} of SOC for the entire 20 year period. Tuan *et al.* (2015), also on steep slopes in Yen Chau district, reported losses of 21 to 23 kg N ha^{-1} a^{-1} under maize mono-cropping.

A loss at the plot scale is not necessarily associated with a loss at the watershed or even basin scale – as nutrients that disappear through erosion are not automatically lost to the whole watershed (van Noordwijk *et al.*, 1997; Valentin *et al.*, 2008). The eroded nutrients could either be redeposited in lower parts of the catchment, or be exported from the catchment altogether, in which case other catchments or water bodies downstream will be affected. As such, rice fields can benefit from the nutrient

re-allocation processes in the landscape by trapping, or alternatively become additional sources of nutrient loss, depending on the topography. Sink-source relationships at the landscape level are therefore highly variable, and this variability occurs not only in space but also in time. Rice fields can be net sinks during specific periods of the cropping season but become a source due to ploughing and leveling practices at the onset of the season (Kundarto *et al.*, 2002, in Indonesian; cited in Maglinao *et al.*, 2003). Furthermore, depending on the water level of paddies, the irrigation and/or rainfall pattern, additional runoff can be created, turning paddies from nutrient sinks into sources during the rainy season. Therefore, a high temporal resolution of nutrient re-allocation in the catchment is needed to understand upland-lowland sink-source relationships and in particular the role of rice fields in intensively cultivated upland areas. This type of nutrient budget studies requires new techniques that continuously quantify sediment and nutrient loads, both within and exported from paddies, in combination with assessments of nutrient flows into and out of the watershed.

In this study, a turbidity-based method developed by Slaets *et al.* (2014) was applied to quantify the re-allocation of sediment-associated OC, sediment-associated and dissolved N transport in an intensely cultivated, irrigated watershed containing continuous maize cultivation on the uplands and paddy rice in the valley. Our specific aims were (i) to determine the effect of irrigation derived from an upstream surface reservoir on sediment-associated OC and N as well as dissolved N inputs for paddy fields, (ii) to quantify the effect of overland flow from surrounding upland areas on sediment-associated OC and N inputs for paddy rice, (iii) to estimate the load of sediment-associated OC and N exported from the paddy area and lost from the watershed, and (iv) to assess the proportion of plant-available N in the total N inputs from irrigation water and overland flow and thus the potential impacts of these upland-lowland linkages on rice production.

5.3 Material and methods

5.3.1 Study site

The study was conducted in Chieng Khoi commune (Figure 5.1, 350 m a.s.l., 21°7’60’’N, 105°40’0’’E), Yen Chau district, Northwest Vietnam within the framework of the collaborative research center “The Uplands Program”, an international research project funded by the German Research Foundation (DFG) on

the conservation of natural resources and the improvement of livelihoods of the rural population in mountainous areas of Southeast Asia. The rainfall pattern follows a typical monsoon pattern with a rainy season from April till October, and an average annual rainfall of 1200 mm. Alisols and luvisols are the most important soil types in the area (Clemens *et al.*, 2010). The main crops on the hills are maize (*Zea mays* L.) and cassava (*Manihot esculenta* Crantz), whereas paddy rice (*Oryza sativa* L.) dominates in the valleys.

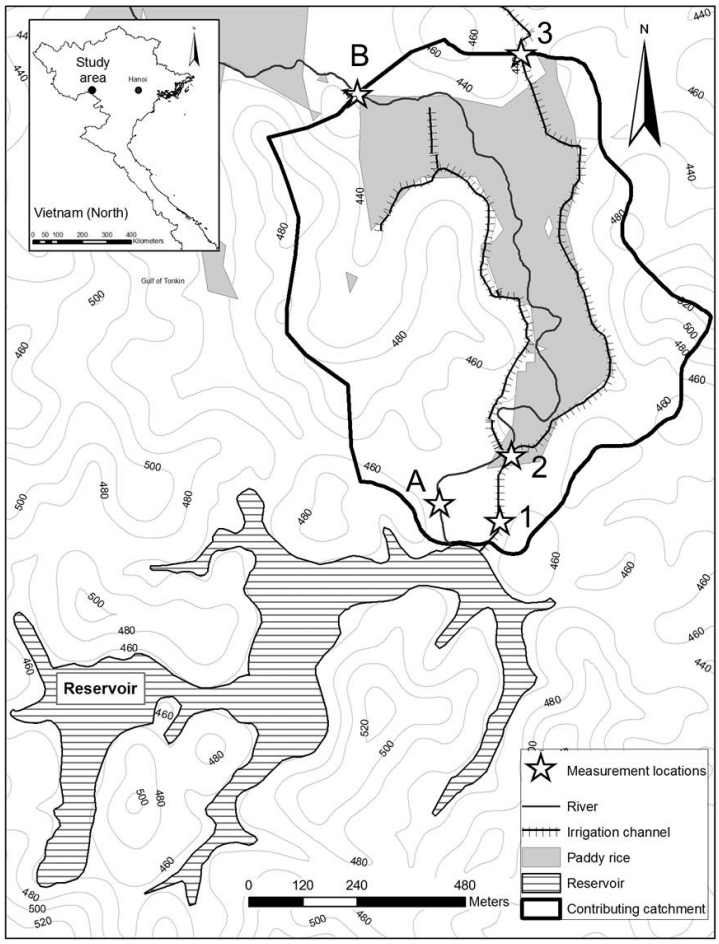

Figure 5.1: Situation of the study site in Chieng Khoi commune, Yen Chau district, Vietnam, showing the surface reservoir, the irrigated paddies, and the measurement locations in the irrigation channel (Locations 1, 2 and 3) and in the river (Locations A and B).

Farmers irrigate the paddy fields with water from a surface reservoir that feeds a concrete irrigation channel. A contributing area of 490 ha, containing maize and cassava upland fields and forest, drains to the reservoir, which has a buffering

capacity of 10^6 m^3 and covers a total surface of 26.3 ha if the maximum water depth of 13.67 m is reached. The reservoir supplies water the whole year around to the 13 ha of paddy fields in the studied watershed, ensuring two rice crops per year: a fully irrigated spring crop from February till June, and a summer (rainy season) crop from July till October that receives supplementary irrigation. The main channel splits into two: one providing water for the paddy fields on the left bank of a river that transects the watershed, and one for the paddy fields on the right bank (Figure 5.1). The water from the left bank of the channel is used up fully within the watershed, while the right bank still contains water as it leaves the catchment and enters a neighboring one. The irrigated paddy fields subsequently drain into the river which in its turn exports the excess water from the watershed.

5.3.2 Measuring sediment-associated OC and N fluxes at the watershed scale

5.3.2.1 Monitoring locations

Two sources contribute sediment-associated OC and N to the paddy fields: irrigation water from the surface reservoir during both the dry and rainy season, and direct overland flow generated on the surrounding steep upland fields draining into the irrigation channel during the rainy season (Figure 5.1). As a part of the irrigation water in the right channel is not used within the studied watershed, a portion of the particulate OC and N released by the reservoir will be transported to the neighboring catchment. To separate these sources and to quantify the amount of water allocated to the left and right channel, three different monitoring locations were installed in the irrigation channel. The station in the channel directly below the reservoir (Location 1 in Figure 5.1) monitored the quantity of and sediment-associated OC and N concentrations in the irrigation water. The site directly below the split of the channel (Location 2 in Figure 5.1) quantified the amount of water going into each branch of the channel and therefore irrigated to each bank of paddy fields. A measurement station at the end of the right concrete channel (Location 3 in Figure 5.1), just before it leaves the catchment, determined the amount of water, N and sediment-associated OC released to the neighbouring catchment and allowed for the quantification of total irrigated OC and N loads to the paddies (i.e., between Locations 2 and 3). Simultaneously monitoring these two sites allowed us to quantify the contribution of overland flow from surrounding upland fields to the OC and N loads. In the river, a similar setup characterized the nutrient loads exported from the paddy rice field: Location A (Figure 5.1) measured nutrient loads before the paddy fields, and

Location B (Figure 5.1) quantified the loads after translocation through the monitored paddy area.

5.3.2.2 Hydrological data

During the monitoring years of 2010 and 2011, water levels were recorded using pressure sensors at two-minute-intervals (Ecotech, Germany). Discharge predictions were obtained using the area-velocity method for the river and the salt dilution method for the channel (Herschy, 1995). Satisfactory accuracy was achieved for all stations (R^2 from 0.97 to 0.99; Slaets *et al.*, 2015). Rainfall was registered by a tipping-bucket rain gauge (accuracy 0.1 mm) which was part of a weather station (Campbell Scientific, USA) that was installed in the upper part of the catchment (Lamers *et al*., 2011).

Turbidity was measured with NEP395 nephalometric turbidity sensors (McVan, Australia) and recorded at 2 minute intervals using CR200 data loggers (Campbell Scientific, USA). The sensors were suspended with the optical eye down in a perforated pipe, installed at the center point of flow but allowing the pipe to be pushed upwards in the water column with rising water levels (Slaets *et al.*, 2014). Automatic wipers were programmed to clean the optical eye every hour to prevent fouling of the sensors.

5.3.2.3 Nutrient concentrations

Water samples were collected in order to establish a relationship between nutrient content and predictor variables such as turbidity and discharge. The sampling was done manually rather than with automatic samplers, as flow-proportional automatic sampling can be challenging in irrigation channels where discharge is affected by management (Schmitter *et al.*, 2012) and composite sampling is not appropriate for calibration of the sensors. A storm-based approach was chosen to catch the full range of OC and N concentrations. Typically ten to twenty samples were collected per event. A 0.5 L samples was taken at each sampling, horizontally and opposite to the flow direction, in order to minimize particle disturbance. The samples were refrigerated on site and transported to the lab after the event, where they were frozen until analysis.

Samples were analyzed for sediment-associated OC, total and dissolved N by a combustion method with a LiquiTOC II (Elementar, Germany) on the full sample containing sediment, and on the supernatants after letting the sediment settle down, as is recommended for water samples with very high sediment concentrations (ASTM, 2013). More details can be found in Slaets *et al.* (2014). Additionally, ammonium and nitrate concentrations were determined for 595 samples (42 samples during base-flow, the remainder during rainfall events). Ammonium was determined using the modified indophenol method (0.1 M KCl extraction; Sparks, 1996) and nitrate was analyzed with the Cataldo method (0.01 M KCl extraction; Cataldo *et al.*, 1975). The ammonium and nitrate concentrations were determined on the water samples containing sediments.

5.3.3 Predicting sediment-associated OC and N loads

5.3.3.1 Data quality control

Discharge and turbidity data were checked before use for concentration predictions by comparing upstream and downstream locations in the same stream against rainfall over the different years. Where discharge data were missing due to malfunctioning of the sensors for short periods of time (defined as less than one day, and during periods of no rainfall only), discharge was linearly interpolated. The two year period encompassed 420 rainfall events (192 events in 2010 and 228 events in 2011). In the dry season of 2011 at the river inlet, there was a more extended period of time with missing turbidity data due to technical problems. In that case, the monthly averaged base-flow values of the previous year were used.

5.3.3.2 Flow component separation

In order to separate the contribution of irrigation water and direct Hortonian overland flow to the OC and N inputs of the paddy fields, the discharge in the irrigation channel was separated into water volume from irrigation and water volume from runoff. The irrigation channel is lined with concrete, so there was no interflow or base-flow present. Therefore the base-flow hydrological balance can be described by

$$Q_{in} = Q_{irr} + Q_{out}, \qquad \text{(Equation 5.1)}$$

where Q_{in} is the discharge at Location 2, Q_{out} is the discharge at Location 3, and Q_{irr} is the discharge irrigated to the paddy fields, all in $m^3\ s^{-1}$. As Q_{in} and Q_{out} were measured directly, the irrigated discharge can be calculated as the difference between

the two. But during rainfall when both direct rainfall and Hortonian overland flow enter the irrigation channel, the balance changes to

$$Q_{pp} + Q_{in} + Q_{of} = Q_{irr} + Q_{out}, \qquad \text{(Equation 5.2)}$$

where Q_{pp} is the direct precipitation into the channel and Q_{of} is the overland flow entering the channel from surrounding uplands during rainfall. As the direct precipitation into the channel can be calculated from the rainfall intensity, which is measured by the rain gauge, and the channel dimensions, we can determine Q_{of} from Equation 5.2 by assuming that the irrigation management does not change during rainfall events. The flow component separation is described in more detail by Schmitter *et al.* (2012).

5.3.3.3 Concentration prediction models

Continuous sediment-associated OC and N concentrations were estimated using a linear mixed model with turbidity, discharge and depth of the surface reservoir as predictor variables (Slaets *et al*., 2014). As a larger dataset was available in this study compared to Slaets *et al.* (2014), a separate model was fitted for each location, rather than one model with location-specific regression coefficients in the previous analysis. Model validation was performed using five-fold cross validation with a SAS macro described in Slaets *et al.* (2014). Sample size and Pearson's correlation coefficient between observed and predicted values for the different monitoring locations are shown in Table 5.1. Input variables were chosen based on forward selection with Pearson's correlation coefficient after cross-validation as selection criterion.

To account for serial correlation in the data, the error was modeled by fitting a first-order autoregressive variance-covariance structure to the data where the events were considered as independent subjects. All statistical analyses were done using the MIXED procedure of SAS 9.4.

Table 5.1: Model fit for the nutrient concentration predictions. Shown are number of observations (n) and squared Pearson's correlation coefficient (r^2) after five-fold cross-validation for sediment-associated Organic Carbon (OC), sediment-associated Nitrogen (N) and Total Nitrogen (TN) concentration predictions for the different measurement locations in Figure 5.1.

	OC		N		TN	
	n	**r^2**	**n**	**r^2**	**n**	**r^2**
Channel	535	0.60	377	0.62	600	0.61
River (A)	102	0.59	108	0.71	112	0.77
River (B)	70	0.71	73	0.62	72	0.62

When applying these models to the whole time series, the predictions showed a small overprediction for base-flow, which is typical (Nearing, 1998) but would have a large effect on annual load estimates. Therefore a qualitative variable for flow regime was included in the model, so that regression coefficients could vary according to the flow regime. To stabilize the variance, the response variable was Box-Cox transformed using a macro developed by Piepho (2009).

Estimated OC and N concentrations during base-flow sometimes yielded negative values, when the total or dissolved concentrations were below the detection limit of the CN analyzer (0.05 mg L^{-1}). Leaving out these values may introduce bias into the model as these low values are not missing at random. But because there was a strong correlation between total and sediment-associated nutrient concentrations, the missing concentration values were imputed using Multiple Imputation as implemented in the MI procedure of SAS 9.4. Specifically, we employed the fully conditional specification method (FCS), which assumes a joint distribution of these variables (van Buuren, 2007). All imputations were done on the log-transformed scale.

5.3.3.4 Load estimates

Instantaneous loads can be calculated by multiplying OC or N concentrations, as predicted from the models, with the discharge at that time point. To obtain load estimates over a time interval, for example an annual load, the instantaneous loads are summed up:

$$\hat{L}_{1\ to\ t} = \sum_{i=1}^{t}(\hat{L}_i * D)\ , \qquad \text{(Equation 5.3)}$$

where $\hat{L}_{1\,to\,t}$ (Mg) is the total load over a time interval 1 to *t*, $\hat{L}_i$ is the instantaneous load at a time *i* (Mg s^{-1}) and *D* the duration of the prediction interval (s), which corresponds to 120 seconds for our two-minute turbidity and discharge recordings.

In order to calculate confidence intervals of the load, a bootstrap method was adopted where both uncertainties on the discharge and concentration predictions were taken into account (Slaets *et al.*, in revision). The imputation of the missing low sediment-associated concentrations was repeated for each bootstrap replicate in order to take this source of uncertainty into account. As the bootstrap also removes bias (Efron and Tibshirani, 1993), load estimates are reported here as the medians of the bootstrap estimates, rather than the direct estimates resulting from Equation 5.3.

Table 5.2: Sediment-associated Organic Carbon budget for rice fields in Chieng Khoi catchment. Contributions are shown for inputs from irrigation water from the surface reservoir and overland flow from the 37 ha upland area surrounding the rice, and export from the 13 ha paddy area in Mg a^{-1} (Figure 5.1). Percentages indicate contributions compared to total combined inputs from irrigation and overland flow. Med = median of bootstrap sample, LL, UL = lower, upper 95% confidence limits. nd = not determined

	2010			2011		
Sediment source	**LL**	**Med**	**UL**	**LL**	**Med**	**UL**
Reservoir water:						
Irrigated to paddy area	12.75	13.84 (90%)	15.85	13.19	14.74 (92%)	19.08
Exported via channel	3.11	3.39	3.99	3.11	3.43	4.35
Spillover to river	nd	nd	nd	5.76	6.72	10.45
Overland flow:						
Irrigated to paddy area	1.04	1.55 (10%)	2.47	0.79	1.35 (8%)	2.55
Exported via channel	0.32	0.50	0.83	0.26	0.40	0.74
Total paddy input		15.39 (100%)			16.09 (100%)	
Paddy outflow	nd	nd	nd	0.03	1.94 (12%)	6.13
Net paddy balance		nd			14.15 (88%)	
Paddy balance per ha		nd			+1.09 Mg ha^{-1} a^{-1}	
Watershed losses		nd			12.4	

5.4 Results

5.4.1 Sediment-associated paddy OC and N inputs from irrigation

Irrigation water from the surface reservoir transported a total of 13.84 Mg of OC in 2010 and 14.74 Mg in 2011 into the 13 ha rice area (Table 5.2). Sediment-associated N loads brought into the paddies amounted to 9.16 Mg in 2010 (Table 5.3) and 9.37 Mg in 2011 (Table 5.4). Percentages of OC and N in the sediments were determined by dividing these sediment-associated OC and N loads by corresponding sediment loads for the same area reported in Slaets *et al.* (2015). The OC and N percentages in the sediment in irrigation water changed throughout the year, being highest at the start of the spring season and at the end of the summer crop (Figure 5.2). They were lowest when surface reservoir water level was very low, e.g. at the end of the spring cropping season (May), as at this time, highly erosive rains fell into a small volume of water, bringing in unfertile sediments, low in nutrients. The OC to N ratio of the sediments in the irrigation water was around 1.6 and changed little throughout the year (Figure 5.3).

Table 5.3: Nitrogen inputs for rice fields in Chieng Khoi catchment in 2010. Shown are sediment-associated and dissolved nitrogen contributions from overland flow from the 37 ha upland area surrounding the paddies and from irrigation water from the surface reservoir. Med = median of bootstrap sample, LL, UL = lower, upper 95% confidence limits. nd = not determined

	Nitrogen (Mg a^{-1})								
	Sediment-associated			Dissolved			Total		
Source	**LL**	**Med**	**UL**	**LL**	**Med**	**UL**	**LL**	**Med**	**UL**
Reservoir water:									
Irrigated to paddy area	8.72	9.16 (97%)	9.92	2.46	5.55 (99%)	11.14	11.79	14.71 (98%)	20.33
Exported via channel	2.12	2.22	2.40	0.60	1.34	2.69	2.87	3.57	4.93
Overland flow:									
Irrigated to paddy area	0.17	0.28 (3%)	0.45	0.00	0.01 (1%)	0.15	0.22	0.29 (2%)	0.38
Exported via channel	0.06	0.11	0.14	0.00	0.00	0.05	0.07	0.09	0.12
Total paddy input		9.44 (100%)			5.56 (100%)			15.00 (100%)	
Inputs per hectare		0.73 Mg ha^{-1}			0.43 Mg ha^{-1}			1.15 Mg ha^{-1}	

The sediment-associated OC and N loads from irrigation water into the paddies showed substantial monthly differences (Figure 5.4). While the percentage of OC and N in the sediments varied throughout the year, differences in monthly loads were mainly driven by alterations in water volume irrigated to the paddies over the year (Figure 5.4a). For both years and both nutrients, the summer rice season received larger OC and N loads than the spring season.

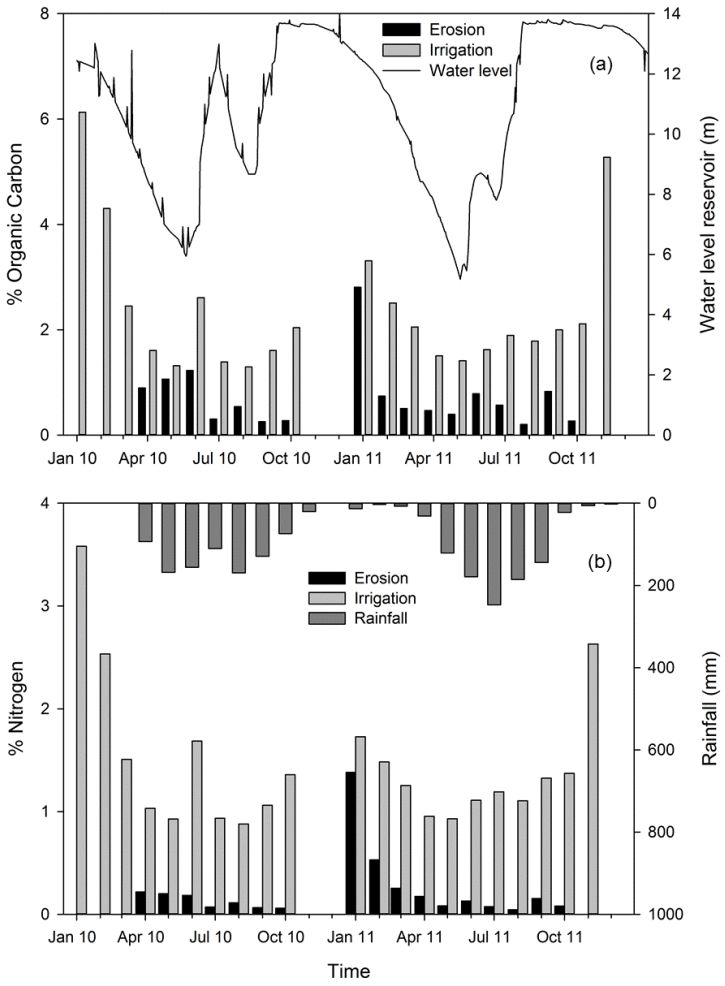

Figure 5.2: Average monthly Organic Carbon (a) and Nitrogen content (b) of the sediments (%) in irrigation water and overland flow. Additionally shown are water level in the surface reservoir (a) and monthly rainfall (b) in the study years 2010 and 2011.

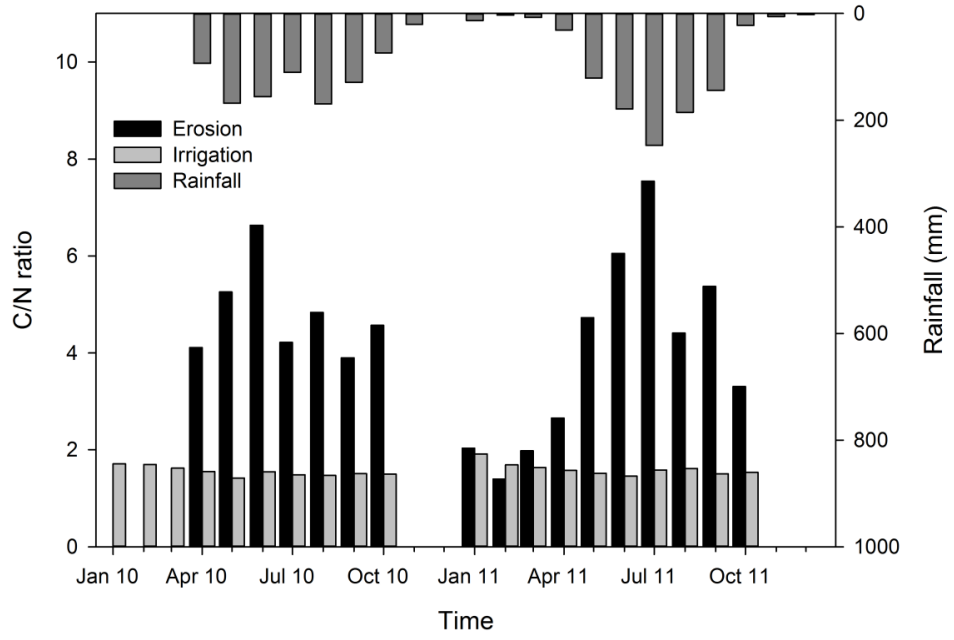

Figure 5.3: Average monthly Organic Carbon to Nitrogen ratio of the sediment in irrigation water and overland flow for the study years 2010 and 2011.

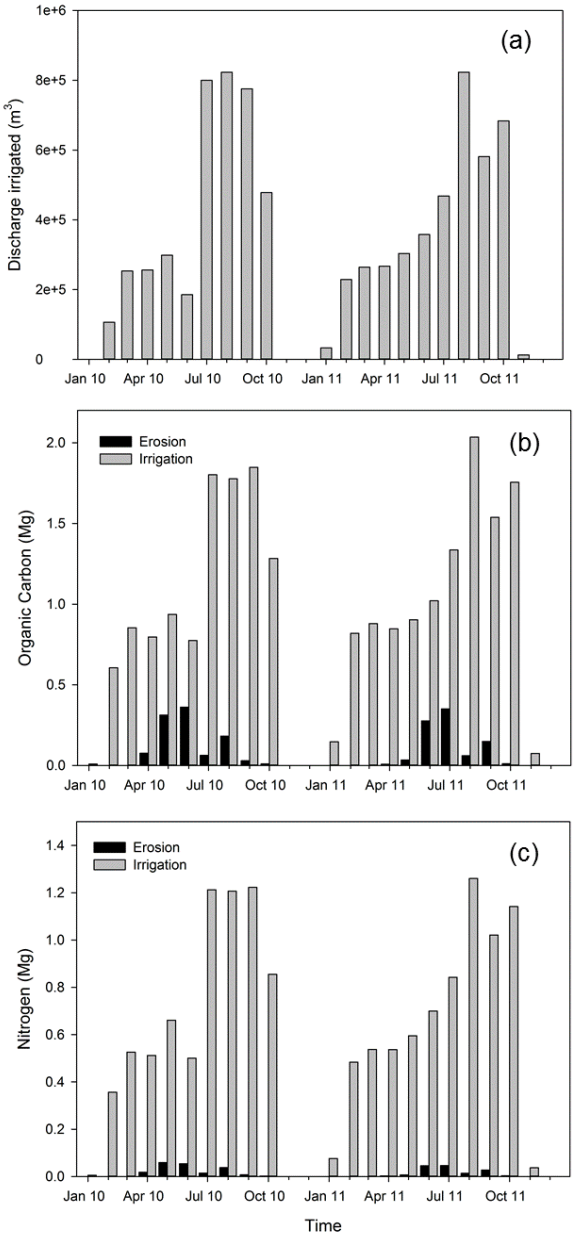

Figure 5.4: Monthly discharge irrigated to the paddies (a), sediment-associated Organic Carbon loads (b) and sediment-associated Nitrogen loads (c) from irrigation and direct upland erosion (37 ha) upland area into the paddy fields (13 ha).

5.4.2 Sediment-associated OC and N paddy inputs from erosion

Nutrient inputs from direct overland flow were much smaller than contributions from irrigation water, amounting to around 10% of inputs in both years for OC, and approximately 1% of inputs for N (Tables 5.2, 5.3 and 5.4 and Figures 5.5 and 5.6). Consequently, erosion from upland areas surrounding paddies carried 1.55 Mg or 0.12 Mg ha^{-1} of sediment-associated OC into the rice area in 2010, and 1.35 Mg or 0.10 Mg ha^{-1} in 2011 during rainfall events. For sediment-associated N, the direct erosion based loads amounted to 0.28 Mg in 2010 and 0.20 Mg in 2011, or about 0.02 Mg $ha^{-1}a^{-1}$ in both years.

Table 5.4: Nitrogen budget for rice fields in Chieng Khoi catchment in 2011. Shown are sediment-associated and dissolved nitrogen contributions from overland flow from the 37 ha upland area surrounding the paddies, inputs from irrigation water from the surface reservoir, export from the 13 ha paddy area, and the net balance for the paddies. Med = median of bootstrap sample, LL, UL = lower, upper 95% confidence limits. (n.a.=not applicable)

Nitrogen (Mg a^{-1})									
	Sediment-associated			Dissolved			Total		
Source	**LL**	**Med**	**UL**	**LL**	**Med**	**UL**	**LL**	**Med**	**UL**
Reservoir water:									
Irrigated to paddy area	8.83	9.37 (98%)	10.43	2.49	5.62 (100%)	10.99	12.06	14.93 (99%)	20.20
Exported via channel	2.08	2.19	2.48	0.53	1.31	2.58	2.84	3.50	4.74
Spillover to river	0.60	0.86	1.23	6.87	7.98	14.47	7.84	8.84	15.36
Overland flow:									
Irrigated to paddy area	0.00	0.20 (2%)	0.35	0.00	0.00 (0%)	0.17	0.09	0.22 (1%)	0.29
Exported via channel	0.04	0.07	0.11	0.00	0.00	0.03	0.05	0.07	0.08
Total paddy input		9.57 (100%)			5.62 (100%)			15.15 (100%)	
Paddy outflow	0.20	0.68	1.58	-0.62	3.72	10.33	0.18	4.44	10.67
Net paddy balance		8.89 (93%)			n.a.			n.a.	
Paddy balance per ha		+0.68 Mg ha-1 a-1			n.a			n.a.	
Watershed losses		3.80			13.01			16.85	

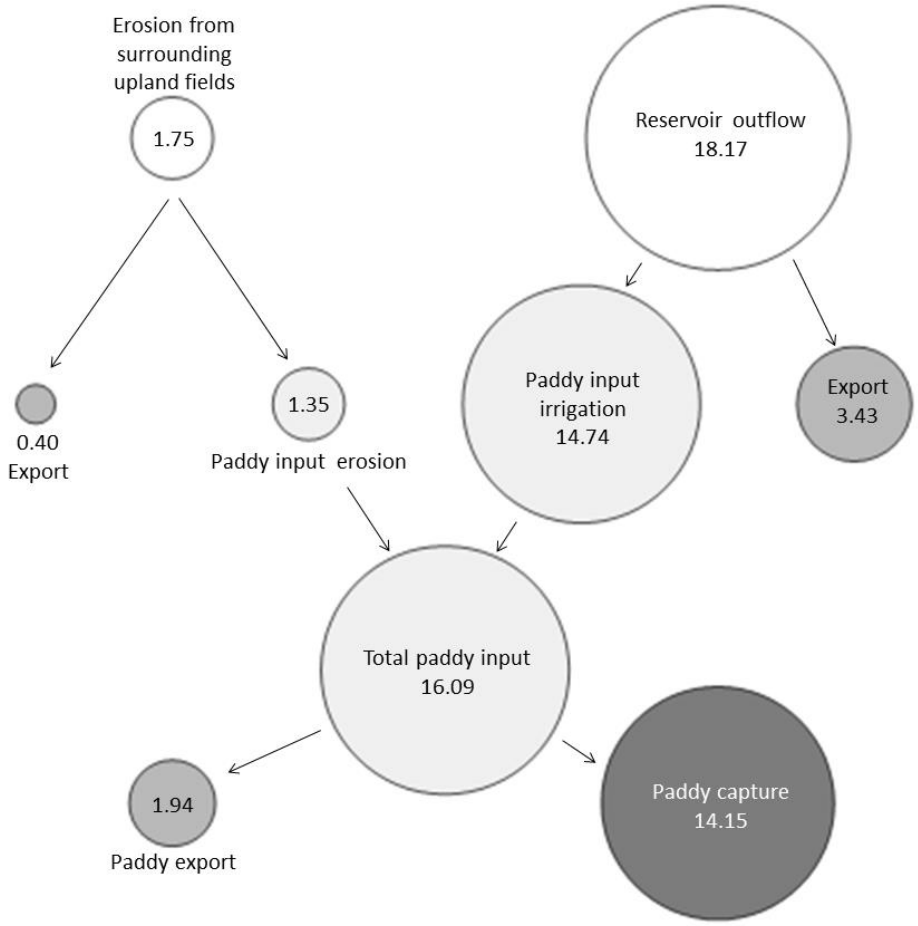

Figure 5.5: Sediment-associated organic carbon flow chart for 2011. Bubble size corresponds to size of the OC load (in Mg a^{-1}).

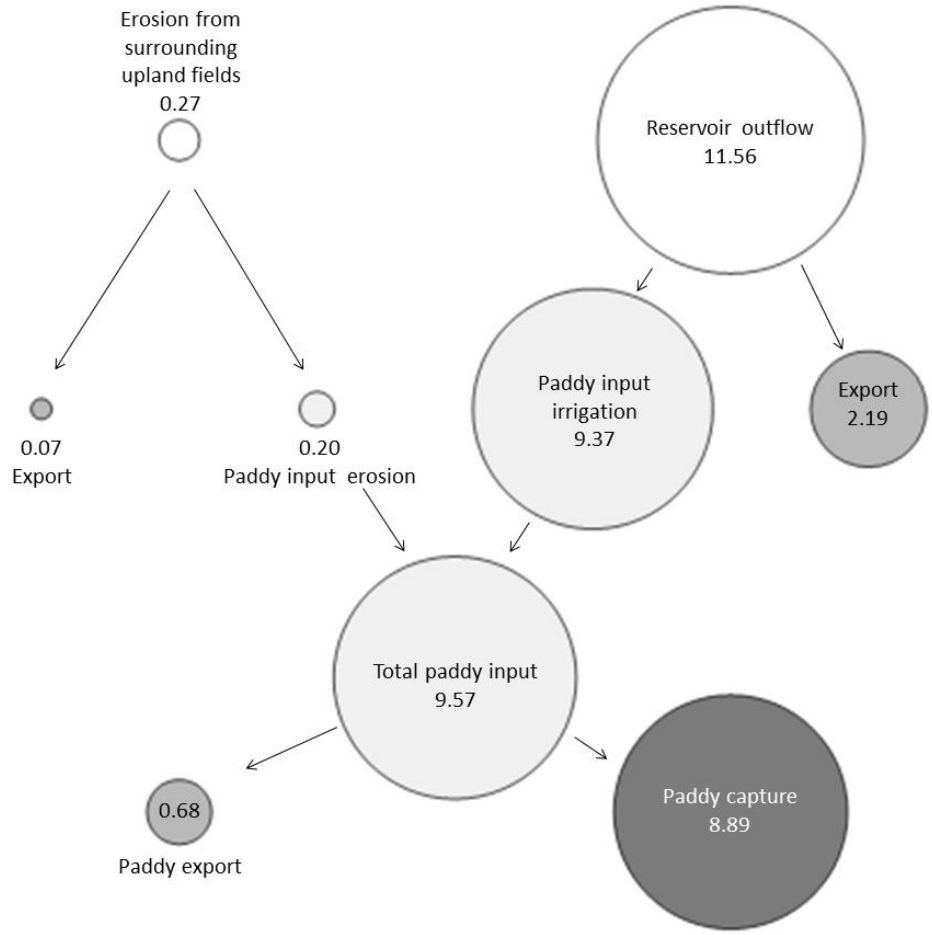

Figure 5.6: Sediment-associated nitrogen flow chart for 2011. Bubble size corresponds to size of the N load (in Mg a^{-1}).

The percentages of OC in sediments originating from erosion, calculated by dividing the sediment-associated OC load from overland flow by the sediment load from overland flow (Slaets *et al.*, 2015) were 0.83% in the first and 0.64% in the second year of the study (Table 5.5). These percentages are low compared to the OC content of sediments in irrigation water, which averaged 2.15% in 2010 and 2.37% in 2011. For N, the difference was even larger, with directly eroded sediments having often a percentage of N an order of magnitude smaller than sediments in irrigation water (Figure 5.2b). In general, the percentage of OC in sediments in overland flow was higher in the first months of the rainy season, after a long dry period, consistent with a first-flush effect when a lot of light and fertile material has built up and is available for eroding (Figure 5.2a). Average monthly OC to N ratios of eroded material varied from 1.4 in February 2011 to a maximum of 7.5 in July 2011, the month with the

largest storm of the study period (on 12/07/2011) in which 70 mm of rain fell in one hour. In 2010, the OC to N ratio was highest during May and June, the months during which upland fields are prepared for maize planting, resulting in a large supply of loose soil and readily erodible sediment at the onset of the rainy season. In 2011, however, the rains came atypically late, resulting in a shifted peak not coinciding with upland field preparation.

Table 5.5: Average organic carbon content (% OC) of sediments from different components of the paddy sediment balance.

	% OC	
Source	**2010**	**2011**
Reservoir water:		
Irrigation channels	2.15	2.37
Spill-over to river	nd	0.52
Overland flow:	0.83	0.64
Paddy outflow:	nd	1.07

nd=not determined

5.4.3 Plant-available nitrogen contributions from irrigation and runoff

As continuous predictions were obtained for both sediment-associated and total N, loads of dissolved N could be estimated as the difference between those two. Irrigation water contributed the vast majority (99%) of dissolved N inputs to the rice fields (5.56 Mg a^{-1}), while overland flow contributed only 0.01 Mg (1%) in the first year of the study and no detectable dissolved N in the second year. Paddy outflow contained 3.72 Mg of dissolved N in 2011.

As ammonium (NH_4^+) and nitrate (NO_3^-) are the main plant-available forms of N, a subset of the sediment containing water samples was analyzed for these N forms. No continuous predictions were obtained, but the samples showed seasonal differences in base-flow NH_4^+ and NO_3^- concentrations in the irrigation water (Table 5.6): NO_3^- concentrations in water samples were particularly high during the months June and July, coinciding with fertilization with NPK of maize on upland areas surrounding the lake. NH_4^+ concentrations were highest during the spring time, NH_4^+ being the dominant form of inorganic N in an anaerobic environment such as the surface reservoir. During the rainy season, NO_3^- concentrations were higher than those of NH_4^+, with averages over the study period of 0.90 mg L^{-1} for NH_4^+ and 2.94 mg L^{-1}

for NO_3^-. During overland flow, storm flow samples contained on average 1.52 mg L^{-1} of NH_4^+ and 6.21 mg L^{-1} of NO_3^- (data not shown).

Table 5.6: Average (av), minimum (min) and maximum (max) monthly ammonium and nitrate concentrations in irrigation water during the maize cropping season (n=42) in mg L^{-1}

	Ammonium			Nitrate		
Month	**min**	**av**	**max**	**min**	**av**	**max**
April	1.42	1.52	1.62	0.89	1.45	8.56
May	0.08	1.58	1.98	0.82	1.19	9.77
June	0.47	2.11	2.56	0.54	4.79	8.64
July	0.20	0.90	2.25	0.80	4.32	8.33
August	0.19	0.75	1.20	0.53	0.80	12.74
September	0.07	0.32	0.71	0.16	1.04	9.67

5.4.4 Organic carbon and nitrogen budgets for irrigated lowland rice

Sediment-associated nutrient losses from the rice area consisted of 1.94 Mg of OC and 0.68 Mg of N in 2011. For dissolved N, a total of 3.72 Mg (or 0.29 Mg ha^{-1}) was exported via paddy outflow in 2011. In 2010, the monitoring station at Location B was not yet installed and, therefore, data are not available for this period. The OC in the sediments in paddy outflow averaged 1.07% in 2011 (Table 5.5). Balancing losses with total inputs, these estimates resulted in an annual net contribution of 14.15 Mg of OC and 8.89 Mg of N (Tables 5.2 and 5.4) from sediments to the nutrient status of the 13 ha paddy area. This contribution corresponded to a trapped amount of 1.09 Mg ha^{-1} a^{-1} sediment-associated OC and 0.68 Mg ha^{-1} a^{-1} of sediment-associated N, revealing that rice fields were a net sink, rather than a net source for sediment-associated nutrients, at landscape level.

Multiplying monthly average concentrations of NH_4^+ and NO_3^- in surface reservoir outflow with monitored discharges to the paddies from irrigation, provided estimates of annual inputs to the rice area of 2.82 Mg of NH_4^+-N and 1.07 Mg of NO_3^--N in 2010, and 1.97 Mg of NH_4^+-N and 0.26 Mg of NO_3^--N in 2011. Accounting for the area of the paddies, which is 13 ha, these results correspond to an average annual input of 0.19 Mg ha^{-1} of NH_4^+-N and 0.09 Mg ha^{-1} of NO_3^--N. This input is the fraction of total N transported into the paddies that is potentially plant-available. Thus dividing by the total N loads (Tables 5.3 and 5.4), which additionally include

organic N, 24% of total N inputs from irrigation was found to be potentially plant-available in both study years. The plant-available proportion (combining sediment-associated and dissolved NH_4^+-N and NO_3^--N) differed between seasons: during the 2010 spring rice crop, from February till June, over half of irrigation water N inputs to the rice fields were in a direct plant-available form (Figure 5.7). In the summer season of 2011, when rainfall did not coincide with upland maize fertilization, 30% of N inputs were found to be plant available. During both summer cropping seasons, from July till November, overall N inputs from irrigation were larger as more water was irrigated (Figure 5.4a), but only 15% of this contribution was plant available N (Figure 5.7).

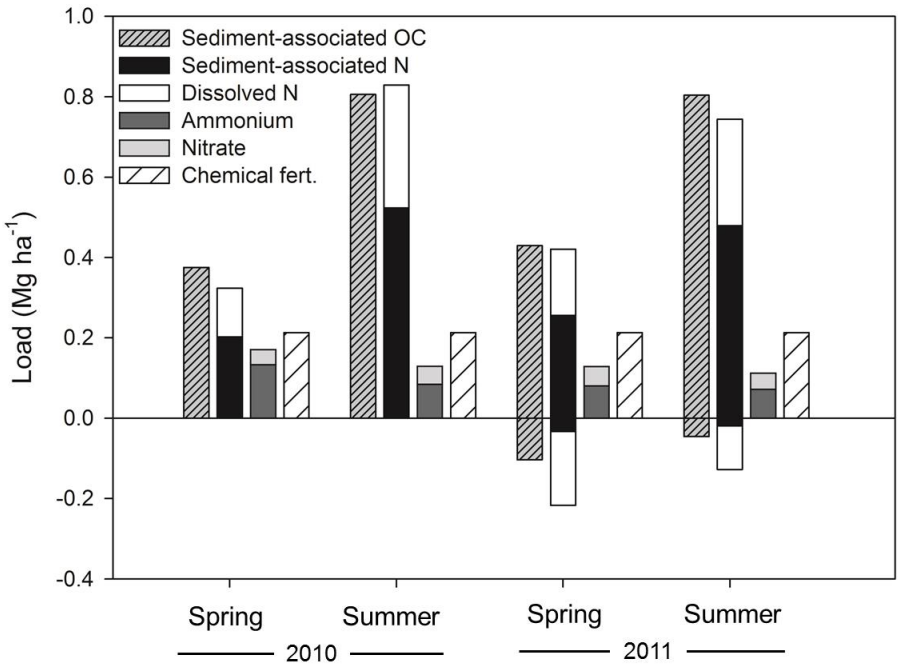

Figure 5.7: Organic Carbon and Nitrogen inputs to the 13 ha paddy area (Mg ha^{-1}) per rice cropping season (spring: Feb-June, summer: July-Nov) for both years in the study. Inputs shown are total sediment-associated OC inputs (from irrigation and erosion), N inputs divided into sediment-associated and particulate fractions, and total plant-available N inputs divided into ammonium-N and nitrate-N. The recommended N inputs from chemical fertilizer according to local agricultural extension guidelines are also indicated. Negative loads are nutrient losses via paddy outflow. Losses were only quantified for OC, sediment-associated and dissolved N in 2011. Losses for ammonium, nitrate and chemical fertilizer were not assessed.

5.4.5 Relocation of organic carbon and nitrogen to neighboring catchments

Nutrients are not only lost via paddy outflow as quantified in the previous section, which for the entire 13 ha paddy area resulted in the export of 1.94 Mg of OC, 0.68

Mg of sediment-associated N and 3.72 Mg of dissolved N in 2011. They are also exported via the irrigation channel, which leaves the catchment and crosses over into a neighboring catchment. In 2010, these losses amounted to 3.39 Mg of OC and 2.22 Mg of N, and in 2011 a total of 3.43 Mg of OC and 2.19 Mg of N were exported this way (Tables 5.2, 5.3 and 5.4). Part of the overland flow that enters the channel during rainfall is also exported in the same way, amounting to 0.50 Mg of OC and 0.11 Mg of N in 2010 and 0.40 Mg of OC and 0.07 Mg of N in 2011. Additionally, watershed losses occurred when excess water was removed from the irrigation supply through the spillover during the rainy season: 6.72 Mg of OC and 0.86 Mg of N left the catchment via reservoir overflow into the river in 2011.

5.5 Discussion

5.5.1 Reservoir influence on upland-lowland nutrient re-allocation in irrigated watersheds

Irrigation water is an important medium for redistribution of nutrients at the watershed scale. Previous work (Slaets *et al*., 2015) has shown that in the same catchment, irrigation mobilized 75% of sediment inputs into the paddy area while 25% originated from erosion. For nutrients, the role of irrigation becomes even more pronounced: 90% of sediment-associated OC and virtually all N, both sediment-associated and dissolved, were brought in by irrigation water while only very little was delivered by erosion (Figures 5.5 and 5.6). Substantial contributions to nutrient loads from overland flow were only made in months of high rainfall and large storms, when mobilized material was characterized by high OC to N ratios. Overland flow therefore still played a role in OC transport, but direct overland flow contributed very little to the N inputs of the rice area. The estimated sediment-associated OC and total N contributions from irrigation are higher than the 0.03 Mg ha^{-1} found by King *et al*. (2009) for a study in Southern California, where regulatory programs protect the reservoir from erosive land use in the contributing area with similar elevation as our study area, showing the importance of the erodibility and land use of the surrounding landscape in irrigated settings. The results are, however, in the same order of magnitude as another study describing nutrient loads from irrigation. Schmitter *et al*. (2012) recorded 1.30 Mg ha^{-1} a^{-1} of OC (both sediment-associated and dissolved) and 0.72 Mg ha^{-1} a^{-1} of total N in the same study area for the two rice cropping seasons from February till October.

While the reservoir discharged a much larger water volume to the paddies than runoff, the higher OC and N loads contribution of the reservoir is not solely related to the released water quantity. The percentage of OC and N in the sediments coming from the surface reservoir was larger than OC and N in sediments from direct overland flow. Both sources, however, receive a relatively similar quality of sediments (i.e. nutrient content), as the drainage area to the lake consists of similar soil types and land uses to those of the 37 ha of upland area draining directly to the irrigation channel. The OC content of erosion sediments was around one third of the OC content in irrigation water, and this difference in nutrient content was therefore caused by biogeochemical processes in the reservoir: breakdown of organic matter and nutrient mobilization in an aquatic environment contribute to the increased nutrient content of the irrigation water. Furthermore, sedimentation of the coarse, sandy material resulted in irrigation water containing fine-textured, fertile sediments higher in OC and N (Lick, 1982; Yamada *et al*., 2015). Results from Slaets *et al.* (2015) on texture analysis for sediments in the same study site also demonstrated that irrigation water sediments were characterized by a finer texture (average 33% sand, 33% silt, 34% clay) than those in overland flow (average 50% sand, 30% silt and 20% clay).

The surface reservoir additionally buffered the seasonal changes in the quality of sediment inputs to the paddies. Brown *et al*. (2011) similarly found surface reservoirs to retain approximately 16% of total N load. While OC to N ratios in sediments from overland flow increased as the rainy season progressed, and light, fertile material disappeared increasingly from the watershed, OC to N ratios of the sediments in the reservoir outflow remained more constant throughout the year. Irrigation water thus provided a constant influx of nutrient-rich sediments beneficial to the rice area, compared to overland flow. Seasonal trends were visible, however, in the plant-available N contribution of irrigation water. In the spring season, the N inputs were dominated by NH_4^+ and NO_3^-, while in the summer, during the rainy season, organic N became more important. This change shows the effect of the N inputs into the reservoir from runoff during the rainy season: runoff during the spring season might easily carry dissolved fertilizer into the reservoir, even if rainfall events are not intense enough to generate substantial erosion.

5.5.2 Irrigation and overland flow in the overall rice organic carbon and nitrogen budget

OC and N inputs from irrigation water were large compared to overland flow, but only part of these inputs will remain long enough on the fields to really be taken up by rice plants. A part will be lost through the quantified pathway of paddy outflow, and also through volatilization or seeping into groundwater. The question therefore remains what was the contribution of irrigation and overland flow to the overall OC and N budget of rice fields in this cascade setting. N inputs from chemical fertilizer to paddy fields vary widely, with average values ranging from 0.06 to 0.15 Mg ha^{-1} per cropping season in Asia (International Plant Nutrition Institute, 2002) depending on soil types, climatic conditions, varieties and cropping intensity (Dobermann and White, 1998). In Chieng Khoi, the local extension service recommended 213 kg N ha^{-1} per rice crop, thus amounting to 426 kg ha^{-1} of N over a year containing two rice crops. Inputs from irrigation water, estimated at 190 kg ha^{-1} a^{-1} of NH_4^+-N and 90 kg ha^{-1} a^{-1} of NO_3^--N, thus potentially provided a load of plant-available N equivalent to 66% of the recommended application of nitrogen through chemical fertilizer, based on our results. As N is usually found to be more limiting than phosphorous or potassium in irrigated rice systems (Dobermann *et al*., 2003; Suprapti *et al*., 2010), the indigenous nutrient supply has a vital role in maintaining rice yields. These results underscore both the importance of upland-lowland linkages and the vulnerability of rice production and food security to changes in land use, such as deforestation, cropping systems and intensification, in the landscape as a whole. Plant-available N inputs, in the form of NH_4^+ and NO_3^-, showed seasonal trends linked to fertilization of maize on upland areas. Therefore upland-lowland linkages do not only affect spatial variability due to differential deposition of sediments (Schmitter *et al*., 2010) but also temporal variation. The summer crop was over-irrigated when the reservoir became full during the rainy season. While the spring crop of 2010 received less irrigation water, and thus less N inputs from irrigation water, it received a larger amount of plant-available N, as the months of May and June coincide with maize cropping on upland areas.

Although the majority (93%) of sediment-associated N inputs were captured in the rice fields, a filtering effect also found by Yan *et al*. (2010) and Marumaya *et al*. (2008), the N export from paddy outflow was driven by the dissolved fraction (Figures 5.6 and 5.7). As the dissolved N exported from the paddies not only consists of inputs from irrigation water, but also from other sources such as chemical fertilizer, green manure and biological N fixation, the dissolved N in the paddy

outflow can be expected to contain a combination of these inputs. Therefore, it was not possible to quantify the proportion of dissolved N contributed by irrigation that is trapped in the rice fields. But losses will also take place for chemical fertilizer, and results showed that in both cropping seasons in both study years, the amount of potentially plant-available N inputs from irrigation formed a substantial contribution, corresponding to over half of the recommended amount of N from chemical fertilizer. These findings demonstrate the importance of upland-lowland linkages in mountainous irrigated watersheds, as maize fertilization on the uplands was linked to a flush of plant-available N into the rice fields. Redistribution mechanisms within watersheds therefore need to be taken into account – not only for site-specific, but also for season-specific fertilizer recommendations. Assuming losses from denitrification of 150 kg ha^{-1} a^{-1} (Yan *et al*., 2010), a net plant-available N capture of 130 kg ha^{-1} a^{-1} would still remain, and therefore N fertilizer application could be reduced without risking N deficiency issues. These implications are further supported by Schmitter *et al*. (2011), who compared fertilized and non-fertilized plots and found no significant differences in rice grain yield between the two in the same study area.

5.5.3 Nutrient re-allocation beyond the watershed scale

Nutrients were not only reallocated within the watershed, the irrigation system also exported nutrients out of the watershed. The main source of these losses was through the surface reservoir spillover: when the lake maximum capacity is reached, the spillover starts to function and releases excess water into the river, through which it is removed from the watershed. Both for OC and dissolved N, this release was the largest export pathway, larger than losses from overland flow or paddy outflow. For sediment-associated N, the largest loss was through irrigation water leaving the catchment via the irrigation channel. Both this water, and discharge from the spillover released to the river, was used further downstream to irrigate paddies in a lower lying catchment. Sediments in the irrigation water were characterized by a higher percentage of OC and N and a lower OC to N ratio compared to runoff, illustrating how the filtering effect of the reservoir releasing nutrient-rich sediments propagates beyond hydrological borders and benefits rice production further downstream as well. Furthermore, the combined load of dissolved N released from the watershed amounted to 13 Mg a^{-1}. Assuming a required amount of N fertilizer according to the local recommendations of 0.43 Mg ha^{-1} a^{-1}, the load of dissolved N

lost from the watershed alone could potentially provide enough N for 30 ha of paddy rice downstream, emphasizing the propagating effect of filtering elements in the landscape such as rice fields and reservoirs, also reported by Brown *et al*. (2011), Lassaletta *et al.* (2012) and Yoshinaga *et al*. (2007). The timing of N inputs from irrigation water depends on both upland fertilization and rainfall events. Maize is typically fertilized in June in the study area, coinciding with the highest NH_4^+ concentrations in the irrigation water, while for rice, local recommendations are a split application where the first dressing, at transplanting, contains 56% N, 100% P and 34% K of the total amount of fertilizer applied in the form of NPK and Urea. Second dressing (at maximum tillering) and third dressing (at flowering) provide the remaining 22% N and 33% K in the form of Urea and Kali. Therefore, even though irrigation water was found to make a substantial contribution to the indigenous N supply of rice, it cannot fully replace good (and timely) fertilizer management.

5.5.4 Implications of uncertainty for nutrient balance

Confidence intervals for OC and N load estimates were large (Tables 5.2, 5.3 and 5.4). Considering all sources of uncertainty affecting load estimates, including spatial and temporal variability (de Vente and Poesen, 2005; Mai *et al*., 2013), non-linearity of sediment transport processes at different scales (Schreier and Brown, 2004) and controls of sediment supply, other than hydrological mobilization and carrying capacity (Gao, 2008) – a very small variance would, in fact, be unexpected. In this type of study, highly accurate predictions are the ones that should invoke closer inspection as they can often be attributed to a lack of validation, an over-parameterization of the model or a too small dataset that simply did not capture the variability in the matter transport.

While the confidence intervals might seem large, especially since they are amongst the first of such results presented, overall, the biophysical interpretation and implications for plant production and sustainability in the area hold. Comparing the confidence intervals for OC and N inputs from overland flow and irrigation water, the contribution of irrigation water remains substantially larger than that of overland flow, emphasizing the dominant role of the surface reservoir in sediment redistribution. The confidence intervals for the sediment loads from irrigation water were wider than those for the load coming from overland flow, confirming that irrigation processes are driving the uncertainty in the OC and N budgets for this

watershed. These results further illustrate the importance of high-temporal resolution data and uncertainty analysis, especially for implementing integrated watershed management strategies or soil and water conservation practices at the watershed level.

5.6 Conclusions

The sediment-associated organic carbon and nitrogen budget for a 13 ha paddy area in this study showed that rice fields were a net sink for sediment-associated OC and N. The paddies trapped 88% of OC and 93% of N, resulting in a net input of 1.09 Mg ha^{-1} a^{-1} of sediment-associated OC and 0.68 Mg ha^{-1} a^{-1} of sediment-associated N. Irrigation water was the dominant driving force of nutrient re-allocation within the watershed, contributing 90% of OC inputs and virtually all N inputs, and provided an additional 0.43 Mg ha^{-1} a^{-1} of N in the dissolved fraction. NH_4^+ and NO_3^- analysis showed that 24% of the combined sediment-associated and dissolved N input into the paddies was potentially plant-available, and therefore irrigation water contributed a substantial amount of plant-available N to the rice, amounting to 66% of the recommended N inputs from chemical fertilizer over the whole vegetation period. The higher percentage of OC and N in sediments in irrigation water, as well as the lower OC to N ratios demonstrated the buffering effect of the surface reservoir on sediment-associated nutrient transport in the watershed. As the sediments in the irrigation water stem from the same erosion processes and from similar sediment sources, the difference in quality between irrigation water and overland flow was attributed to the reservoir capturing coarse, unfertile material and slowly releasing nutrients both to the rice fields within the watershed and, via paddy outflow and the reservoir spillover, to downstream areas as well.

The contribution of irrigation water to the plant-available N inputs highlights the importance of quantifying upland-lowland linkages of maize-rice cropping systems, which are very common throughout montane Southeast Asia. Currently, erosion due to unsustainable maize monocropping on the upland fields results not only in a loss of soil fertility *in situ*, but also in an influx of nutrients to paddy fields. A permanent loss of nutrients from the uplands, for example by removal of the fertile topsoil, would therefore not only result in a loss of income due to a declining yield of the cash crop maize, it would also entail a loss of nutrient inputs to the paddies, associated with a decline of nutrient content of the sediments in the irrigation water.

Such upland-lowland linkages demonstrate the vulnerability of rice yields to landscape level nutrient re-allocation processes. Surface reservoirs help mitigate these consequences with their filtering capacity, but eventually, only sustainable land use practices can ensure continued food security in these cropping systems.

Chapter 6 General discussion

6.1 Overview

This thesis focused on developing methodologies to quantify transport of sediment, organic carbon and nitrogen at the watershed level in irrigated catchments, the implications of these flows for soil fertility, and the resulting effects for upland maize and lowland rice production. These maize-rice cropping patterns have arisen after intense population increase and changes in land use over the last decades, but the crop production system is by no means in a steady state now. Unsustainable practices make the current situation untenable in the long run. Additional drivers of crop yield and matter transport, such as climate change, will add more processes to reckon with in the future. Therefore, filtering elements in landscapes such as paddy fields but also surface reservoirs will gain importance as protective components for lower lying areas.

In this discussion, the overall applicability of the developed turbidity-based and statistical methodology from Chapter 2 is discussed, and the relevancy of the resulting sediment, organic carbon and nitrogen load estimates from Chapters 4 and 5 to other scales is assessed. The role of measurement error and hydrological characteristics on uncertainty, which was quantified in Chapter 3, is determined. The effects of an expected increase in extreme rainfall events and runoff on upland-lowland sediment redistribution processes are assessed and compared to the current re-allocation as computed in Chapter 4. Subsequently, the buffering potential of small reservoirs on sediment re-allocation and the global sediment cycle is examined. Finally, potential future paths for sustainable agricultural practices in montane Southeast Asia are reviewed.

6.2 Methodology transfer and scaling issues

Mountainous agricultural catchments in the tropics are challenging to monitor in terms of water and matter flows. Topography, geology and soil properties are highly variable in montane areas. Strong anthropogenic influences furthermore lead to highly diverse land use on small plots, which changes rapidly and results in altered soil cover and soil quality over time. As rainfall patterns in the tropics tend to be erratic and display higher spatial and temporal variability compared to temperate regions (Callaghan and Bonell, 2005), large differences in antecedent moisture

conditions, rainfall intensity and duration, and varying runoff and erosion between events, seasons and years pose additional complications in the quantification of water and matter flows. In combination with irrigation management, which disturbs the natural link between stream flow and matter transport, classic monitoring strategies such as direct measurement by integrating values from automatic water samples, or a sediment rating curve based on discharge (Gao, 2008) are not suitable for this type of environment. The turbidity-based method developed in Chapter 2, however, is able to accommodate these specific issues, as the use of multiple predictor variables overcomes the distorted relationship between water flow and particulate concentration and difficulties with sensor limits due to extreme concentration peaks, and the use of a linear mixed model allows a storm-based sampling strategy that captures the full range of flow conditions by modeling the serial correlation in the data. The result is a widely applicable method that is not only suitable for irrigated, intensely cultivated or mountainous catchments, but for many non-natural environments as well, including mined areas, catchments disturbed by logging or controlled reservoir release related to hydropower and regulated rivers. Additionally, the sensor-based approach is not only suitable for monitoring sediment transport, but the same sensor can be used to continuously quantify organic carbon and nitrogen flows as well. Using one sensor is a cost-effective and practical way to simultaneously monitor several constituents important to water quality, landscape re-allocation processes and catchment sediment and nutrient losses.

While the method is suited for a range of environments and applications, results obtained at one scale do not necessarily apply to another scale: the spatial level at which constituent fluxes are monitored is an important consideration when interpreting load estimates. Results at the plot level are not necessarily meaningful at the watershed, regional or national level, as several factors affect the relevance of the results. Firstly, different processes dominate over different area sizes. Ecological theory dictates that lower spatial scales tend to be dominated by processes acting at plant level, while higher spatial scales are dominated by climatic and geomorphological processes (O'Neill *et al.*, 1991). Schreier and Brown (2004) found indications that surface erosion dictates sediment transport in small catchments, while erosion and resuspension from stream banks and flood plain deposits drive erosion rates in large watersheds. Rill and gully erosion can contribute a large proportion of the watershed sediment load, but are not uniformly distributed in

landscapes. Redeposition, under influence of sediment trapping landscape elements such as hedges or grass barriers, hardly plays a role in bounded plot measurements, but becomes important when upscaling. Therefore, the change in erosion rates between different scales depends strongly on the nature of the landscape. A monitored plot containing rill or gully erosion might have a much larger soil loss than the average over the watershed. In a catchment with a mosaic landscape, features can act both as sources and as sinks depending on antecedent moisture, rainfall patterns and location, influencing the spatio-temporal variability of sediment and nutrient transport processes. In a mountainous, cultivated area such as Chieng Khoi, many sediment trapping elements in the landscape and hence opportunities for redeposition can result in plot-level erosion rates much larger than the watershed sediment yield.

Secondly, spatial variability of erosion and runoff can be large, especially in fragmented landscapes with small field size and diverse land use such as the situation in the study site of this thesis. Schreier and Brown (2004) found the spatial variability between fields for a mountainous catchment in Nepal to be larger than the temporal variability between runoff events on the same field. Due to this variability, all plots must be measured in order to summarize plot results over the whole area, which is only feasible if census data are available for the whole watershed. This is almost never the case, not in the least because watershed borders do not tend to follow administrative boundaries.

As a result, there is a non-linearity when comparing the change in area-specific erosion rates at different scales. Schreier and Brown (2004) used a nested approach and compared sediment export over four different spatial scales (at 0.01 ha, 72 ha, 532 ha and 11 100 ha). They found that the area-specific suspended sediment yield monitored at 11 100 ha was 30% smaller than the sediment yield at 0.01 ha, as a result of sediment sources and sinks present in the landscape, resulting in redeposition and retention as well as sediment diversion into an irrigation system. For the below-watershed scales, there was no clear reduction effect.

Table 6.1: Scaling effect on area-specific sediment yield for Chieng Khoi catchment in 2011

Scale	Contributing area (ha)	Sediment yield (Mg ha^{-1} a^{-1})	Relative change (%)
Bounded plot (Tuan *et al.*, 2014)	0.0072	10 - 110	22 - 244
Unbounded plot (Tuan *et al.*, 2014)	0.042 - 0.159	14 - 55	31 - 122
Upland area (Chapter 4)	17	7.5	17
Sub-watershed (Chapter 4)	50	45	**100**
Watershed (Chapter 4)	200	28	62

Using the results from Chapter 4 and data from Tuan *et al.* (2014) regarding bounded plot and sediment fence erosion measurements in the same study site, Table 6.1 contains the measured sediment yield over different scales for the watershed in this thesis. The range of sediment yields in the bounded plots in Chieng Khoi illustrates the high spatial variability of plot scale measurements in the study site. This large range is not unexpected in such an intensely cultivated mountainous watershed: large inherent differences due to geological and topographic conditions affect hydraulic conductivity, which is one of the key soil properties driving sediment delivery. Additionally, soil management and changes in vegetation cover in such an intensely cultivated area with high population pressure, and thus small farm size, constantly alter infiltration and runoff properties.

Looking at sediment yield from the hills only, excluding the paddies, the data display a decrease in sediment yield from the bounded and unbounded plot measurements to the complete 17 ha upland area, showing the capacity of this mountainous landscape to retain runoff and sediment: the highly fragmented land use on the uplands and mixture of homesteads, linear elements such as roads and ditches, and uneven topography make naïve upscaling by extrapolating plot level results not meaningful. The plot level measurements, however, are the only relevant assessments of loss of soil fertility at the field for farmers and agricultural extension, which are needed for example for accurate recommendations on soil and water conservation at the field scale. As landscape measurements taking into account large redeposition processes that take place only beyond the farm, they will inevitably underestimate soil loss on the farm. Therefore, due to the characteristics of the study site, which is highly divided and heterogeneous, there are not only problems with upscaling which are typical (Swallow *et al.*, 2002), but also with downscaling.

The increase in sediment yield from upland area to sub-watershed, and from sub-watershed to watershed is unexpected, as one would normally suppose a decrease. But in Chieng Khoi watershed, the surface reservoir affects sediment budgets that include the lowland areas: for the sub-watershed, the vast majority of exported sediments are actually originating from reservoir overflow into the river, and therefore these sediments do not really come from the sub-watershed but rather from the 490 ha contributing area surrounding the lake. They are propelled to the outlet at the sub-watershed and subsequently pass the main outlet of the watershed. In irrigated or dammed catchments, normal scaling factors for natural flow regime catchments (Williams, 1975; Lu *et al.*, 2005) can thus not be expected to hold true.

In conclusion, reliably assessing watershed management problems at different hierarchical scales requires monitoring strategies to be integrated across those scales (Swallow *et al.*, 2002). As the process understanding we have is typically at the plot level, most budgets for catchment scale or larger tend to be derived from models and are often poorly calibrated (Schreier and Brown, 2004). The sediment budget in this thesis, however, was quantified at the catchment scale, and validated using cross-validation and a bootstrap uncertainty assessment, thus providing a strong physical foundation for model inputs. The turbidity-based methodology developed in Chapter 2 provides a powerful tool for future studies to measure constituent transport beyond the plot, thus contributing to overcoming scaling issues that have thus far hindered accurate assessments of sediment and nutrient redistribution at the landscape, regional and national level.

6.3 Drivers of accuracy in constituent transport monitoring for irrigated watersheds

6.3.1 The role of measurement error in improving sediment concentration predictions

In Chapter 3, the uncertainty on the sediment concentration predictions was considered as a component in the uncertainty on annual sediment load estimates. Conceptually, the concentration prediction error can also be separated into an underlying latent autoregressive process generating the true concentrations, and an independently distributed measurement error corresponding to white noise in time series data. The variance of the data is then given by

$$var(y) = \sigma_p^2 \Omega + \sigma^2 I \,, \qquad \text{(Equation 6.1)}$$

where y is the response variable i.e. the sediment concentration, σ_p^2 is the latent process variance, Ω is the correlation matrix containing the autocorrelation parameter ρ, σ^2 is the measurement error variance, and I is the identity matrix. The white noise, i.e. the second term in Equation 6.1, is equal to the error that would remain if two measurements were conducted at almost coinciding time points. This variability is typically attributable to measurement error and in spatial statistics, this is what is known as a nugget effect. Convergence problems are very common when trying to fit nugget models as these models tend to be difficult to fit. Particularly AR(1) type error structures are prone to these issues, as there is an inherent confounding between the independent white noise component and the autocorrelated variance component (Piepho *et al.*, 2015). In a bootstrap setting where convergence was already an issue, adding such an effect would be an impractical choice. But for exploratory purposes, the nugget can be fitted to the original dataset without bootstrapping, in order to examine the contributions of the respective error components. The sediment concentration prediction model in Chapter 2 had a spatial power error structure with a power decay of the serial correlation over time, which allows for non-constant time lags between samples, but as this structure gave convergence issues in the bootstrap resampling, it was replaced with a first-order autoregressive structure. Therefore in Table 6.2 the nugget effect is tested for both covariance structures.

Table 6.2: Contribution of measurement error to the variance of the sediment concentration predictions. Parameter estimates of variance components due to latent process (autocorrelation and latent process variance) and measurement error variance for two different covariance structures (first-order autoregressive or spatial power), for the irrigation channel sediment concentration prediction model. The response variable, suspended sediment concentration, was log-transformed. Model fit for the two different covariance structures is assessed with the Akaike Information Criterion (AIC, smaller is better).

	Covariance structure	
Variance parameter	**AR(1)**	**Power decay**
Autocorrelation	0.84	0.97
Latent process variance	0.65	0.99
Measurement error variance	0.31	0.29
AIC	857	827

Results show that, for the irrigation channel sediment concentration predictions, the measurement error is large (Table 6.2) and does not differ much when changing from an AR(1) to a power decay covariance structure, although the latent process variance

is larger than the measurement error in both models. The asymptotic correlations between the variance-covariance parameter estimates, obtained from the information matrix, indicate that there are substantial correlations between the covariance parameters which are the cause of the frequently observed convergence issues, even though the correlations did not reach the boundary values of -1 and 1 (Table 6.3).

Table 6.3: Asymptotic correlations of the three variance-covariance parameter estimates (shown in Table 6.2) for the first-order autoregressive covariance structure and the power decay structure.

	Correlation	
Variance	**AR(1)**	**Power decay**
Autocorrelation – latent process variance	0.02	0.35
Latent process variance – measurement error variance	-0.50	-0.27
Autocorrelation – measurement error variance	0.58	0.40

The presence of a nugget effect implies that decreasing the measurement error could be an important factor in improving sediment concentration predictions. While the latent process error is also large, improvement there is not a possibility, as this scatter is inherent to the underlying physical process of sediment transport. Even if an unlimited number of water samples were to be obtained, the sediment rating curve would not become perfectly accurate: sediment source heterogeneity gives rise to equifinality of combinations of sediment texture and organic matter content, and sediment concentration does not only depend on hydrological carrying capacity but also on sediment supply, meaning that there is simply no perfect relationship between sediment concentration and hydrological predictor variables to be found. The measurement error, on the other hand, indicates that if two measurements are performed at almost coinciding time points, they would still yield substantially different results. Factors contributing to this measurement error include sensor error, both from the turbidity sensors and the pressure sensors for discharge, the manual grab sample process which may not always capture the center point of flow, and laboratory error in determining the sediment concentrations. The error separation thus indicates that focusing on these factors could yield substantial improvement in the sediment rating curve.

6.3.2 Hydrological and climatic influences on error for better sampling strategies

Monitoring landscape processes is an essential step in improvement of agricultural and water quality management practices, design of hydrological structures such as reservoirs and irrigation systems, and land planning. In order to further explore sources of variance, which can lead to improved process understanding and sampling recommendations as to where and how to measure these landscape processes, the variance-covariance parameter estimates for sediment concentration were examined for differences between seasons, flow regimes (base-flow versus storm-flow), and rainfall event characteristics. This was done by using the group option in the repeated statement of PROC MIXED in SAS, which allows variance components to vary between groups of observations. The first-order autoregressive covariance structure was used as the power decay again resulted in non-convergence.

Table 6.4: Flow-specific and season-specific variance components and model fit (AIC) for the suspended sediment concentration predictions

	Flow regime	Estimate	Season	Estimate
Process variance	Base-flow	1.20	Spring	0.99
Process variance	Storm-flow	0.83	Summer	0.98
Autocorrelation	Base-flow	0.43	Spring	0.59
Autocorrelation	Storm-flow	0.64	Summer	0.41
AIC		848		879

Results in Table 6.4 show that the variance of sediment concentration on the log-scale is larger during periods of no rainfall. Event concentrations are correlated with hydrological variables such as rainfall and discharge, while variations in irrigation water base-flow do not necessarily have the same drivers. Turbidity is then the most powerful predictor variable, but as the results from Chapter 2 showed, turbidity is affected not only by sediment concentration but also by sediment texture and organic matter content, hence the large variance for the base-flow samples. Seasonal changes in reservoir outflow quality entail differences in sediment texture and organic matter content, further confounding the predictive power of turbidity sensors and underscoring the additional difficulties that quantifying matter flows in irrigated catchments poses. The seasonality group effect also showed that the variance is larger in the spring season than in the summer season, which could be related to higher intensity spring storms on bare upland hills, and flushing effects at the onset of the rainy season that bring different qualities of sediment, with higher amounts of

organic matter, into the channel compared to later in the season. Organic matter was shown to affect the turbidity signal in Chapter 2. Comparing models, however, the AIC for fitting flow-specific variance components is smaller indicating better model fit and therefore flow regime has a more important effect on the variance than season.

The variance separation underscores that water and matter fluxes in irrigated catchments behave differently than they do in natural catchments. Base-flow in particular plays a more important role in sediment and nutrient transport when irrigation is present. This dominance of base-flow in our study is at odds with the old adage that, in natural catchments, 90% of sediment is typically transported in only 10% of the time – during extreme rainfall events (Horowitz, 1995). In Chieng Khoi watershed, irrigation water was the dominant driver of sediment, organic carbon and nitrogen transport, mobilizing around 75% of sediment, 90% of organic carbon and 99% of nitrogen inputs into the paddy area, and causing the vast majority of catchment sediment yield. Irrigation water samples were also the main source of variability for the sediment concentration prediction model. While the vast majority of load assessments are performed in natural watersheds, irrigation affects large areas of agricultural land, especially in Southeast Asia. Over 60% of the world's irrigated agriculture is in Asia, and approximately two thirds of that area concerns cereal production, most of which consists of rice (Barker and Molle, 2004). The importance of irrigation water in sediment re-allocation is reinforced further by land use intensification leading to increased erosion and thus higher sediment concentrations in reservoir water. Strategies that can quantify loads in irrigated catchments are therefore widely applicable.

The influence of base-flow irrigation affects the suitability of monitoring strategies for constituent flows. Any approach that relies exclusively on the natural link between discharge and constituent load in non-managed streams will not be appropriate in irrigated watersheds. Turbidity as a predictor variable is a viable alternative, as long as the sampling strategy includes enough base-flow samples to obtain model convergence, which is more difficult when a resampling method such as the bootstrap is used for assessing uncertainty and removing bias. Based on the results in Chapter 3, a minimum of around 25 base-flow samples per location

sufficed to allow an independent resampling of no-rain samples without convergence issues for the bootstrap replicates.

When focusing on storm-flow samples exclusively, group-specific variance components were used to explore the effect of rainfall characteristics on variance. Group-specific variance parameters were fitted for rainfall maximum intensity, cumulative event rainfall, rainfall duration and duration of the antecedent dry period. The nugget or measurement error was assumed not to be group-specific, as factors such as sensor and lab error do not depend on hydrological characteristics. The 25, 50 and 75% quantiles of the 420 rainfall events in the two year study period were used as the limits to classify four groups for each rainfall characteristic. The vast majority of events are small: 371 events mobilized less than 1 Mg of erosion each. 16 events resulted in between 1 and 2 Mg of sediment eroded, and the remaining 33 events which are the largest in the study, are shown in Appendix C. As the rains came late in 2011, the erosive storms appeared further in summer, while in 2010 they occurred earlier in the season, in May and June.

Classifying events according to the maximum event rainfall intensity (in mm h^{-1}) yielded the largest drop in AIC, showing improved model fit. Furthermore, variance is largest for the largest rainfall intensities. Making recommendations for sampling strategies based on these results, however, is rather difficult as no one can predict when a certain type of event will take place, making it hard to adjust the strategy towards anything else than catching as many events as possible. In conclusion, in order to obtain improved load estimates, based on the variance component analysis, sampling efforts in irrigated catchments should ideally focus on capturing a variety of base-flow conditions, as well as early season and high-intensity events. As land preparation activities such as ploughing and clearing typically take place in spring, intensely erosive and highly variable runoff events typically take place during this time of year in many agricultural systems, and taking these field processes into account during data collection could result in improved constituent load estimates in a broad range of environments.

Table 6.5: Group-specific variance estimates for rainfall characteristic-based event classification. Four groups were formed, and groups were separated by the 25%, 50% and 75% quantiles of the full event dataset for cumulative rainfall, maximum event 30 minute rainfall intensity, duration of the antecedent dry period and duration of the event (Group 1 < 25% quantile, 25% < Group 2 < 50% quantile, 50% quantile < Group 3 < 75% quantile, 75% quantile < Group 4).

	Group	Cumulative rainfall	Maximum rainfall	Duration dry period	Event duration
Process variance	1	0.05	0.20	1.60	0.66
Process variance	2	1.48	0.97	1.12	1.22
Process variance	3	0.89	1.12	1.38	1.13
Process variance	4	1.47	1.50	1.58	1.67
Autocorrelation	1	0.99*	0.94	0.89	0.99*
Autocorrelation	2	0.99*	0.99*	0.81	0.39
Autocorrelation	3	0.57	0.93	0.87	0.86
Autocorrelation	4	0.48	0.81	0.68	0.80
Measurement error variance		0.12	0.08	0.05	0.06
AIC		558	536	554	549

* Boundary value set to achieve convergence

6.3.3 Implications of uncertainty for load studies

Quantifying uncertainty has become increasingly important in assessments of water and matter fluxes; especially since databases are more and more being used as input for more complex, larger-scale (both spatially and temporally) studies. In Chapter 3 of this thesis, the importance of error propagation in calculating annual sediment loads was shown: ignoring the uncertainty on discharge estimation, which is commonly done in load studies, can underestimate confidence interval widths by 10%, even when the stage-discharge relationship has a high accuracy (R^2 of 0.95) – in fact, a much higher accuracy than the sediment concentration predictions. Uncertainty assessments should not be implemented as a last step in evaluating results, but rather be carried out through entire dynamic modelling studies (Lippe, 2014), for example by including not only the uncertainty on constituent concentration predictions, but also the error on discharge estimates, as was shown to affect confidence intervals on annual constituent load estimates in Chapter 3.

If these assessments are implemented consistently, the uncertainties might turn out to seem relatively large, compared to expectations based on the type of validations typically shown in erosion or sedimentation studies. But taking into account all sources of uncertainty addressed in this discussion – ranging from spatial variability

to temporal changes, from the non-linearity of sediment transport processes at different scales to the controls of sediment supply, rather than only hydrological mobilization and carrying capacity – a very small variance would, in fact, be unexpected. In this type of study, highly accurate predictions are the ones that should invoke closer inspection as they can often be attributed to a lack of validation, an over-parameterization of the model or a too small dataset that simply did not capture the variability in the matter transport. And while the confidence intervals determined in Chapter 4 might seem large, especially since they are amongst the first of such results presented, overall, the biophysical interpretation and implications for plant production and sustainability in the area hold. Comparing the confidence intervals for sediment inputs from overland flow and irrigation water, the contribution of irrigation water remains substantially larger than that of overland flow, emphasizing the dominant role of the surface reservoir in sediment redistribution. The confidence intervals for the sediment loads from irrigation water were wider than those for the load coming from overland flow (Chapter 4), and the variance of the sediment concentration predictions was larger for the base-flow samples, confirming that irrigation processes are driving the uncertainty in the sediment budget.

While the paddy fields were determined to be a net sink for sediments, the lower limit of the confidence interval of the net paddy balance was negative (Chapter 4). The range of values covered by the 95% confidence interval therefore indicates the possibility that the rice area could act as a sediment source, rather than a sediment sink. In this case, the consequences of upland agricultural intensification would propagate even faster downstream, both negatively affecting rice production within the watershed and water quality and sediment re-allocation downstream, as all upland erosion would be propelled through the paddies. These results illustrate the importance of high-temporal resolution data and uncertainty analysis, especially for implementing integrated watershed management strategies or soil and water conservation practices at the watershed level.

6.4 Extreme rainfall event impact on sediment re-allocation in light of climate change

Adapting agricultural systems to the threats of climate change is one of the biggest challenges in guaranteeing future food security and safeguarding the livelihoods of people depending on agriculture, including the majority of the world's poor (Lipper

et al., 2014). In Vietnam, rice production in particular could be affected by climate change, specifically through increased temperatures, rising atmospheric CO_2 levels and changes in water cycles that could lead to flooding, but also to water scarcity and droughts (GFDRR, 2011; Redfern *et al.*, 2012). Higher night temperatures from global warming will result in reduced rice yields (Peng *et al*., 2004), but consequences are expected to differ between regions, and different studies report different projected yield trends. Ko *et al*. (2014) described an increase in yields for mountainous paddies, as simulated water and nitrogen use efficiency increased under rising CO_2 levels, which dominated the yield decrease due to temperature increase.

Rising sea levels and associated flooding are projected to affect 10% of Vietnam's surface area in the south, where rice is cultivated in vast lowlands of the Mekong and Red River delta's (Redfern *et al.*, 2012) – areas which are currently of prime importance for agriculture. Such a loss of cropping area puts great pressure on the population in Vietnam's lowlands and their food production. But these changes would not remain confined to the lowlands. Vietnam has already experienced a very similar chain of events in the last decades, the consequences of which formed the foundation of the project in which this thesis was conducted: population pressure in the South led to migration to the North, which subsequently became overpopulated itself and suffered from the resulting crop production intensification and associated land degradation. If large areas of lowland rice production are lost under the influence of climate change, these national upland-lowland linkages will come into play again, and the mountainous North will not remain isolated from impacts.

Additionally, rice production in the North of Vietnam has already been affected by flooding: in the study area an entire summer rice crop was lost in October 2007 due to typhoon Lekima (Schad *et al.*, 2012), showing the region's vulnerability to extreme rainfall events. Climate change is predicted to alter rainfall patterns globally: some regions are expected to receive seasonal shifts, while others will experience more intense, extreme precipitation (Christensen *et al.*, 2007; cited in Zeppel, 2014) – monsoonal Southeast Asia being in the latter category (IPCC, 2013). The results in Chapter 4 of this thesis have highlighted the importance of this type of events for sediment re-allocation in maize-rice cropping systems, as a storm on the 12^{th} of July 2011, consisting of 73 mm of rainfall in three hours, mobilized one quarter of the water erosion in that study year. Table 6.5 furthermore showed that large storms with

high maximum rainfall intensity contribute most to the uncertainty in sediment concentration predictions. In Vietnam, runoff is projected to increase by 7% by 2050 under influence of climate change (GFDRR, 2011). But the specific consequences on food production, of altered runoff resulting from climate change in mountainous areas, remain poorly understood to date.

Making a first step towards increased understanding of higher runoff on erosion rates and sediment re-allocation, the sediment budget of 2011 of Chapter 4 is here recalculated for the projected 7% increase in runoff. In a first scenario, all rainfall peaks are increased proportionally to their original size to result in a 7% total increase in runoff. As more extreme events are likely to occur, rather than a general increase, in a second scenario the largest runoff event in the study was increased with 7% of the total annual runoff. Concentrations were kept the same as the observed concentrations in both scenarios, which results in a conservative estimate, as increased erosion would increase the sediment concentrations as well. During long and intense storms, however, sediment exhaustion effects will come into play, but these factors are difficult to estimate exactly and therefore the cautious choice of keeping them unchanged was selected. Estimates resulting from the simulation can thus be interpreted as minimum impact scenarios.

Table 6.6: Simulated change in sediment load from upland area (17 ha) under influence climate change. Scenarios shown are the observed runoff, a 7% increase in annual runoff and a 7% increase in runoff during the largest monitored event.

Scenario	Sediment load (Mg a^{-1})
Observed	139
7% increase in runoff overall	149
7% increase in runoff peak-event	172

Results in Table 6.6 show that proportionally increasing all peaks has a small effect on the annual water erosion, while increasing the largest peak increases the eroded sediment load with 24%. The difference between the two is the very high peak sediment concentrations during the largest storm, which result in a larger amount of simulated erosion. The corresponding change in erosion rate is from 8 Mg ha^{-1} a^{-1} monitored in 2011 to a simulated erosion rate of 10 Mg ha^{-1} a^{-1}. As around 80% of overland flow enters the paddies (Chapter 4), this could potentially imply an additional 26 Mg of sediments brought in. Mid-infrared spectroscopy analysis

showed that overland flow has predominantly sandy texture (Chapter 4) and is thus preferentially being deposited into the rice fields, and therefore climate change has the potential to further exacerbate detrimental effects of maize-rice systems on rice yields in Southeast Asia.

The discussion based on the results in Table 6.6 focuses on an increase in total runoff and erosion and does not take changes in variance into account. As the predictions of the sediment loads have a log-normal distribution as both discharge and concentration are predicted on the log-scale, however, the variance on the original scale increases quadratically with the mean even if the variance on the log-scale is assumed to remain unaltered (Johnson *et al.*, 1994), as was done in this simulation. The variance of rainfall, and consequently of runoff and sediment load, however, can also be expected to increase, both intra- and inter-annually, resulting in larger load differences between years and larger uncertainty on annual load estimates. It is hard to assess the size of this change in a statistical modelling approach, as features of climate variability such as the El Nino Southern Oscillation introduce large uncertainty at the regional scale (McSweeney *et al.*, 2008). Dynamic modelling simulations disagree widely in projected changes in future amplitude of these events, and the manner in which they influence monsoonal variability in Southeast Asia is not well understood. As a result, climate projections for this region are characterised by great uncertainty (McSweeney *et al.*, 2008).

6.5 Sediment buffering capacity of small surface reservoirs

In Chapter 4, the focus was on the sediment trap capacity of paddy fields. As the study area is irrigated with water from a surface reservoir, there is an additional landscape element affecting water and matter transport, in a manner potentially very similar to rice fields. And due to the massive expansion in irrigated agriculture in Southeast Asia in the 1970s (Svendsen and Rosegrant, 1994), which has resulted in an abundance of surface reservoirs used for irrigation, the repercussions of reservoirs on water and matter fluxes potentially affect a large number of watersheds. In recent years, impoundments for hydropower, built to provide green energy, have also appeared increasingly throughout Africa and Asia, resulting in an additionally increased number of surface reservoirs. Impact studies related to these reservoirs, however, have mainly focused on population displacement (Singer and Watanabe, 2014), siltation rates (Lantican *et al.*, 2003), effects on the water balance,

competition for water and water scarcity (Barker and Molle, 2004). But small surface reservoirs, such as the one in the study site, can also store water, allow for part of the sediments to settle, thereby buffering particularly the coarse particle fluxes, and then slowly release sediments with the irrigation water. These trap and release processes, and their environmental impact on the watershed and downstream area, remain little studied to date.

The contributing area to the surface reservoir in Chieng Khoi consists of 490 ha of surrounding uplands. Assuming that the average watershed-level erosion rate for the upland area of 7.5 Mg ha^{-1} a^{-1} determined in this thesis is representative for these upland areas as well, that area-specific erosion rate results in a total annual sediment input to the reservoir of 3 675 Mg (Table 6.7). Irrigation water exported around 762 Mg a^{-1} from the reservoir, and another 1 557 Mg a^{-1} was lost through the spillover as the water level reached maximum storage capacity. Therefore, the reservoir trapped 1 356 Mg a^{-1} of sediments per year or 37% of the inputs. The trapped amount of 1 356 Mg a^{-1} corresponds to an average reservoir sedimentation rate of 0.43 cm a^{-1} as the lake surface area is 26.3 ha. Walz (2015) determined sedimentation rates based on fallout radio nuclides (^{210}Pb) which resulted in an estimated sedimentation rate of 1.1 cm a^{-1}. Based on charcoal analysis in the profile pits at the lake bottom, Weiss (2008) calculated average sedimentation rates between 2.5 and 3.3 cm a^{-1}. As those estimates were based on sediment accumulation in profiles directly below lake-adjacent plots with these three different land uses, the rates do not account for redeposition processes that occur at the landscape scale, when sediment sources are not located directly at the lake shore, which explains the larger sedimentation rate compared to the results based on the average watershed-level erosion rate from this thesis.

Table 6.7: Estimated trap efficiency of the surface reservoir (26.3 ha) in Chieng Khoi watershed, in Mg ha^{-1}, for 2011, based on data from Chapter 4. Shown are upscaled inputs from overland flow (see Chapter 4) of the 490 ha upland area, the combined sediment export from irrigation and the spillover, and particle size distribution for each component (See Chapter 4). Percentages add up to 100% in rows.

	Sediment (Mg a^{-1})	Sand (Mg a^{-1} (%))	Silt (Mg a^{-1} (%))	Clay (Mg a^{-1} (%))
Input	3 675	1 838 (50%)	1 102 (30%)	735 (20%)
Export	2 319	789 (34%)	789 (34%)	741 (32%)
Trapped	1 356	1 049 (77%)	314 (23%)	0 (0%)

Using average overland flow and irrigation water texture values measured in this study, the annually trapped sediment would consist of 1 049 Mg (77%) of sand and 314 Mg (23%) of silt, while the clay fraction would entirely be exported from the reservoir based on the clay concentrations present in the reservoir outflow in irrigation channel and spillover river water (Table 6.7). These results fit in with soil profiles that were dug in the reservoir bottom during the lowest water level, which showed a texture of between 40 and 75% of sand, 20 to 50% of silt and 5 to 14% of clay (Weiss, 2008). This preferential trapping ability demonstrates the protective power of reservoirs in mountainous watersheds, buffering increased erosion from changes in land cover on the hills surrounding them, by capturing coarse sediments and slowly releasing fertile sediments. Reservoirs can thus play a role in the safeguarding of downstream areas from large inputs of unfertile material, related to land use change processes in the headwater area of the reservoir.

This buffering effect is not limited to the watershed in which the reservoir is located, as reservoir water is used further downstream for irrigation, or is exported to major rivers via tributaries. The effect reservoirs can have on regional and global sediment and nutrient fluxes is well established for large artificial impoundments (up to 0.5 km^3) which are typically estimated to trap around 30% of incoming sediment (Vörösmarty *et al.*, 2003). The same study also included smaller reservoirs that were officially registered with UNESCO, and large and small impoundments combined (n≈45 000) were reported to intercept a total of 4 to 5 Gt a^{-1} of the world's sediment export to oceans, around 25 to 30% of the total global sediment flux. The role of even smaller, unregistered surface reservoirs, such as the one studied in this thesis, is not well understood, although there are an estimated 800 000 of these basins in the world (Vörösmarty *et al.*, 2003).

The results in this thesis demonstrate that these smaller reservoirs, with a similar ratio of reservoir size to contributing area, have a trapping potential of around 37% of the total incoming sediment (1356 of 3675 Mg a^{-1}, Table 6.1). Assuming this figure to be a representative trapping efficiency for reservoirs of this size, as well as the contributing area of 490 ha representative for other reservoirs, and calculating with an average global erosion rate of 10.2 Mg ha^{-1} a^{-1} (Yang *et al.*, 2003), the estimated 800 000 small unregistered reservoirs have the potential to retain 1.5 Gt of sediment annually or roughly 10% of the total global sediment flux. Due to their large number and this high filtering efficiency, buffering effects of small surface reservoirs thus need to be considered explicitly in global water and constituent flux estimates.

6.6 Escaping the maize trap: the future of maize-rice cropping systems in montane Southeast Asia

The results in this thesis demonstrated that permanent maize cultivation on upland fields in maize-rice systems is not only certain to result in a loss of soil fertility on the slopes, but also negatively impacts long-term rice production through the deposition of sandy sediments, low in organic carbon and nitrogen, in paddy fields. Surface reservoirs can buffer these repercussions by trapping coarse sediments and releasing fertile sediments and dissolved nutrients downstream through irrigation. Direct erosion entering the paddies, however, does not pass this filtering mechanism and thus poses a threat to the long term productivity of the paddies under continued degrading upland soil quality. Simulations in Chapter 6 showed that under the impact of climate change, more extreme rainfall events can be expected to intensify these negative upland-lowland linkages in the future. But maize prices on the world market are so high, that finding sustainable alternatives attractive to farmers proves very difficult, hence people are trapped in choosing maize for upland cultivation. In order to emerge from this maize trap, solutions must be adjusted to site conditions and have a local support base. These requirements are challenging to fulfill in any situation, but particularly so in light of the socio-cultural context of the ethnic minorities historically inhabiting the mountainous North of Vietnam, seeing them as state-escaping people (Scott, 2009). Top-down approaches or blanket recommendations in such a highly fragmented environment are doomed to fail (Neef, 2012). The economic and socio-cultural circumstances thus result in a failure of both state and market mechanisms to promote sustainable resource use.

Alternatives to escape the maize trap then need to be locally acceptable, economically feasible and robust against the consequences of climate change. As for the stakeholder acceptability and economic reality, payment for environmental services is one strategy that can bypass destructive land use types that generate a lot of cash (Neef, 2012). Climate-smart agricultural systems that are able to adapt to the reality of changed temperature, rainfall patterns and CO_2 levels, require not simply a status-quo at the current production levels, but a tool box that allows the agricultural sector to keep improving crop production under various scenarios that climate change might result in (Redfern, 2012). Specific examples of such strategies include adapting planting date, developing resilient varieties and site-specific nutrient management (Redfern, 2012), the latter being particularly important in view of intensified sediment redistribution in landscapes. Spatial variability in rice crop response to nutrient inputs is large, at the region, watershed and even cascade level (Dobermann, 2003) and in fact tends to be larger than seasonal variability on the same field. Furthermore, the crop nutrient response is related to the indigenous nutrient supply through sediment-induced soil fertility gradients (Schmitter *et al.*, 2011) making site-specific fertilizer recommendations for mountainous paddies particularly interesting. Additionally, results in Chapter 5 showed that the nitrogen supply not only varies spatially, but also temporally, as plant-available nitrogen inputs from irrigation are coupled to fertilization of maize on surrounding uplands. Nitrogen fertilizer recommendations must therefore consider temporal, as well as spatial variability.

As for specific upland land uses to replace for maize, several potential candidates have emerged in recent years. One possibility is to implement conservation practices in combination with maize cropping on upland areas. Several techniques have been tested locally in Chieng Khoi watershed: grass barriers, minimum tillage with *Arachis pintoi* as cover crop, and minimum tillage with *Phaseolus calcaratus* as a relay crop (Tuan *et al.*, 2014). The third option reduced soil losses on experimental plots by 94% while providing comparable maize yields, thus making it an attractive option. Relay crops did increase labor required, either due to increased weeding for *Arachis pintoi* or because maize harvest was more challenging due to the proliferating *Phaseolus calcaratus*, and could be a constraint on local adoption of these methods. Soil and water conservation practices additionally reduce available

cropping area, which is not always compensated by an increase in yield, which can be another limiting factor for stakeholder acceptance.

Looking for completely different crops as alternatives, the maize trap is more and more replaced by the rubber juggernaut: rubber plantations have spread rapidly in montane Southeast Asia, and are projected to cover up to 150 000 ha by 2050 (Ziegler *et al.*, 2009b). The environmental impacts of rubber plantations in mountainous areas, however, are not well assessed: biophysical consequences are typically quantified for natural forest to rubber conversion, but this change is not equivalent to the impacts of converting land already under permanent upland cultivation. Erosion processes also change as the trees age, with young trees having particularly high soil loss rates. One alternative to mitigate changes in ecosystem services is the implementation of diversified agroforestry systems, in which rubber is part of a landscape mosaic, rather than planted in monoculture. In a similar vein, production forests in general could provide improved ecosystem services in combination with sustainable income, although land transformations from agriculture to forest tend to be sluggish in nature (Rutten *et al.*, 2014).

It remains an open question how aware local stakeholders are of the finiteness of their current practices. Regarding erosion, Clemens *et al.* (2010) showed that farmers are able to accurately assess soil fertility qualities and identify erosion hotspots, but underestimate the extent of erosion in the landscape. Re-allocation and sedimentation processes make the picture more complex, and most likely also make it more difficult to assess impacts for end users. If linkages between upland fertility loss and rice production were better understood, and better known, the far-ranging impacts of permanent maize cultivation would be clearer. As combined redistribution of sediment, organic carbon and nitrogen through erosion and irrigation water substantially affects paddy topsoil fertility, upland maize is a double curse, affecting both upland and lowland agricultural potential. At the same time, a double opportunity presents itself: an improved nutrient status of upland fields will entail better quality sediment inputs for downstream agriculture, and the effects propagate well beyond the watershed scale, as irrigation water, reservoir spillover water and paddy outflow are all exported from the watershed.

References

Akaike, H. (1974). New look at the statistical model identification. *IEEE Transactions on Automatic Control, AC-19*(6), 716-723.

Alvarez-Cobelas, M., Angeler, D.G., Sánchez-Carrillo, S., & Almendros, G. (2012). A worldwide view of organic carbon export from catchments. *Biogeochemistry, 107*(1-3), 275-293.

Amelung, W., & Zech, W. (1999). Minimisation of organic matter disruption during particle-size fractionation of grassland epipedons. *Geoderma, 92*(1-2), 73-85.

Anderson, C.A. (2005). *Turbidity, National Field Manual for the Collection of Water-Quality Data* (Vol. 9). Reston, VA: USGS.

Anh, P.T.Q., Gomi, T., MacDonald, L.H., Mizugaki, S., Van Khoa, P., & Furuichi, T. (2014). Linkages among land use, macronutrient levels, and soil erosion in northern Vietnam: A plot-scale study. *Geoderma, 232-234*, 352-362.

Anyusheva, M., Lamers, M., La, N., Nguyen, V.V., & Streck, T. (2012). Fate of pesticides in combined paddy rice-fish pond farming systems in northern Vietnam. *Journal of Environmental Quality, 41*(2), 515-525.

App, A., Santiago, T., Daez, C., Menguito, C., Ventura, W., Tirol, A., Po, J., Watanabe, I., De Datta, S.K., & Roger, P. (1984). Estimation of the nitrogen balance for irrigated rice and the contribution of phototrophic nitrogen fixation. *Field Crops Research, 9*(C), 17-27.

ASTM (2013). Standard D3977-97. Standard Test Methods for Determining Sediment Concentration in Water Samples. ASTM International, West Conshohocken, PA.

Barker, R., & Molle, F. (2004). Evolution of irrigation in South and Southeast Asia *Comprehensive Assessment Research Report* (Vol. 5). Colombo, Sri Lanka: IWMI.

Berg, R.D., & Carter, D.L. (1980). Furrow erosion and sediment losses on irrigated cropland. *Journal of Soil & Water Conservation, 35*(6), 267-270.

Berk, R.A. (2008). *Statistical learning from a regression perspective*. New York: Springer.

Beusen, A.H.W., Dekkers, A.L.M., Bouwman, A.F., Ludwig, W., & Harrison, J. (2005). Estimation of global river transport of sediments and associated particulate C, N, and P. *Global Biogeochemical Cycles, 19*(4).

Brasington, J., & Richards, K. (2000). Turbidity and suspended sediment dynamics in small catchments in the Nepal Middle Hills. *Hydrological Processes, 14*(14), 2559-2574.

Bräuer, T., Grootes, P.M., Nadeau, M.J., & Andersen, N. (2013). Downward carbon transport in a 2000-year rice paddy soil chronosequence traced by radiocarbon measurements. *Nuclear Instruments and Methods in Physics Research, Section B: Beam Interactions with Materials and Atoms, 294*, 584-587.

Bray F. 1986. The Rice Economies: Technology and Development in Asian Societies. London, (UK): B. Blackwell

Brown, J.B., Sprague, L.A., & Dupree, J.A. (2011). Nutrient Sources and Transport in the Missouri River Basin, with Emphasis on the Effects of Irrigation and Reservoirs. *Journal of the American Water Resources Association, 47*(5), 1034-1060.

Bruun, T.B., de Neergaard, A., Lawrence, D., & Ziegler, A.D. (2009). Environmental consequences of the demise in Swidden cultivation in Southeast Asia: Carbon storage and soil quality. *Human Ecology, 37*(3), 375-388.

Burnham, K.P., & Anderson, D.R. (1998). *Model Selection and Inference: A Practical Information-Theoretic Approach*. New York: Springer-Verlag GmbH.

Callaghan, J., & Bonell, M. (2005). An overview of the meteorology and climatology of the humid tropics *Forests, Water and People in the Humid Tropics: Past, Present and Future Hydrological Research for Integrated Land and Water Management* (pp. 158-193). Cambridge, United Kingdom: Cambridge University Press.

Cao, W., Zhu, H., & Chen, S. (2007). Impacts of urbanization on topsoil nutrient balances—a case study at a provincial scale from Fujian, China. *Catena, 69*(1), 36-43.

Cao, Z.H., Ding, J.L., Hu, Z.Y., Knicker, H., Kögel-Knabner, I., Yang, L.Z., Yin, R., Lin, X.G., Dong, Y.H., Cao, Z.H., Hu, Z.Y., Yang, L.Z., Yin, R., Lin, X.G., & Dong, Y.H. (2006). Ancient paddy soils from the Neolithic age in China's Yangtze River Delta. *Naturwissenschaften, 93*(5), 232-236.

Cassman, K.G., & Pingali, P.L. (1995). Intensification of irrigated rice systems: Learning from the past to meet future challenges. *GeoJournal, 35*(3), 299-305.

Cassman, K.G., Dobermann, A., Sta Cruz, P.C., Gines, G.G., Samson, M.I., Descalsota, J.P., Alcantara, J.M., Dizon, M.A., & Olk, D.C. (1996). Soil organic matter and the indigenous nitrogen supply of intensive irrigated rice systems in the tropics. *Plant and Soil, 182*(2), 267-278.

Cassman, K.G., Peng, S., Olk, D.C., Ladha, J.K., Reichardt, W., Dobermann, A., & Singh, U. (1998). Opportunities for increased nitrogen-use efficiency from improved resource management in irrigated rice systems. *Field Crops Research, 56*(1-2), 7-39.

Cataldo, D.A., Haroon, M., Schrader, L.E., & Youngs, V.L. (1975). Rapid colorimetric determination of nitrate in plant tissue by nitration of salicylic acid. *Commun. Soil Sci. Plant Anal., 6*(1), 71-80.

Chaplot, V., Khampaseuth, X., Valentin, C., & Le Bissonnais, Y. (2007). Interrill erosion in the sloping lands of northern Laos subjected to shifting cultivation. *Earth Surface Processes and Landforms, 32*(3), 415-428.

Chaplot, V., & Poesen, J. (2012). Sediment, soil organic carbon and runoff delivery at various spatial scales. *Catena, 88*(1), 46-56.

Cho, J.Y., Han, K.W., & Choi, J.K. (2000). Balance of nitrogen and phosphorus in a paddy field of Central Korea. *Soil Science and Plant Nutrition, 46*(2), 343-354.

Christensen, J.H., Hewitson, B., Busuioc, A., Chen, A., Gao, X., Held, R., Jones, R., Kolli, R.K., Kwon, W.-T., Laprise, V., Magana Rueda, L., Mearns, G.G., Menendez, C.G., Rainsanen, J., Rinke, A., Sarr, A., & Whetton, P. (2007) Regional Climate Projections. Climate Change 2007: The Physical Science Basis. Contribution of Working Group I to the Fourth Assessment report of the Intergovernmental Panel on climate Change. Cambridge, United Kingdom: Cambridge University Press.

Clemens, G., Fiedler, S., Cong, N.D., Van Dung, N., Schuler, U., & Stahr, K. (2010). Soil fertility affected by land use history, relief position, and parent material under a tropical climate in NW-Vietnam. *Catena, 81*(2), 87-96.

Cox, N.J., Warburton, J., Armstrong, A., & Holliday, V.J. (2008). Fitting concentration and load rating curves with generalized linear models. *Earth Surface Processes and Landforms, 33*(1), 25-39.

Cuisinier, J. (1948). *Les Muong: Géographie humaine et sociologie*. Paris: Institut d'ethnologie.

De Datta, S.K. (1981). *Principles and Practices of Rice Production*. New York: John Wiley & Sons, Inc.

de Vente, J., & Poesen, J. (2005). Predicting soil erosion and sediment yield at the basin scale: Scale issues and semi-quantitative models. *Earth-Science Reviews, 71*(1–2), 95-125.

Di Baldassarre, G., & Montanari, A. (2009). Uncertainty in river discharge observations: a quantitative analysis. *Hydrol. Earth Syst. Sci., 13*(6), 913-921.

Dobermann, A., Cassman, K., Mamaril, C., & Sheehy, J. (1998). Management of phosphorus, potassium, and sulfur in intensive, irrigated lowland rice. *Field Crops Research, 56*(1), 113-138.

Dobermann, A., & White, P.F. (1998). Strategies for nutrient management in irrigated and rainfed lowland rice systems. *Nutrient Cycling in Agroecosystems, 53*(1), 1-18.

Dobermann, A. (2000) Future intensification of irrigated rice systems. *Vol. 7* (pp. 229-247).

Dobermann, A., Witt, C., Abdulrachman, S., Gines, H.C., Nagarajan, R., Son, T.T., Tan, P.S., Wang, G.H., Chien, N.V., Thoa, V.T.K., Phung, C.V., Stalin, P., Muthukrishnan, P., Ravi, V., Babu, M., Simbahan, G.C., & Adviento, M.A.A. (2003). Soil fertility and indigenous nutrient supply in irrigated rice domains of Asia. *Agronomy Journal, 95*(4), 913-923.

Dove, M.R. (1983). Theories of swidden agriculture, and the political economy of ignorance. *Agroforestry Systems, 1*(2), 85-99.

Duan, N. (1983). Smearing estimate: a nonparametric retransformation method. *Journal of the American Statistical Association, 78*(383), 605-610.

Dung, N.V., Vien, T.D., Lam, N.T., Tuong, T.M., & Cadisch, G. (2008). Analysis of the sustainability within the composite swidden agroecosystem in northern Vietnam. 1. Partial nutrient balances and recovery times of upland fields. *Agriculture, Ecosystems and Environment, 128*(1-2), 37-51.

Dung, N.V., Vien, T.D., Cadisch, G., Lam, N.T., Patanothai, A., Rambo, T., & Truong, T. (2009). A nutrient balance analysis of the composite swiddening agroecosystem. In T.D. Vien, T.A. Rambo & N.T. Lam (Eds.), *Farming with Fire and Water-the Human Ecology of a Composite Swiddening Community in Vietnam's Northern Mountains* (pp. 456). Melbourne: Kyoto University Press and Trans Pacific Press.

Durrenberger, E.P. (1981). The economy of a Shan village. *Ethnos, 46*(1-2), 64-79.

Duvert, C., Gratiot, N., Anguiano-Valencia, R., Némery, J., Mendoza, M.E., Carlón-Allende, T., Prat, C., & Esteves, M. (2011). Baseflow control on sediment flux connectivity: Insights from a nested catchment study in Central Mexico. *Catena, 87*(1), 129-140.

Ebtehaj, M., Moradkhani, H., & Gupta, H.V. (2010). Improving robustness of hydrologic parameter estimation by the use of moving block bootstrap resampling. *Water Resources Research, 46*(7), W07515.

Efron, B., & Tibshirani, R.J. (1993). *An Introduction to the Bootstrap*. Boca Raton: Chapman & Hall/CRC.

Evrard, O., Navratil, O., Ayrault, S., Ahmadi, M., Némery, J., Legout, C., Lefèvre, I., Poirel, A., Bonté, P., & Esteves, M. (2011). Combining suspended sediment monitoring and fingerprinting to determine the spatial origin of fine sediment in a mountainous river catchment. *Earth Surface Processes and Landforms, 36*(8), 1072-1089.

FAO. (2014). FAO country profile: Vietnam.

FAO Aquastat. (2014). General Summary Asia - Irrigation. Retrieved 20th August 2015.

Ferguson, R.I. (1986). River loads underestimated by rating curves. *Water Resources Research, 22*(1), 74-76.

Foster, I.D.L., Millington, R., & Grew, R.G. (1992). *The impact of particle size controls on stream turbidity measurement; some implications for suspended sediment yield estimation.* Paper presented at the Erosion and Sediment Monitoring Programmes in River Basins, Proceedings of the Oslo symposium, pp. 51–62.

Fox, J., & Vogler, J.B. (2005). Land-use and land-cover change in Montane Mainland Southeast Asia. *Environmental Management, 36*(3), 394-403.

Fox, J., Fujita, Y., Ngidang, D., Peluso, N., Potter, L., Sakuntaladewi, N., Sturgeon, J., & Thomas, D. (2009). Policies, political-economy, and swidden in Southeast Asia. *Human Ecology, 37*(3), 305-322.

Freeman, J., & Modarres, R. (2006). Inverse Box–Cox: the power-normal distribution. *Statistics & Probability Letters, 76*(8), 764-772.

Gafur, A., Jensen, J.R., Borggaard, O.K., & Petersen, L. (2003). Runoff and losses of soil and nutrients from small watersheds under shifting cultivation (Jhum) in the Chittagong Hill Tracts of Bangladesh. *Journal of Hydrology, 274*(1-4), 30-46.

Gao, P., Pasternack, G.B., Bali, K.M., & Wallender, W.W. (2007). Suspended-sediment transport in an intensively cultivated watershed in southeastern California. *Catena, 69*(3), 239-252.

Gao, P. (2008). Understanding watershed suspended sediment transport. *Progress in Physical Geography, 32*(3), 243-263.

Gao, P., Pasternack, G.B., Bali, K.M., & Wallender, W.W. (2008). Estimating suspended sediment concentration using turbidity in an irrigation-dominated Southeastern California watershed. *Journal of Irrigation and Drainage Engineering, 134*(2), 250-259.

GFDRR. (2011). Vulnerability, risk reduction and adaptation to climate change: Vietnam. Retrieved 16/09/2015, 2015, from http://sdwebx.worldbank.org/climateportalb/home.cfm?page=country_profile&CCode=VNM&ThisTab=Overview

Gilvear, D.J., & Petts, G.E. (1985). Turbidity and suspended solids variations downstream of a regulating reservoir. *Earth Surface Processes & Landforms, 10*(4), 363-373.

Gippel, C.J. (1995). Potential of turbidity monitoring for measuring the transport of suspended solids in streams. *Hydrological Processes, 9*(1), 83-97.

Gong, Z.T., Zhang, G.L., & Chen, Z.C. (2007). *Pedogenesis and Soil Taxonomy*. Bejing: Science Press.

Göransson, G., Larson, M., & Bendz, D. (2013). Variation in turbidity with precipitation and flow in a regulated river system-river Göta Älv, SW Sweden. *Hydrology and Earth System Sciences, 17*(7), 2529-2542.

Grayson, R.B., Finlayson, B.L., Gippel, C.J., & Hart, B.T. (1996). The potential of field turbidity measurements for the computation of total phosphorus and suspended solids loads. *Journal of Environmental Management, 47*(3), 257-267.

Hamilton, A.S., & Moore, R.D. (2012). Quantifying uncertainty in streamflow records. *Canadian Water Resources Journal, 37*(1), 3-21.

Häring, V., Fischer, H., Cadisch, G., & Stahr, K. (2013). Implication of erosion on the assessment of decomposition and humification of soil organic carbon after land use change in tropical agricultural systems. *Soil Biology and Biochemistry, 65*, 158-167.

Häring, V., Fischer, H., & Stahr, K. (2014). Erosion of bulk soil and soil organic carbon after land use change in Northwest Vietnam. *Catena, 122*, 111-119.

Harmel, R.D., Smith, D.R., King, K.W., & Slade, R.M. (2009). Estimating storm discharge and water quality data uncertainty: A software tool for monitoring and modeling applications. *Environmental Modelling and Software, 24*(7), 832-842.

Helsel, D.R., & Hirsch, R.M. (1992). *Statistical methods in water resources*. Amsterdam: Elsevier.

Heong, K., Teng, P., & Moody, K. (1995). Managing rice pests with less chemicals. *GeoJournal, 35*(3), 337-349.

Herschy, R.W. (1995). *Streamflow measurement*. Boca Raton: CRC Press.

Horowitz, A.J. (1995). *The use of suspended sediment and associated trace elements in water quality studies*. Wallingford, Oxfordshire, United Kingdom: International Association of Hydrological Sciences.

Horowitz, A.J. (2003). An evaluation of sediment rating curves for estimating suspended sediment concentrations for subsequent flux calculations. *Hydrological Processes, 17*(17), 3387-3409.

Horowitz, A.J. (2008). Determining annual suspended sediment and sediment-associated trace element and nutrient fluxes. *Science of the Total Environment, 400*(1-3), 315-343.

Horowitz, A.J., Clarke, R.T., & Merten, G.H. (2014). The effects of sample scheduling and sample numbers on estimates of the annual fluxes of suspended sediment in fluvial systems. *Hydrological Processes, 29*(4), 531-543.

Huang, L.M., Thompson, A., Zhang, G.L., Chen, L.M., Han, G.Z., & Gong, Z.T. (2015). The use of chronosequences in studies of paddy soil evolution: A review. *Geoderma, 237*, 199-210.

Hung, N.N., Delgado, J.M., Güntner, A., Merz, B., Bárdossy, A., & Apel, H. (2014). Sedimentation in the floodplains of the Mekong Delta, Vietnam. Part I: Suspended sediment dynamics. *Hydrological Processes, 28*(7), 3132-3144.

International Plant Nutrition Institute (2002). *Rice Series: Rice - A Practical Guide to Nutrient Management*. Norcross, Georgia, USA: IPNI.

International Rice Research Institute (2015). World Rice Statistics Online Query Facility. Retrieved 07/09, 2015

IPCC (2013). Climate change 2013: The physical science basis. Contribution of working group I to the fifth assessment report of the intergovernmental panel on climate change. In T.F. Stocker, D. Qin, G.-K. Plattner, M. Tignor, S.K. Allen, J. Boschung, A. Nauels, Y. Xia, V. Bex & P.M. Midgley (Eds.), (pp. 1535). Cambridge, United Kingdom and New York, NY, USA.

Istvánovics, V., Osztoics, A., & Honti, M. (2004). Dynamics and ecological significance of daily internal load of phosphorus in shallow Lake Balaton, Hungary. *Freshwater Biology, 49*(3), 232-252.

Jamieson, N. (1991). *Culture and Development in Vietnam*. Honolulu: East-West Center, EAPI, Working Papers Series of Indochina Initiative.

Jamieson, N.L., Le, T.C., & Rambo, A.T. (1998). The development crisis in Vietnam's mountains. *East-West Center Special Reports (6), 1–32.*

Johnson, J.A., Runge, C.F., Senauer, B., Foley, J., & Polasky, S. (2014). Global agriculture and carbon trade-offs. *Proceedings of the National Academy of Sciences, 111*(34), 12342-12347.

Johnson, N.L., Kotz, S., & Balakrishnan, N. (1994). *Continuous univariate distributions* (Vol. 1). New York: Wiley.

Jones, A.S., Stevens, D.K., Horsburgh, J.S., & Mesner, N.O. (2011). Surrogate Measures for Providing High Frequency Estimates of Total Suspended Solids and Total Phosphorus Concentrations. *Journal of the American Water Resources Association, 47*(2), 239-253.

Keil, A., Saint-Macary, C., & Zeller, M. (2008). Maize boom in the uplands of Northern Vietnam: economic importance and environmental implications: Discussion Paper No. 4/2008, Universitaet Hohenheim, Department of Agricultural Economics and Social Sciences in the Tropics and Subtropics.

Kim, J.S., Oh, S.Y., & Oh, K.Y. (2006). Nutrient runoff from a Korean rice paddy watershed during multiple storm events in the growing season. *Journal of Hydrology, 327*(1-2), 128-139.

King, A.P., Evatt, K.J., Six, J., Poch, R.M., Rolston, D.E., & Hopmans, J.W. (2009). Annual carbon and nitrogen loadings for a furrow-irrigated field. *Agricultural Water Management, 96*(6), 925-930.

Ko, J., Kim, H.Y., Jeong, S., An, J., Choi, G., Kang, S., & Tenhunen, J. (2014). Potential impacts on climate change on paddy rice yield in mountainous highland terrains. *Journal of Crop Science and Biotechnology, 17*(3), 117-126.

Koyama, T., & App, A. (1979). *Nitrogen balance in flooded rice soils*. Los Baños, Philippines: The International Rice Research Institute.

Krause, G., & Ohm, K. (1984). A method to measure suspended load transports in estuaries. *Estuarine, Coastal and Shelf Science, 19*(6), 611-618.

Kronvang, B., Laubel, A., & Grant, R. (1997). Suspended sediment and particulate phosphorus transport and delivery pathways in an arable catchment, Gelbæk Stream, Denmark. *Hydrological Processes, 11*(6), 627-642.

Kroon, F.J., Kuhnert, P.M., Henderson, B.L., Wilkinson, S.N., Kinsey-Henderson, A., Abbott, B., Brodie, J.E., & Turner, R.D.R. (2012). River loads of suspended solids, nitrogen, phosphorus and herbicides delivered to the Great Barrier Reef lagoon. *Marine Pollution Bulletin, 65*(4–9), 167-181.

Kuhnert, P.M., Henderson, B.L., Lewis, S.E., Bainbridge, Z.T., Wilkinson, S.N., & Brodie, J.E. (2012). Quantifying total suspended sediment export from the Burdekin River catchment using the loads regression estimator tool. *Water Resources Research, 48*(4), W04533.

Kulasova, A., Smith, P.J., Beven, K.J., Blazkova, S.D., & Hlavacek, J. (2012). A method of computing uncertain nitrogen and phosphorus loads in a small stream from an agricultural catchment using continuous monitoring data. *Journal of Hydrology, 458–459*(0), 1-8.

Kundarto, M., Agus, F., Maas, A., & Sunarminto, B.H. (2002). *Water balance, soil erosion and lateral transport of NPK in rice-field systems of sub watershed Kalibabon Semarang*. Paper presented at the Multifunctionality of Paddy Fields, Bogor (in Indonesian).

Lacombe, G., Ribolzi, O., de Rouw, A., Pierret, A., Latsachak, K., Silvera, N., Pham Dinh, R., Orange, D., Janeau, J.L., Soulileuth, B., Robain, H., Taccoen, A., Sengphaathith, P., Mouche, E., Sengtaheuanghoung, O., Tran Duc, T., & Valentin, C. (2015). Afforestation by natural regeneration or by tree planting: examples of opposite hydrological impacts evidenced by long-term field monitoring in the humid tropics. *Hydrol. Earth Syst. Sci. Discuss., 12*(12), 12615-12648.

Lahiri, S.N. (2003). *Resampling methods for dependent data*. New York: Springer.

Lamers, M., Anyusheva, M., La, N., Nguyen, V.V., & Streck, T. (2011). Pesticide pollution in surface- and groundwater by paddy rice cultivation: A case study from Northern Vietnam. *Clean - Soil, Air, Water, 39*(4), 356-361.

Lantican, M.A., Guerra, L.C., & Bhuiyan, S.I. (2003). Impacts of soil erosion in the upper Manupali watershed on irrigated lowlands in the Philippines. *Paddy Water Environ., 1*(1), 19-26.Lassaletta, L., Romero, E., Billen, G., Garnier, J., García-Gómez, H., & Rovira, J. (2012). Spatialized N budgets in a large agricultural Mediterranean watershed: high loading and low transfer. *Biogeosciences, 9*(1), 57-70.

Lee, S.B., Lee, C.H., Jung, K.Y., Park, K.D., Lee, D., & Kim, P.J. (2009). Changes of soil organic carbon and its fractions in relation to soil physical properties in a long-term fertilized paddy. *Soil and Tillage Research, 104*(2), 227-232.

Lessels, J.S., & Bishop, T.F.A. (2013). Estimating water quality using linear mixed models with stream discharge and turbidity. *Journal of Hydrology, 498*(0), 13-22.

Lewis, J. (1996). Turbidity-controlled suspended sediment sampling for runoff-event load estimation. *Water Resources Research, 32*(7), 2299-2310.

Lewis, J., & Eads, R. (2001). *Turbidity threshold sampling for suspended sediment load estimation*. Paper presented at the Seventh Federal Interagency Sedimentation Conference, Reno, Nevada.

Lick, W. (1982). Entrainment, deposition, and transport of fine-grained sediments in lakes. *Hydrobiologia, 91-92*(1), 31-40.

Lippe, M., Thai Minh, T., Neef, A., Hilger, T., Hoffmann, V., Lam, N.T., & Cadisch, G. (2011). Building on qualitative datasets and participatory processes to simulate land use change in a mountain watershed of Northwest Vietnam. *Environmental Modelling & Software, 26*(12), 1454-1466.

Lippe, M. (2015). *Simulating the impact of land use change on ecosystem functions in data-limited watersheds of Mountainous Mainland Southeast Asia.* (PhD), University of Hohenheim, Shaker, Germany.

Lipper, L., Thornton, P., Campbell, B.M., Baedeker, T., Braimoh, A., Bwalya, M., Caron, P., Cattaneo, A., Garrity, D., Henry, K., Hottle, R., Jackson, L., Jarvis, A., Kossam, F., Mann, W., McCarthy, N., Meybeck, A., Neufeldt, H., Remington, T., Sen, P.T., Sessa, R., Shula, R., Tibu, A., & Torquebiau, E.F. (2014). Climate-smart agriculture for food security. *Nature Climate Change, 4*(12), 1068-1072.

López-Tarazón, J., Batalla, R., Vericat, D., & Balasch, J. (2010). Rainfall, runoff and sediment transport relations in a mesoscale mountainous catchment: the River Isábena (Ebro basin). *Catena, 82*(1), 23-34.

Lu, H., Moran, C.J., & Sivapalan, M. (2005). A theoretical exploration of catchment-scale sediment delivery. *Water Resources Research, 41*(9), 1-15.

Lu, X.X., Li, S., He, M., Zhou, Y., Li, L., & Ziegler, A.D. (2012). Organic carbon fluxes from the upper Yangtze basin: An example of the Longchuanjiang River, China. *Hydrological Processes, 26*(11), 1604-1616.

Ludwig, W., Probst, J.L., & Kempe, S. (1996). Predicting the oceanic input of organic carbon by continental erosion. *Global Biogeochemical Cycles, 10*(1), 23-41.

Maglinao, A.R., Valentin, C., & Penning de Vries, F. (2003). . *From soil research to land and water management: harmonizing people and nature.* In: Proceedings of the IWMI-ADB Project Annual Meeting and 7th MSEC Assembly, 2nd till 7th December 2002, Vientiane, Laos.

Mai, V.T., van Keulen, H., Hessel, R., Ritsema, C., Roetter, R., & Phien, T. (2013). Influence of paddy rice terraces on soil erosion of a small watershed in a hilly area of Northern Vietnam. *Paddy and Water Environment, 11*(1-4), 285-298.

Mailhot, A., Rousseau, A.N., Talbot, G., Gagnon, P., & Quilbé, R. (2008). A framework to estimate sediment loads using distributions with covariates: Beaurivage River watershed (Québec, Canada). *Hydrological Processes, 22*(26), 4971-4985.

Maruyama, T., Hashimoto, I., Murashima, K., & Takimoto, H. (2008). Evaluation of N and P mass balance in paddy rice culture along Kahokugata Lake, Japan, to assess potential lake pollution. *Paddy and Water Environment, 6*(4), 355-362.

Mc Sweeney, C., New, M., & Lizcano, G. (2008). UNDP climate change country profiles: Vietnam. School of Geography and the Environment of the University of Oxford: Oxford: UNDP, 27p.

McHugh, A.D., Bhattarai, S., Lotz, G., & Midmore, D.J. (2008). Effects of subsurface drip irrigation rates and furrow irrigation for cotton grown on a vertisol on off-site movement of sediments, nutrients and pesticides. *Agronomy for Sustainable Development, 28*(4), 507-519.

Mertz, O., Leisz, S., Heinimann, A., Rerkasem, K., Dressler, W., Pham, V., Vu, K.C., Schmidt-Vogt, D., Colfer, C.J.P., & Epprecht, M. (2009). Who Counts? Demography of Swidden Cultivators in Southeast Asia. *Human Ecology, 37*(3), 281-289.

Meyfroidt, P., & Lambin, E.F. (2008). The causes of the reforestation in Vietnam. *Land Use Policy, 25*(2), 182-197.

Milliman, J.D., & Syvitski, J.P.M. (1992). Geomorphic/tectonic control of sediment discharge to the ocean: the importance of small mountainous rivers. *The Journal of Geology*, 525-544.

Minella, J.P.G., Merten, G.H., Reichert, J.M., & Clarke, R.T. (2008). Estimating suspended sediment concentrations from turbidity measurements and the calibration problem. *Hydrological Processes, 22*(12), 1819-1830.

Minella, J.P.G., Walling, D.E., & Merten, G.H. (2014). Establishing a sediment budget for a small agricultural catchment in southern Brazil, to support the development of effective sediment management strategies. *Journal of Hydrology, 519, Part B*(0), 2189-2201.

Mingzhou, Q., Jackson, R.H., Zhongjin, Y., Jackson, M.W., & Bo, S. (2007). The effects of sediment-laden waters on irrigated lands along the lower Yellow River in China. *Journal of Environmental Management, 85*(4), 858-865.

Minot, N. (2006). *Income diversification and poverty in the Northern Uplands of Vietnam* (Vol. 145): Intl Food Policy Res Inst.

Moatar, F., & Meybeck, M. (2005). Compared performances of different algorithms for estimating annual nutrient loads discharged by the eutrophic River Loire. *Hydrological Processes, 19*(2), 429-444.

Navratil, O., Esteves, M., Legout, C., Gratiot, N., Nemery, J., Willmore, S., & Grangeon, T. (2011). Global uncertainty analysis of suspended sediment monitoring using turbidimeter in a small mountainous river catchment. *Journal of Hydrology, 398*(3-4), 246-259.

Nearing, M.A. (1998). Why soil erosion models over-predict small soil losses and under-predict large soil losses. *Catena, 32*(1), 15-22.

Neef, A. (2012). Fostering Incentive-Based Policies and Partnerships for Integrated Watershed Management in the Southeast Asian Uplands. *Southeast Asian Studies, 1*(2), 247-271.

Némery, J., Mano, V., Coynel, A., Etcheber, H., Moatar, F., Meybeck, M., Belleudy, P., & Poirel, A. (2013). Carbon and suspended sediment transport in an impounded alpine river (Isère, France). *Hydrological Processes, 27*(17), 2498-2508.

Nguyen, T.T. (2009). *Assessment of land cover change in Chieng Khoi Commune, Northern Vietnam, by combining remote sensing tools and historical local knowledge.* (Msc.), University of Hohenheim, Stuttgart, Germany.

Nyssen, J., Clymans, W., Poesen, J., Vandecasteele, I., De Baets, S., Haregeweyn, N., Naudts, J., Hadera, A., Moeyersons, J., Haile, M., & Deckers, J. (2009). How soil conservation affects the catchment sediment budget – a comprehensive study in the north Ethiopian highlands. *Earth Surface Processes and Landforms, 34*(9), 1216-1233.

O'Neill, R.V., Turner, S., Cullinan, V., Coffin, D., Cook, T., Conley, W., Brunt, J., Thomas, J., Conley, M., & Gosz, J. (1991). Multiple landscape scales: an intersite comparison. *Landscape Ecology, 5*(3), 137-144.

Pagendam, D.E., Kuhnert, P.M., Leeds, W.B., Wikle, C.K., Bartley, R., & Peterson, E.E. (2014). Assimilating catchment processes with monitoring data to estimate sediment loads to the great barrier reef. *Environmetrics, 25*(4), 214-229.

Pampolino, M.F., Laureles, E.V., Gines, H.C., & Buresh, R.J. (2008). Soil carbon and nitrogen changes in long-term continuous lowland rice cropping. *Soil Science Society of America Journal, 72*(3), 798-807.

Pan, G., Zhou, P., Li, Z., Smith, P., Li, L., Qiu, D., Zhang, X., Xu, X., Shen, S., & Chen, X. (2009). Combined inorganic/organic fertilization enhances N efficiency and increases rice productivity through organic carbon accumulation in a rice paddy from the Tai Lake region, China. *Agriculture, Ecosystems and Environment, 131*(3-4), 274-280.

Pansak, W., Hilger, T.H., Dercon, G., Kongkaew, T., & Cadisch, G. (2008). Changes in the relationship between soil erosion and N loss pathways after establishing soil conservation systems in uplands of Northeast Thailand. *Agriculture, Ecosystems and Environment, 128*(3), 167-176.

Patterson, H.D., & Thompson, R. (1971). Recovery of inter-block information when block sizes are unequal. *Biometrika, 58*(3), 545-554.

Peng, S., Huang, J., Sheehy, J.E., Laza, R.C., Visperas, R.M., Zhong, X., Centeno, G.S., Khush, G.S., & Cassman, K.G. (2004). Rice yields decline with higher night temperature from global warming. *Proceedings of the National Academy of Sciences of the United States of America, 101*(27), 9971-9975.

Pfannkuche, J., & Schmidt, A. (2003). Determination of suspended particulate matter concentration from turbidity measurements: Particle size effects and calibration procedures. *Hydrological Processes, 17*(10), 1951-1963.

Piepho, H.P. (2009). Data transformation in statistical analysis of field trials with changing treatment variance. *Agronomy Journal, 101*(4), 865-869.

Piepho, H.P., Möhring, J., Pflugfelder, M., Hermann, W., & Williams, E.R. (2015). Problems in parameter estimation for power and AR(1) models of spatial correlation in designed field experiments. *Communications in Biometry and Crop Science, 10*(1), 3-16.

Poch, R.M., Hopmans, J.W., Six, J.W., Rolston, D.E., & McIntyre, J.L. (2006). Considerations of a field-scale soil carbon budget for furrow irrigation. *Agriculture, Ecosystems and Environment, 113*(1-4), 391-398.

Poffenberger, M., & Nguyen, H.P. (1998). The national forest sector. In M. Poffenberger (Ed.), *Stewards of Vietnam's upland forests*. Berkeley, CA, USA: Center for Southeast Asia Studies.

Porterfield, G. (1972). Computation of fluvial-sediment discharge *United States Geological Survey Techniques of Water-Resources Investigations, Book 3*.

Poulenard, J., Legout, C., Némery, J., Bramorski, J., Navratil, O., Douchin, A., Fanget, B., Perrette, Y., Evrard, O., & Esteves, M. (2012). Tracing sediment sources during floods using Diffuse Reflectance Infrared Fourier Transform Spectrometry (DRIFTS): A case study in a highly erosive mountainous catchment (Southern French Alps). *Journal of Hydrology, 414-415*, 452-462.

Pucher, J., Mayrhofer, R., El-Matbouli, M., & Focken, U. (2014). Effects of modified pond management on limnological parameters in small-scale aquaculture ponds in mountainous Northern Vietnam. *Aquaculture Research , 47(1), 56-70.*

Rambo, A.T. (1995). Defining highland development challenges in Vietnam: Some themes and issues emerging from the conference. *The Challenges of Highland Development in Vietnam*, xi-xxvii.

Rasmussen, P.P., Bennet, T., Lee, C., & Christensen, V.G. (2002). *Continuous in-situ measurement of turbidity in Kansas streams*. Paper presented at the Turbidity and Other Surrogates Workshop, April 30 – May 2, 2002 Reno, NV.

Redfern, S.K., Azzu, N., & Binamira, J.S. (2012). Rice in Southeast Asia: facing risks and vulnerabilities to respond to climate change. *Build Resilience Adapt Climate Change Agri Sector, 23*, 295.

Reichardt, W., Dobermann, A., & George, T. (1998). Intensification of rice production systems: opportunities and limits. In N.G. Dowling, S.M. Greenfield & K.S. Fischer (Eds.), *Sustainability of rice in the global food system* (pp. 127-144). Manila, Philippines.: International Rice Research Institute.

Rerkasem, K., & Rerkasem, B. (1994). *Shifting Cultivation in Thailand: Its Current Situation and Dynamics in the Context of Highland Development*, IIED forestry and land use series, London.

Rerkasem, K., Lawrence, D., Padoch, C., Schmidt-Vogt, D., Ziegler, A.D., & Bech-Brun, T. (2009). Consequences of Swidden Transitions for Crop and Fallow Biodiversity. *Human Ecology, 37(3)*, 347-360.

Riley, S.J. (1998). The sediment concentration-turbidity relation: Its value in monitoring at Ranger Uranium Mine, Northern Territory, Australia. *Catena, 32*(1), 1-14.

Roger, P.A. (1996). *Biology and management of the floodwater ecosystem in rice fields*. Los Banos, Philippines: International Rice Research Institute.

Römkens, M.J., Helming, K., & Prasad, S. (2002). Soil erosion under different rainfall intensities, surface roughness, and soil water regimes. *Catena, 46*(2), 103-123.

Rustomji, P., & Wilkinson, S.N. (2008). Applying bootstrap resampling to quantify uncertainty in fluvial suspended sediment loads estimated using rating curves. *Water Resources Research, 44*(9), W09435.

Rüth, B., & Lennartz, B. (2008). Spatial variability of soil properties and rice yield along two catenas in southeast China. *Pedosphere, 18*(4), 409-420.

Rutten, M., Van Dijk, M., Van Rooij, W., & Hilderink, H. (2014). Land use dynamics, climate change, and food security in Vietnam: A global-to-local modeling approach. *World Development, 59*, 29-46.

Ryberg, K.R. (2006). Continuous Water-quality Monitoring and Regression Analysis to Estimate Constituent Concentrations and Loads in the Red River of the North, Fargo, North Dakota *United States Geological Survey Scientific Investigations Report 2006-5241*.

Saito, M., & Kawaguchi, K. (1971). Flocculating tendency of paddy soils (Part 4). Soil structure of paddy plow-layers. *Jpn. J. Soil Sci. Plant Nutr, 42*, 95-96 (in Japanese).

Sanchez, P.B., Oliver, D.P., Castillo, H.C., & Kookana, R.S. (2012). Nutrient and sediment concentrations in the Pagsanjan–Lumban catchment of Laguna de Bay, Philippines. *Agricultural Water Management, 106*, 17-26.

Sauer, V.B., & Meyer, R.W. (1992). *Determination of error in individual discharge measurements*. Washington, D.C.: US Department of the Interior, US Geological Survey.

Schad, I., Schmitter, P., Saint-Macary, C., Neef, A., Lamers, M., Nguyen, L., Hilger, T., & Hoffmann, V. (2012). Why do people not learn from flood disasters? Evidence from Vietnam's northwestern mountains. *Natural hazards, 62*(2), 221-241.

Schertz, D.L. (1983). The basis for soil loss tolerances. *Journal of Soil and Water Conservation, 38*(1), 10-14.

Schmidt-Vogt, D., Leisz, S.J., Mertz, O., Heinimann, A., Thiha, T., Messerli, P., Epprecht, M., Van Cu, P., Chi, V.K., & Hardiono, M. (2009). An assessment of trends in the extent of swidden in Southeast Asia. *Human Ecology, 37*(3), 269-280.

Schmitter, P., Dercon, G., Hilger, T., Thi Le Ha, T., Huu Thanh, N., Lam, N., Duc Vien, T., & Cadisch, G. (2010). Sediment induced soil spatial variation in paddy fields of Northwest Vietnam. *Geoderma, 155*(3-4), 298-307.

Schmitter, P., Dercon, G., Hilger, T., Hertel, M., Treffner, J., Lam, N., Duc Vien, T., & Cadisch, G. (2011). Linking spatio-temporal variation of crop response with sediment deposition along paddy rice terraces. *Agriculture, Ecosystems and Environment, 140*(1-2), 34-45.

Schmitter, P., Fröhlich, H.L., Dercon, G., Hilger, T., Huu Thanh, N., Lam, N.T., Vien, T.D., & Cadisch, G. (2012). Redistribution of carbon and nitrogen through irrigation in intensively cultivated tropical mountainous watersheds. *Biogeochemistry, 109*(1-3), 133-150.

Schreier, H., & Brown, S. (2004). Multiscale approaches to watershed management: land-use impacts on nutrient and sediment dynamics. *IAHS Publications-Series of Proceedings and Reports, 287*, 61-76.

Scott, J.C. (2009). *The art of not being governed: An anarchist history of upland Southeast Asia*. New Haven and London: Yale University Press.

Seitzinger, S.P., Harrison, J.A., Dumont, E., Beusen, A.H.W., & Bouwman, A.F. (2005). Sources and delivery of carbon, nitrogen, and phosphorus to the coastal zone: An overview of Global Nutrient Export from Watersheds (NEWS) models and their application. *Global Biogeochemical Cycles, 19*(4).

Selle, B., & Hannah, M. (2010). A bootstrap approach to assess parameter uncertainty in simple catchment models. *Environmental Modelling & Software, 25*(8), 919-926.

Sharma, P.K., & De Datta, S.K. (1985). Effects of puddling on soil physical properties and processes *Soil physics and rice* (pp. 217-234). Los Banos Laguna, Philippines: International Rice Research Institute.

Singer, J., & Watanabe, T. (2014). Reducing reservoir impacts and improving outcomes for dam-forced resettlement: Experiences in central Vietnam. *Lakes and Reservoirs: Research and Management, 19*(3), 225-235.

Slaets, J.I.F., Schmitter, P., Hilger, T., Lamers, M., Piepho, H.P., Vien, T.D., & Cadisch, G. (2014). A turbidity-based method to continuously monitor sediment, carbon and nitrogen flows in mountainous watersheds. *Journal of Hydrology, 513*, 45-57.

Slaets, J.I.F., Schmitter, P., Hilger, T., Vien, T.D., & Cadisch, G. (2015). Sediment trap efficiency of paddy fields at the watershed scale in a mountainous catchment in Northwest Vietnam. *Biogeosciences Discuss., 12*(24), 20437-20473.

Slaets, J.I.F., Piepho, H.P., Schmitter, P., Hilger, T., & Cadisch, G. Quantifying uncertainty on sediment loads using bootstrap confidence intervals. In revision.

Smith, C., and B. Croke (2005), Sources of uncertainty in estimating suspended sediment load, IAHS-AISH Publication 292, pp. 136-143.

Sparks, D.L., Page, A.L., Helmke, P.A., Loeppert, R.H., Soltanpour, P.N., Tabatabai, M.A., Johnston, C.T., & Summer, M.E. (1996). Part 3 Chemical Methods *SSA Book Series 5: Methods of Soil Analysis*. Madison, USA: Soil Science Society of America.

Stubblefield, A.P., Reuter, J.E., Dahlgren, R.A., & Goldman, C.R. (2007). Use of turbidometry to characterize suspended sediment and phosphorus fluxes in the Lake Tahoe basin, California, USA. *Hydrological Processes, 21*(3), 281-291.

Suprapti, H., Mawardi, M., & Shiddieq, D. (2010). *Nitrogen transport and distribution on paddy rice soil under water efficient irrigation method*. Paper presented at the International Seminar of ICID, Yogyakarta, Indonesia.

Susumu, Y., Akihiro, K., Hiroshi, K., Masaaki, Y., Alex, M., & Masahiko, M. (2015). Sediment and 137 Cs transport and accumulation in the Ogaki Dam of eastern Fukushima. *Environmental Research Letters, 10*(1), 014013.

Svendsen, M., & Rosegrant, M.W. (1994). Irrigation development in Southeast Asia beyond 2000: will the future be like the past? *Water International, 19*(1), 25-35.

Swallow, B.M., Garrity, D.P., & Van Noordwijk, M. (2002). The effects of scales, flows and filters on property rights and collective action in watershed management. *Water policy, 3*(6), 457-474.

Teixeira, E.C., & Caliari, P.C. (2005). *Estimation of the concentration of suspended solids in rivers from turbidity measurement: error assessment.* Paper presented at the IAHS-AISH Publication.

Thollet, F., Le Coz, J., Antoine, G., François, P., Saguintaah, L., Launay, M., & Camenen, B. (2013). Influence of grain size changes on the turbidity measurement of suspended solid fluxes in watercourses. *Houille Blanche*(4), 50-56.

Thongmanivong, S., Fujita, Y., & Fox, J. (2005). Resource use dynamics and land-cover change in Ang Nhai Village and Phou Phanang National Reserve Forest, Lao PDR. *Environmental Management, 36*(3), 382-393.

Tomkins, K.M. (2014). Uncertainty in streamflow rating curves: Methods, controls, and consequences. *Hydrol. Processes, 28*(3), 464-481.

Tuan, V.D., Hilger, T., MacDonald, L., Clemens, G., Shiraishi, E., Vien, T.D., Stahr, K., & Cadisch, G. (2014). Mitigation potential of soil conservation in maize cropping on steep slopes. *Field Crops Research, 156*, 91-102.

Tuan, V.D., Hilger, T., & Cadisch, G. (2015). Identifying resource competition in maize-based soil conservation systems using 13C and 15N isotopic discrimination. *Archives of Agronomy and Soil Science*, 1-20.

Uexkuell, H.v., & Beaton, J. (1992). A review of fertility management of rice soils. In J. Kimble (Ed.), *Characterization, classification, and utilization of wet soils. Proceedings of the 8th International Soil Correlation Meeting (VIII. ISCOM). Soil Conservation Service* (pp. 288-300). Lincoln, Neb. (USA): United States Department of Agriculture.

Uncles, R.J., Frickers, P.E., Easton, A.E., Griffiths, M.L., Harris, C., Howland, R.J.M., King, R.S., Morris, A.W., Plummer, D.H., & Tappin, A.D. (2000). Concentrations of suspended particulate organic carbon in the tidal Yorkshire Ouse River and Humber Estuary. *Science of the Total Environment, 251-252*, 233-242.

Valentin, C., Agus, F., Alamban, R., Boosaner, A., Bricquet, J.P., Chaplot, V., de Guzman, T., de Rouw, A., Janeau, J.L., Orange, D., Phachomphonh, K., Do Duy, P., Podwojewski, P., Ribolzi, O., Silvera, N., Subagyono, K., Thiébaux, J.P., Tran Duc, T., & Vadari, T. (2008). Runoff and sediment losses from 27 upland catchments in Southeast Asia: Impact of rapid land use changes and conservation practices. *Agriculture, Ecosystems and Environment, 128*(4), 225-238.

van Buuren, S. (2007). Multiple imputation of discrete and continuous data by fully conditional specification. *Statistical Methods in Medical Research, 16*(3), 219-242.

Van Dijk, A.I.J.M., & Bruijnzeel, L.A.S. (2005). *Key controls and scale effects on sediment budgets: Recent findings in agricultural upland Java, Indonesia.* Paper presented at the IAHS-AISH Publication.

Van Mai, T., & To, P.X. (2015). A Systems Thinking Approach for Achieving a Better Understanding of Swidden Cultivation in Vietnam. *Human Ecology, 43*(1), 169-178.

van Noordwijk, M., Cerri, C., Woomer, P.L., Nugroho, K., & Bernoux, M. (1997). Soil carbon dynamics in the humid tropical forest zone. *Geoderma, 79*(1-4), 187-225.

van Reeuwijk, L.P. (1992). *Procedures for Soil Analysis*. Wageningen: International Soil Reference and Information Centre.

Verbeke, G., & Molenberghs, G. (2009). *Linear mixed models for longitudinal data*. New York: Springer.

Verstraeten, G., & Poesen, J. (2001). Factors controlling sediment yield from small intensively cultivated catchments in a temperate humid climate. *Geomorphology, 40*(1–2), 123-144.

Vien, T.D., Rambo, T.A., & Lam, N. (2009). *Farming with fire and water: The human ecology of a composite swiddening community in Vietnam's Northern Mountains*. Melbourne: Kyoto University Press.

Vigiak, O., & Bende-Michl, U. (2013). Estimating bootstrap and Bayesian prediction intervals for constituent load rating curves. *Water Resources Research, 49*(12), 8565-8578.

Vörösmarty, C.J., Meybeck, M., Fekete, B., Sharma, K., Green, P., & Syvitski, J.P.M. (2003). Anthropogenic sediment retention: Major global impact from registered river impoundments. *Global and Planetary Change, 39*(1-2), 169-190.

Walling, D. E. (1977), Limitations of the rating curve technique for estimating suspended sediment loads, with particular reference to British rivers, *IAHS-AISH Publication* 122, pp. 34-118.

Walling, D.E., & Webb, B.W. (1981, June 1981). *The reliability of suspended sediment load data (River Creedy, UK). Erosion and sediment transport measurement. IAHS-AISH Publication* 133.

Walling, D.E., & Webb, B.W. (1996). Erosion and sediment yield: A global overview. *IAHS-AISH Publication, 236*, pp. 3-19.

Walz, L. (2015). *Linking compound specific stable isotopes (CSSI) with fallout radionucleides (FRN) to investigate sources of soil erosion sedimentation processes and land use history in the Chieng Khoi watershed, Vietnam* (Msc), University of Hohenheim, Stuttgart, Germany.

Wang, Y.G., Kuhnert, P., & Henderson, B. (2011). Load estimation with uncertainties from opportunistic sampling data - A semiparametric approach. *Journal of Hydrology, 396*(1-2), 148-157.

Wass, P.D., & Leeks, G.J.L. (1999). Suspended sediment fluxes in the Humber catchment, UK. *Hydrological Processes, 13*(7), 935-953.

Weiss, A.M. (2008). *Charcoal in sediment layers: A way to estimate land use intensification on reservoir siltation?* (MSc. Thesis), University of Hohenheim, Stuttgart, Germany.

Wezel, A., Luibrand, A., & Thanh, L.Q. (2002). Temporal changes of resource use, soil fertility and economic situation in upland Northwest Vietnam. *Land Degradation & Development, 13*(1), 33-44.

Wheatcroft, R.A., Goñi, M.A., Hatten, J.A., Pasternack, G.B., & Warrick, J.A. (2010). The role of effective discharge in the ocean delivery of particulate organic carbon by small, mountainous river systems. *Limnology and Oceanography, 55*(1), 161-171.

Williams, G.P. (1989). Sediment concentration versus water discharge during single hydrologic events in rivers. *Journal of Hydrology, 111*(1-4), 89-106.

Williams, J.R. (1975). Sediment routing for agricultural watersheds. *JAWRA Journal of the American Water Resources Association, 11*(5), 965-974.

Wold, H. (1966). Estimation of principal components and related models by iterative least squares. *Multivariate analysis, 1*, 391-420.

Xu, J., Fox, J., Zhang, P., Fu, Y., Yang, L., Qian, J., Leisz, S., & Vogler, J. (2005). Land Use/Land Cover Change and Farmer Vulnerability in Xishuangbanna. *Environmental Management, 36*, 3404-3413.

Yamada, S., Kitamura, A., Kurikami, H., Yamaguchi, M., Malins, A., & Machida, M. (2015). Sediment and 137Cs transport and accumulation in the Ogaki Dam of eastern Fukushima. *Environmental Research Letters, 10*(1), 014013.

Yan, X., Cai, Z., Yang, R., Ti, C., Xia, Y., Li, F., Wang, J., & Ma, A. (2010). Nitrogen budget and riverine nitrogen output in a rice paddy dominated agricultural watershed in eastern China. *Biogeochemistry*.

Yang, D., Kanae, S., Oki, T., Koike, T., & Musiake, K. (2003). Global potential soil erosion with reference to land use and climate changes. *Hydrological processes, 17*(14), 2913-2928.

Yoshinaga, I., Miura, A., Hitomi, T., Hamada, K., & Shiratani, E. (2007). Runoff nitrogen from a large sized paddy field during a crop period. *Agricultural Water Management, 87*(2), 217-222.

Zeppel, M.J.B., Wilks, J.V., & Lewis, J.D. (2014). Impacts of extreme precipitation and seasonal changes in precipitation on plants. *Biogeosciences, 11*(11), 3083-3093.

Ziegler, A.D., Giambelluca, T.W., Tran, L.T., Vana, T.T., Nullet, M.A., Fox, J., Vien, T.D., Pinthong, J., Maxwell, J.F., & Evett, S. (2004). Hydrological consequences of landscape fragmentation in mountainous northern Vietnam: evidence of accelerated overland flow generation. *Journal of Hydrology, 287*(1–4), 124-146.

Ziegler, A.D., Bruun, T.B., Guardiola-Claramonte, M., Giambelluca, T.W., Lawrence, D., & Thanh Lam, N. (2009a). Environmental consequences of the demise in swidden cultivation in montane mainland southeast asia: Hydrology and geomorphology. *Human Ecology, 37*(3), 361-373.

Ziegler, A.D., Fox, J.M., & Xu, J. (2009b). The rubber juggernaut. *Science, 324*(5930), 1024-1025.

Ziegler, A.D., Xi, L.X., & Tantasarin, C. (2011). *Sediment load monitoring in the Mae Sa catchment in Northern Thailand.* Paper presented at the AHS-AISH Publication.

Ziegler, A.D., Sidle, R.C., Phang, V.X.H., Wood, S.H., & Tantasirin, C. (2014). Bedload transport in SE Asian streams-Uncertainties and implications for reservoir management. *Geomorphology, 272*, 31-48.

Summary

Anthropogenic influences have caused landscapes to change worldwide in the last decades, and changes have been particularly intense in montane Southeast Asia. Traditional swiddening cropping systems with low environmental impacts have been largely replaced by forms of permanent upland cultivation, often with maize. The associated soil fertility loss at the plot scale is well documented. In valley bottoms of these areas, paddies have been cultivated for centuries, and are considered some of the most sustainable production systems in the world – in part maintained by the influx of fertile sediments through irrigation. Altered cropping patterns on the slopes therefore also have potential repercussions on rice production, and hence on food security, but the consequences of shifted sediment and nutrient redistribution at the landscape scale are not well understood. In order to assess these effects, methodologies were developed in this thesis that enable low-cost, continuous monitoring of sediment and nutrient transport in irrigated watersheds (Chapter 2), as well as quantification of the uncertainty on constituent loads (Chapter 3). These methods are applied in a case study to determine sediment, organic carbon and nitrogen trap efficiency of paddy rice fields in a mountainous catchment in Vietnam (Chapters 4 and 5).

Specifically, in order to quantify on- and off-site effects of land use change in intensely cultivated landscapes, monitoring strategies are required that are suitable for the catchment scale, are practical in terms of costs and sample size, and provide continuous data with a fine temporal resolution. In irrigated catchments, traditional hydrological predictors for constituent transport, such as discharge, fail due to water management. Therefore, in Chapter 2, a turbidity-based methodology was developed that enables continuous monitoring of sediment, organic carbon and nitrogen concentrations in irrigated watersheds. The use of a linear mixed model accounted for temporal correlation in the data, thus supporting storm-based manual sampling with samples taken closely together in time in order to capture rapid changes during rainfall events. As turbidity was shown to be not only affected by sediment concentration but also by texture and organic matter content, results demonstrated that organic carbon could be predicted with greater accuracy than sediment. With the developed methodology, sediment and nutrient transport can be quantified

simultaneously with a single sensor, at the landscape level and beyond, making it cost-effective and time-saving.

As the quantified constituent loads are frequently used as basis for modeling or decision-making, it is crucial to assess the accuracy of our estimates. Determining measures of uncertainty on annual loads is not trivial, because a load is a product of concentration and discharge per time point, summed up over time intervals. Due to the time series nature of the data and the fact that these variables are typically not normally distributed, error assessments are rarely performed. In Chapter 3, a bootstrap based approach was developed which enables the calculation of confidence intervals on constituent loads. The results showed that while the discharge predictions generally have a much higher accuracy than the sediment rating curve, ignoring the uncertainty on the discharge will typically underestimate the width of 95% confidence intervals with around 10%. Furthermore, as confidence intervals were shown to be asymmetric with the largest uncertainty on the upper limit, maximum impact scenarios could frequently be underestimating true consequences.

In Chapter 4, the developed methodology was applied in a case study of a maize-rice cropping system in the commune of Chieng Khoi, in Northwest Vietnam. The upland area had an average erosion rate of 7.5 Mg ha^{-1} a^{-1}. Sediment inputs to the paddy area consisted of 64 Mg ha^{-1} a^{-1}, of which irrigation water provided 75% and the remainder came from erosion during rainfall events. Erosion contributed one third of the sand inputs, while sediments from irrigation water were predominantly silty, demonstrating the protective effect of the reservoir which buffered the coarse, unfertile material. Almost half of the total sediment inputs were trapped in the rice area. As all of the sand inputs remained in the rice fields, the upland-lowland linkages could entail a long-term change in topsoil fertility and eventually a rice yield loss.

Quantification of nutrient re-allocation in Chapter 5 showed that irrigation was even more important as a driver of sediment-associated organic carbon and nitrogen inputs into the rice fields, contributing 90% of carbon and virtually all nitrogen. Direct contributions from erosion to the nutrient status of the paddies were negligible, again underscoring the protective function of the surface reservoir in buffering irrigated areas from unfertile sediment inputs. 88% of the sediment-associated organic carbon

and 93% of the nitrogen were captured by the rice fields. Irrigation water additionally brought in dissolved nitrogen, resulting in a total nitrogen input of 1.11 Mg ha^{-1} a^{-1}. Of this amount, 24% was determined to be in the plant-available forms of ammonium and nitrate, a contribution equivalent to 66% of the recommended nitrogen application via chemical fertilizer.

The dependence of paddy soil fertility on agricultural practices in the uplands illustrates the vulnerability of irrigated rice to unsustainable land use in the surrounding landscape. Unfortunately, alternatives for upland land use that are not detrimental to soil quality are hard to come by, due to the economic reality of high maize prices on the world market. Conservation measures and agroforestry systems offer potential, but without some form of payment for environmental services, adoption rates remain low.

Finding sustainable solutions is especially urgent as climate change is likely to increase the number of extreme rainfall events and hence intensify the redistribution processes already taking place. In this light, the role of trapping elements in landscapes such as paddy fields and surface reservoirs becomes more important as well. As these features are widely spread throughout tropical landscapes, their role in global sediment and nutrient cycles must be taken into account. The methodologies developed in this thesis, for sediment and nutrient transport monitoring and for uncertainty assessment, can aid in closing the data gap that currently hinders a reliable assessment of the consequences of anthropogenic and climate change, both on food security and on environmental impacts, locally, regionally and globally.

German Summary

Weltweit haben anthropogene Einflüsse Landschaften in den letzten Jahrzehnten wesentlich verändert. Dieser Wandel war besonders stark in Bergregionen Südostasiens. Traditioneller Wanderackerbau mit geringen Umweltauswirkungen wurde weitgehend durch Formen permanenten Anbaus - oft auf Basis von Mais - ersetzt. Der damit einhergehende Verlust an Bodenfruchtbarkeit auf Feldebene ist gut beschrieben. In Tallagen dieser Region werden Reisfelder seit Jahrhunderten kultiviert und gelten als einige der nachhaltigsten Pflanzenproduktionssysteme der Welt. Dies wird teilweise durch den Eintrag fruchtbarer Sedimente über das Bewässerungswasser ermöglicht. Veränderte Landnutzungsmuster in Hanglagen können sich daher auch auf die Reisproduktion auswirken und in Folge die Nahrungssicherung beeinträchtigen. Allerdings werden die Konsequenzen einer veränderten Sediment- und Nährstoffumverteilung auf der Landschaftsebene bisher kaum verstanden. Um diese Auswirkungen zu erfassen, wurden im Rahmen dieser Dissertation Methoden entwickelt, die ein kostengünstiges, kontinuierliches Monitoring der Sediment- und Nährstofftransports in bewässerten Wassereinzugsgebieten (Kapitel 2) sowie die Quantifizierung von Ungewissheiten in deren Zusammensetzung erlauben (Kapitel 3). Diese Methoden werden in einer Fallstudie angewandt, um den Wirkungsgrad des Sedimenteintrags in bewässerten Reisfeldern auf Wassereinzugsgebietsebene in einer Bergregion Vietnams zu bestimmen (Kapitel 4 und 5).

Um Auswirkung von Einflüssen von Landnutzungsänderung innerhalb und außerhalb eines intensiv kultivierten Wassereinzugsgebietes quantifizieren zu können, bedarf es Strategien für das Monitoring, die für diese Skala geeignet und hinsichtlich der Kosten und Probenanzahl praktikabel sind sowie kontinuierlich Daten mit einer hohen zeitlichen Auflösung liefern. Wegen des geregelten Wassermanagements in bewässerten Einzugsgebiet versagen herkömmliche, hydrologische Kenngrößen, z. B. Ablauf, für den Transport von Inhaltsstoffen. Daher wurde in Kapitel 2 eine turbiditätsbasierte Methode entwickelt, die ein kontinuierliches Monitoring von Sedimenten sowie von organischen Kohlenstoff- und Stickstoffkonzentrationen in bewässerten Einzugsgebieten erlaubt. Die Verwendung eines gemischten linearen Models konnte die zeitliche Korrelation der Daten erklären. Dadurch konnten Aussagen zu starkregenbasierter, manueller

Beprobung in Verbindung mit zeitlich eng gestaffelten automatisierten Proben verifiziert werden, um rasche Veränderungen während Regenereignisse zu erfassen. Allerdings konnte der organische Kohlenstoff mit höherer Genauigkeit vorhergesagt werden als Sediment, da die Turbidität nicht nur von der Sedimentkonzentration, sondern auch von Textur und Gehalt an organischer Substanz beeinflusst wird. Mit dieser Methode lassen sich Sediment- und Nährstofftransport auf Landschaftsebene und darüber hinaus mit einem einzelnen Sensor quantifizieren. Dadurch ist die Methode kosteneffizient und zeitsparend.

Da die quantifizierte Schwebstofffracht oft als Basis für Modellierungen oder Entscheidungsfindung herangezogen wird, ist es ausschlaggebend die Genauigkeit unserer Schätzwerte zu erfassen. Das Bestimmen des Ausmaßes der Unsicherheit in annuellen Frachten ist nicht einfach, da die Fracht ein Produkt aus Konzentration und Abfluss pro Zeitpunkt, summiert über Zeitintervalle, ist. Wegen des Zeitreihencharakters der Daten und der Tatsache, dass diese Variablen typischerweise nicht normal verteilt sind, werden Fehlererfassungsverfahren selten eingesetzt. In Kapitel 3 wird ein Bootstrap-Ansatz erläutert, der eine Berechnung von Konfidenzintervallen der Ladungsfracht ermöglicht. Die Ergebnisse zeigen, dass bei generell besserer Genauigkeit Abflussvorhersagen gegenüber der Sedimenteichkurve ein Vernachlässigen der Ungewissheit in Bezug auf den Abfluss die Breite des 95 % Konfidenzintervalls typischerweise um rund 10 % unterschätzt. Ferner können Szenarien maximaler Auswirkungen wahre Folgen häufig unterschätzen, weil die Konfidenzintervalle asymmetrisch sind, wobei die größte Ungewissheit im oberen Limit liegt. Kapitel 4 beschreibt die Anwendung der entwickelten Methode in einer Fallstudie mit Mais-Reis Anbausystemen in der Chieng Khoi Kommune, Nordwestvietnam. In der Hangzone lag die durchschnittliche Erosionsrate bei 7.5 Mg/ha und Jahr. Der Sedimenteintrag in die Nassreisfläche betrug 64 Mg/ha und Jahr. Hierzu trug das Bewässerungswasser 75 % bei, der Rest durch Erosion während Starkregenereignissen. Erosion lieferte ein Drittel des Sandeintrags, während die Sedimente des Bewässerungswassers überwiegend schluffig waren. Dies demonstriert den Puffereffekt des Stausees, der das gröbere, unfruchtbare Material aufnahm. Fast die Hälfte der Sedimentfracht verblieb in der Reisanbauzone. Da der gesamte Sandanteil in den Reisfeldern verblieb, könnte sich in der Beziehung zwischen Hang- und Tallagen langfristig eine Veränderung der Bodenfruchtbarkeit im Oberboden einstellen und in Folge eventuell ein Verlust an Reiserträgen.

Die Quantifizierung der Nährstoffumverteilung in Kapitel 5 zeigte, dass die Bewässerung einen noch größeren Einfluss auf die Einträge an organischem Kohlenstoff und Stickstoff in die Reisfelder hatte und dabei 90% des Kohlenstoffs und fast den gesamten Stickstoff beitrug. Direkte Beiträge der Erosion zur Nährstoffversorgung der Reisfelder waren vernachlässigbar, was wiederum die Schutzfunktion des Stausees im Hinblick auf den Schutz des Bewässerungsgebietes vor unfruchtbaren Sedimenteinträgen unterstreicht. 88% der Sedimentfracht an organischem Kohlenstoff und 93% des Stickstoffs verblieben in den Reisfeldern. Das Bewässerungswasser trug zusätzlich gelösten Stickstoff ein, was einen Gesamteintrag an Stickstoff in Höhe von 1.11 Mg ha^{-1} a^{-1} zur Folge hatte. Hiervon waren 24% pflanzenverfügbar in Form von Ammonium und Nitrat, wodurch das Bewässerungswasser einen Beitrag zum pflanzenverfügbaren N lieferte, äquivalent zu der Hälfte der empfohlenen chemischen Dünger-Anwendung.

Die Abhängigkeit der Bodenfruchtbarkeit der Reisböden von Anbaupraktiken in den Hanglagen illustriert die Anfälligkeit des Nassreises gegenüber einer nicht nachhaltigen Landnutzung in der umgebenden Landschaft. Alternativen für eine Nutzung der Hanglagen, die nicht abträglich für die Bodenqualität sind, sind leider rar wegen der hohen Weltmarktpreise für Mais. Bodenschonende Anbausysteme oder Agroforstsysteme haben Potenzial, werden aber ohne irgendeine Form der Kompensationszahlung für Ökosystemleistungen in ihrer Übernahmerate gering bleiben.

Das Finden nachhaltiger Lösungen ist besonders dringend, da der Klimawandel vermutlich eine Zunahme extremer Regenereignisse bewirkt, in deren Folge die bereits bestehenden Umlagerungsprozesse noch intensiviert werden. In diesem Zusammenhang gewinnen Landschaftselemente wie Nassreisfelder und Stauseen als Filter zunehmend an Bedeutung. Da diese Merkmale in Landschaften der Tropen weit verbreitet sind, muss man ihre Rolle im Zusammenhang mit globalen Sediment- und Nährstoffkreisläufen sehen. Die im Rahmen dieser Dissertation zum Monitoring von Sediment- und Nährstofftransport sowie zur Überprüfung von Messunsicherheit entwickelten Methoden können helfen, Wissenslücken zu schließen, die aktuell eine verlässliche Einschätzung der Konsequenzen anthropogenem Handelns einschließlich der Auswirkungen des Klimawandels in Hinblick auf

Nahrungssicherheit und Auswirkungen auf die Umwelt im lokalen, regionalen und globalen Kontext erschweren.

Appendices

Appendix A: Simulating data with a fixed realized R^2

In order to obtain (log(Q), log(h))-pairs with a certain R^2 (eg. 0.95), we started by simulating a dataset of the same number of observations of the original dataset. We thus obtained pairs of $\log(Q_i)$ and $\log(h_i)$ using the original discharge rating curve, which is a regression model $y_i = \eta_i + e_i$, where $\eta_i = \alpha + \beta x_i$ and the errors were randomly drawn from a normal distribution which can have any variance, as the errors will be rescaled later.

Next, we computed the total sum of squares, SS_y, and the residual sum of squares, SS_e, for this simulated dataset. We subsequently replaced the simulated errors e_i by re-scaled errors $e_i^* = ce_i$ and used these to compute re-scaled simulated data $y_i^* = \eta_i + e_i^*$. A scaling constant c was chosen in such a way that the desired coefficient of determination results:

(A1) $R^2 = 1 - SS_e/SS_y$ and $R^{2*} = 1 - SS_e^*/SS_y^*$,

(A2) The residual error sum of squares is a quadratic form of errors only. It follows that

$$SS_e^* = c^2 SS_e$$

(A3)

$$SS_y^* = \sum_{i=1}^{n} (y_i^* - \bar{y}_\cdot^*)^2 = \sum_{i=1}^{n} (\eta_i + ce_i - \bar{\eta}_\cdot - c\bar{e}_\cdot)^2 = \sum_{i=1}^{n} [(\eta_i - \bar{\eta}_\cdot) + c(e_i - \bar{e}_\cdot)]^2$$

$$= \sum_{i=1}^{n} (\eta_i - \bar{\eta}_\cdot)^2 + 2c \sum_{i=1}^{n} (\eta_i - \bar{\eta}_\cdot)(e_i - \bar{e}_\cdot) + c^2 \sum_{i=1}^{n} (e_i - \bar{e}_\cdot)^2 = z_1 + z_2 c + z_3 c^2$$

where z_1, z_2 and z_3 are computable constants for given simulated (η_i, e_i).

(A4)

$$R^{2*} = 1 - SS_e^*/SS_y^* \Leftrightarrow$$

$$0 = SS_e^*/SS_y^* - 1 + R^{2*} \Leftrightarrow$$

$$0 = SS_e^* + (R^{2*} - 1)SS_y^* = c^2 SS_e + (R^{2*} - 1)(z_1 + z_2 c + z_3 c^2) = Ac^2 + Bc + C$$

This is a quadratic equation in *c*, which can be solved for *c* by standard procedures. There are two distinct solutions but they result in errors that only differ in the sign, and so either solution can be chosen.

SAS-code to perform this simulation can be found below.

```
In the original dataset, Q is discharge and h is the water height.
Simulate a dataset of log(Q) and log(h) that:
-has the same size as the original dataset (i=1 to n_original)
-is simulated from the original stage-discharge equation (enter parameters for logQ=a*logh + b)
-has residual errors drawn randomly for a normal distribution with any variance, as the variance will
be rescaled later
*/

data Q_simset;
do i=1 to 20;
  logh=-1.0727485+4.1546429*rannor(-1);
  logQ_perf=0.0466*logh + 0.1254;
  logQ=logQ_perf+ (0.1*rannor(-1));
            *add any variance, then rescale;
  output;
end;
run;

/*
This simulated dataset is the input dataset for the macro which rescales the errors so we obtain the
desired R-square.
The macro variables are
sim= the simulated dataset from the first step
Rsquare_desired= the required R2, for example 0.95
*/
%macro Rsquare(sim=, Rsquare_desired=);

            proc mixed data=&sim;
            model logQ= logh /outpm=pred;
            run;
            quit;

            data pred;
            set pred;
            resid_sq=resid**2;
            run;
```

```
proc univariate data=pred noprint;
var resid resid_sq logQ pred;
output out=sum_resid sum=sum_resid sum_resid_sq sumQ sumpred mean=mean_resid
mean_resid_sq mean_logQ mean_pred;
run;

data sum_resid;
set sum_resid;
call symput('SS_resid',trim(left(sum_resid_sq)));
call symput('mean_resid',trim(left(mean_resid)));
call symput('mean_logQ',trim(left(mean_logQ)));
call symput('mean_pred',trim(left(mean_pred)));
run;

data data_sim;
set pred;
z2_pred=(pred-&mean_pred);
z2_err=(resid-&mean_resid);
run;

data data_sim;
set data_sim;
z1_calc=(pred-&mean_pred)**2;
z2_calc=z2_pred*z2_err;
z3_calc=(resid-&mean_resid)**2;
run;

proc univariate data=data_sim noprint;
var z1_calc z2_calc z3_calc;
output out=explained_error sum=sum_z1 sum_z2 sum_z3;
run;

data explained_error;
set explained_error;
z1=sum_z1;
z2=2*sum_z2;
z3=sum_z3;
run;


data explained_error;
set explained_error;
call symput('z1',trim(left(z1)));
call symput('z2',trim(left(z2)));
call symput('z3',trim(left(z3)));
run;


*solve for c: Ac2 + bc + C = 0 with
C= (Rsquare_desired-1)*z1
B= (Rsquare_desired-1)*z2
A= SSe + (Rsquare_desired-1)*z3

-> solution
x1,2= ( -B +/- Sqrt( B**2 - 4*A*C) ) / (2*A)
;

data rescale;
set explained_error;
A= &SS_resid + ((&Rsquare_desired-1)*&z3);
B= (&Rsquare_desired-1)*&z2;
C= (&Rsquare_desired-1)*&z1;
```

```
run;

data rescale;
set rescale;
D=(B**2) - (4*A*C);
run;

data rescale;
set rescale;
sqrtD=sqrt(D);
run;

data rescale;
set rescale;
c1= (-B + sqrtD)/(2*A);
c2= (-B - sqrtD)/(2*A);
run;

data rescale;
set rescale;
call symput('c1',trim(left(c1)));
call symput('c2',trim(left(c2)));
run;

data data_sim;
set data_sim;
c1=&c1;
c2=&c2;
SS_error=&SS_resid;
run;

data data_sim;
set data_sim;
resid_rescaled1=c1*resid;
resid_rescaled2=c2*resid;
run;

data data_sim;
set data_sim;
logQ_new_1=pred+resid_rescaled1;
logQ_new_2=pred+resid_rescaled2;
run;

data data_sim;
set data_sim;
keep logQ_new_1 logQ_new_2 logh;
run;


%mend;

%Rsquare(sim=Q_simset, Rsquare_desired=0.95);

/*
The final dataset is called data_sim.
As there are two distinct solutions, there are two rescaled variables that both give the desired Rsquare:
logQ_new_1 and logQ_new_2
The desired Rsquare can be demonstrated in PROC GLM
*/

proc glm data=data_sim;
model logQ_new_1=logh;
run;
```

```
quit;

proc glm data=data_sim;
model logQ_new_2=logh;
run;
```

Appendix B: Map of Chieng Khoi catchment

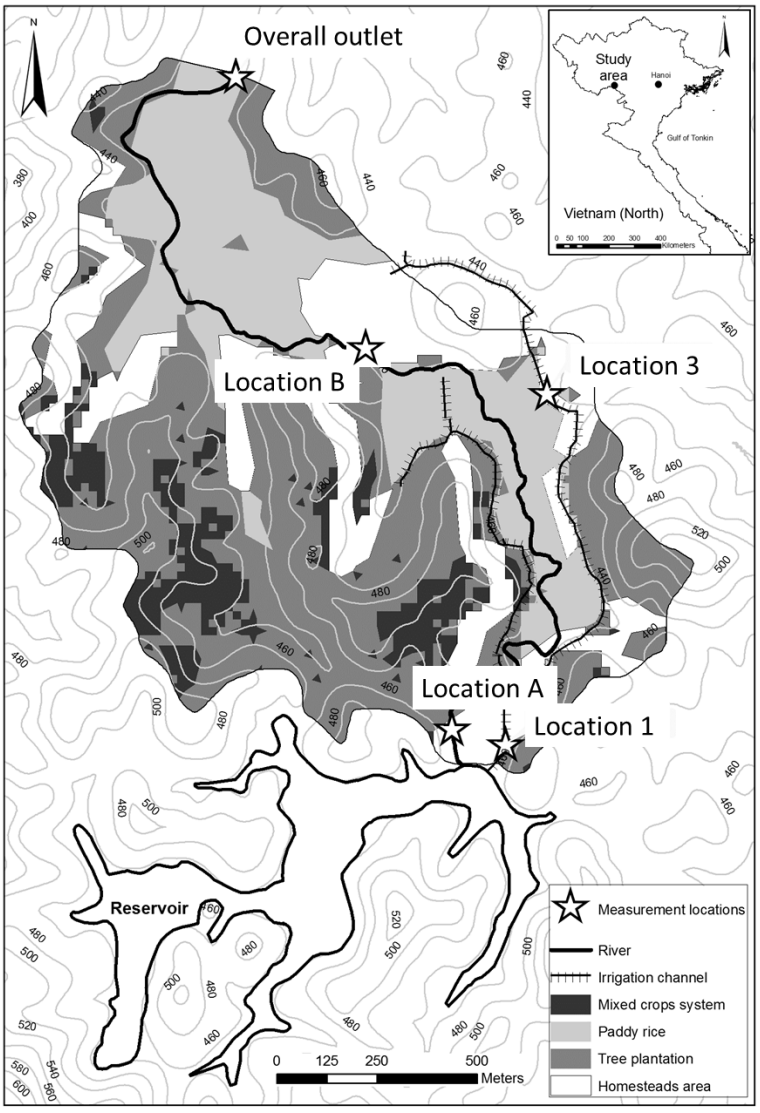

Figure B1: Map of Chieng Khoi watershed, showing land use types and measurement locations (modified after Slaets *et al.*, 2014).

Appendix C: Event table

Table C.1: Erosion and rainfall characteristics of the 33 events in the study that mobilized more than 2 Mg of sediment, shown in descending order according to their event load. Total rainfall (P total), duration of the event, maximum event rainfall intensity (Max P int) and average event rainfall intensity (Av P int) are displayed.

	Erosion	**P total**	**Event duration**	**Max P int**	**Av P int**
Date	(Mg)	(mm)	(min)	(mm/hour)	(mm/hour)
13/07/2011	31.43	73	186	156.0	23.5
05/06/2010	27.28	52	236	48.0	13.2
20/06/2011	21.58	55	274	132.0	12.1
24/08/2011	8.82	37	332	81.0	6.6
10/09/2011	8.46	32	118	90.0	16.3
28/05/2010	7.44	43	52	126.0	49.6
24/05/2010	7.10	12	122	6.1	5.8
05/05/2011	6.54	40	182	84.0	13.3
18/07/2010	6.31	30	546	18.0	3.2
19/08/2010	6.12	34	70	72.0	29.0
04/08/2010	6.10	32	120	78.0	16.2
01/07/2011	5.41	23	126	75.0	11.0
02/09/2011	5.33	23	152	33.0	9.0
18/06/2011	4.78	21	66	81.0	19.4
11/08/2010	4.60	12	78	57.0	9.5
22/06/2010	4.40	33	86	48.0	22.7
17/08/2010	4.15	24	342	48.0	4.3
31/05/2010	4.06	17	46	78.0	21.8
21/06/2010	3.88	25	210	54.0	7.2
26/04/2010	3.65	19	108	54.0	10.5
24/07/2010	3.40	20	48	99.0	25.1
10/05/2010	3.39	4	56	6.1	4.3
25/05/2010	3.19	18	194	60.0	5.6
19/07/2011	2.85	17	270	30.0	3.8
23/07/2011	2.76	25	152	54.0	9.8
13/07/2011	2.66	18	70	90.0	15.0
26/08/2010	2.61	13	66	96.0	12.2
06/10/2011	2.53	13	422	6.0	1.8
22/06/2010	2.50	17	52	96.0	19.0
15/08/2011	2.22	33	48	139.4	40.7
29/05/2010	2.18	15	54	126.0	16.1
27/06/2011	2.10	13	262	15.0	2.9
13/07/2010	2.07	20	254	21.0	4.6